Thermoresponsive Colloidal Microgels and Polymeric Solutions at Rest and Under Shear

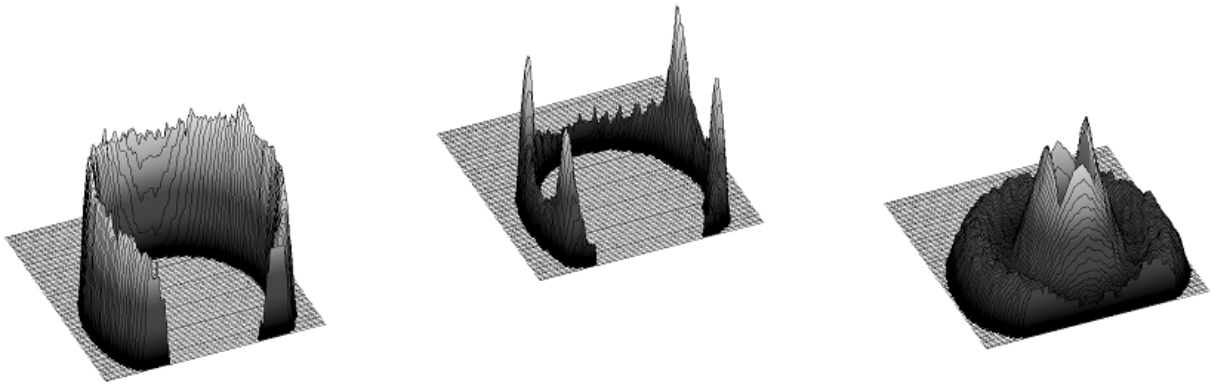

PhD thesis

submitted in partial fulfillment of the requirements
for the degree of “Doktor rerum naturae”
to the Faculty of Mathematics and Science
Christian-Albrechts University of Kiel

Markus Stieger

Kiel 2004

This PhD work was carried out at the Institute of Macromolecular Chemistry at Albert-Ludwigs University of Freiburg from October 1999 until October 2000 and continued at the Institute of Physical Chemistry at Christian-Albrechts University of Kiel from November 2000 until March 2004. I certify that this thesis does not incorporate, without acknowledgement, any material previously submitted for a degree or diploma in any university, and that, to the best of my knowledge, it does not contain any material previously published or written by another person except where due reference is made in the text. The work in this thesis is my own, except for the contributions made by others as described in the Acknowledgements.

Markus Stieger

Referent:	Prof. Dr. W. Richtering
Korreferent:	Prof. Dr. Dr. h. c. G. Lagaly
Tag der Disputation:	27.04.2004
Zum Druck genehmigt, Kiel den	
	Der Dekan

Thermoresponsive Colloidal Microgels and Polymeric Solutions at Rest and Under Shear

The structure of temperature-sensitive poly(*N*-isopropylacrylamide) (PNiPAM) microgels in dilute suspension was investigated by means of small-angle neutron scattering (SANS). A direct modeling expression for the scattering intensity was derived which includes the overall particle form as well as the internal structure of the microgel network. The influences of temperature, cross-linking density and particle size on the structure were revealed by the radial density profiles and clearly showed that the segment density in the swollen state was not homogeneous but gradually decayed at the surface. The density profile revealed a box profile only when the particles were collapsed at elevated temperatures. An increase of the cross-linking density resulted in both an increase of the polymer volume fraction in the inner region of the particle and a reduction of the smearing of the surface. The structural changes were in good agreement with the kinetics of the emulsion copolymerization used to prepare the microgel colloids.

The model expression was extended by a structure factor to describe concentrated PNiPAM microgel suspensions. A direct real space description of the spatial ordering in the neighborhood of a single particle was obtained. The overall particle size and the correlation length of the concentration fluctuations of the internal polymer network decreased with concentration revealing the increasing compression of the spheres. The particle form factor of the swollen PNiPAM microgels depended on concentration. The interaction potential did not change significantly between 25°C and 32°C. Microgels with different degrees of cross-linking and particle size resembled true hard sphere behavior up to effective volume fractions of ϕ_{eff}<0.35. At higher effective volume fractions strong deviations from true hard spheres were observed. In agreement with this, the equilibrium colloidal phase behavior and rheology also had some features of soft sphere systems. At temperatures well above the LCST the interaction potential became strongly attractive. The collapsed microgel spheres formed aggregates consisting of flocculated particles without significant long-range order.

Rheo-SANS experiments revealed that the shear-induced particle arrangements strongly depend on the interaction potential. When the interaction potential was repulsive at temperatures below the LCST, no significant deformation of the swollen PNiPAM particles was observed. Shear-induced ordering was found resulting in the formation of two dimensional hexagonal close packed layers that aligned along the flow direction giving rise to shear thinning. At temperatures near the LCST, when the particle interaction potential is not yet strongly attractive, shear flow induced the collapse of an individual particle. A so-called butterfly scattering pattern indicated the shear-induced enhancement of concentration fluctuations along the flow direction leading to solvent being squeezed out of the particles.

The influence of shear flow on the phase separation of PNiPAM microgels was investigated by means of rheo-turbidity and rheo-SANS and compared to the behavior of linear PNiPAM macromolecules. The rheological behavior of concentrated microgel suspensions depended strongly on temperature, but flow and viscoelastic properties of concentrated solutions of the linear polymer were not significantly affected by temperature changes. Shear induced phase separation was observed for both polymer architectures, although the viscoelastic properties of the two systems have different structural origins. For solutions of aqueous linear chain PNiPAM in the semi-dilute regime at different shear rates the existence of a threshold shear stress was observed and the phase separation process became faster with increasing stress. The two dimensional scattering patterns remained isotropic even during the phase separation process and the correlation length increased. The influence of shear flow on the phase separation process has apparently an analogous effect as a temperature increase.

Temperatursensitive Kolloidale Mikrogele und Polymerlösungen in Ruhe und unter Scherung

Die Struktur temperatursensitiver Poly(*N*-isopropylacrylamid) (PNiPAM) Mikrogele wurde mittels Kleinwinkelneutronenstreuung (SANS) in verdünnter Lösung untersucht. Ein Modell für die Streuintensität wurde hergeleitet, welches sowohl die Gesamtform des Teilchens als auch die innere Struktur des Mikrogel Netzwerkes berücksichtigt. Der Einfluß von Temperatur, Vernetzungsdichte und Teilchengröße auf die Struktur wurde durch Polymerdichteprofile verdeutlicht. Die Polymersegmentdichte im gequollenen Zustand war nicht homogen verteilt, sondern nahm zur Teilchenoberfläche hin ab. Nur wenn die Teilchen bei Temperaturen oberhalb der Entmischungstemperatur (LCST) kollabiert waren, zeigten die Dichteprofile ein homogenes Rechteckprofil. Mit zunehmenden Vernetzungsgrad nahm die Polymerdichte im Inneren des Teilchens zu und gleichzeitig die Verschmierung der Oberfläche ab. Die strukturellen Änderungen sind in guter Übereinstimmung mit der Kinetik der Emulsionscopolymerisation, mit der die Mikrogel Kolloide dargestellt wurden.

Das Modell wurde um einen Strukturfaktor erweitert, um konzentrierte PNiPAM Suspensionen zu beschreiben. Auf diese Weise wurde die räumlichen Struktur in der Nachbarschaft eines einzelnen Teilchens erhalten. Die Gesamtteilchengröße und die Korrelationslänge der Konzentrationsfluktuationen des inneren Polymernetzwerkes nahmen mit steigender Konzentration ab. Das Wechselwirkungspotential änderte sich zwischen 25°C und 32°C nicht signifikant. Mikrogele mit unterschiedlicher Vernetzungsdichte und Teilchengröße konnten mit Harte-Kugel Modellen bis zu Volumenbrüchen von ϕ_{eff}<0.35 beschrieben werden. Bei höheren Volumenbrüchen traten starke Abweichungen vom Harte-Kugel Verhalten auf. Dies war in exzellenter Übereinstimmung mit dem Phasenverhalten und der Rheologie, die ebenfalls Charakteristika von Weichen-Kugeln aufwiesen. Bei Temperaturen oberhalb der Entmischungstemperatur wurde das Wechselwirkungspotential stark attraktiv. Die kollabierten Mikrogelteilchen bildeten Aggregate aus ausgeflockten Partikeln ohne langreichweitige Ordnung.

Rheo-SANS Untersuchungen zeigten eine starke Abhängigkeit der scherinduzierten Strukturen vom Wechselwirkungspotential. Bei Temperaturen unterhalb der LCST war das Wechselwirkungspotential abstoßend und es wurde keine Deformation der gequollenen PNiPAM Teilchen beobachtet. Scherung führte zur Bildung von zweidimensional hexagonal dicht gepackten Schichten, welche sich entlang der Fließrichtung orientierten und somit eine Abnahme der Viskosität hervorriefen. Bei Temperaturen nahe der LCST war das Wechselwirkungspotential leicht attraktiv und der Kollaps eines individuellen Teilchens wurde unter Scherung beobachtet. Ein sogenanntes “butterfly”-Streubild zeigte die Zunahme der Konzentrationsfluktuationen entlang der Fließrichtung unter Scherung an, die zum Herauspressen von Lösungsmittel aus dem Teilchen führten.

Desweiteren wurde der Einfluß von Scherung auf die Phasenseparation von PNiPAM Mikrogelen mittels Trübungs- und SANS Messungen untersucht und mit dem Verhalten von Lösungen von linearem PNiPAM Makromolekülen verglichen. Die Fließ- und viskoelastischen Eigenschaften von konzentrierten Mikrogelsuspensionen hingen stark von der Temperatur ab. Im Gegensatz dazu zeigte das rheologische Verhalten der Lösungen des linearen PNiPAM keine ausgeprägte Temperaturabhängigkeit. Scherinduzierte Entmischung wurde für beide Polymerarchitekturen beobachtet, obwohl die viskoelastischen Eigenschaften der beiden Systeme unterschiedliche strukturelle Ursachen haben.

Im halbverdünnten Bereich nahe der LCST zeigten Experimente mit Lösungen des linearen PNiPAM bei verschiedenen Scherraten die Existenz eines Grenzwertes der Schubspannung, ab dem scherinduzierte Entmischung beobachtet wurde. Der Phasenseparationsprozeß wurde mit zunehmender Schubspannung schneller. Der Einfluß der Scherströmung auf die Phasenseparation hat offensichtlich einen analogen Effekt wie eine Temperaturerhöhung.

List of Publications and Presentations

Paper:

Markus Stieger, Walter Richtering; *Macromolecules*, **2003**, *36*, 8811-8818.
Shear-Induced Phase Separation in Aqueous Polymer Solutions: Temperature-Sensitive Microgels and Linear Polymer Chains

Markus Stieger, Walter Richtering, Jan Skov Pedersen, Peter Lindner; *J. Chem. Phys.*, **2004**, *in press.*
Small-Angle Neutron Scattering Study of Structural Changes in Temperature-Sensitive Microgel Colloids

Markus Stieger, Walter Richtering, Jan Skov Pedersen, Peter Lindner; *Langmuir*, **2004**, *submitted.*
Are Thermoresponsive Microgels Model Systems for Concentrated Colloidal Suspensions? A Rheology and Small-Angle Neutron Scattering Study

Markus Stieger, Peter Lindner, Walter Richtering; *Journal of Physics: Condensed Matter*, **2004**, *submitted.*
Structure Formation of Thermoresponsive Microgels Suspensions Under Shear Flow

Markus Stieger, Peter Lindner, Walter Richtering; *e-Polymers*, **2004**, *in preparation.*
Small-Angle Neutron Scattering Study of Shear-Induced Phase Separation in Aqueous Poly(*N*-isopropylacrylamide) Solutions

Ekkehard Müh, Markus Stieger, Joachim E. Klee, Holger Frey, Rolf Mülhaupt; *J. Polym. Sci. A: Polym. Chem.*, **2001**, *39*, 4274-4282.
Organic-Inorganic Hybrid Networks by the Sol-Gel Process and Subsequent Photopolymerization

Stefan Mecking, Ulf Schlotterbeck, Ralf Thomann, Matthias Soddemann, Markus Stieger, Walter Richtering, Holger Kautz; *Polym. Mat. Sci. Eng.*, **2001**, *84*, 511-512
Formation of Metal Nanoparticles in Modified Hyperbranched Polyglycerols and Use as Soluble Separable Catalysts.

Martin Baumert, Jörg Fröhlich, Markus Stieger, Holger Frey, Rolf Mülhaupt, Herbert Plenio; *Macromol. Rapid Commun.*, **1999**, *20*, 203-209.
Styrene-Vinylferrocene Random and Block Copolymers by TEMPO-Mediated Radical Polymerization

Markus Stieger; *Applied Rheology*, **2002**, *3*, 232 (Book Review).
The Rheology Handbook – For Users of Rotational and Oscillatory Rheometers

Talks:

Markus Stieger, Walter Richtering; *5th European School on Scattering Methods Applied to Soft Condensed Matter*, **June 2000**, Bombannes, Gironde, France
Shear-Induced Structures in Concentrated Colloidal Suspensions

Markus Stieger, Peter Lindner, Walter Richtering; *73rd Annual Meeting of the Society of Rheology*, **October 2001**, Bethesda, Maryland, USA
Shear Induced Demixing of Temperature-Sensitive Microgel Suspensions

Markus Stieger, Johannes Zipfel, Peter Lindner, Walter Richtering; *Bunsentagung*, **Mai 2002**, Potsdam
Temperatursensitive Mikrogele: Struktur und Phasenverhalten in Ruhe und unter Scherung

Poster:

Markus Stieger, Holger Senff, Walter Richtering; *13th Colloid and Interface Science Society Conference*, **September 1999**, Dublin, Ireland
Temperature-Sensitive Microgel Suspensions: Rheology and Phase Behavior at Rest and under Shear

Markus Stieger, Holger Senff, Walter Richtering; *Makromolekulares Kolloquium*, **Februar 2000**, Freiburg
Rheologie und Phasenverhalten temperatursensitiver Mikrogele

Markus Stieger, Johannes Zipfel, Peter Lindner, Walter Richtering; *Jülich Soft Matter Days*, **November 2001**, Kerkrade, Netherlands
Shear Induced Demixing of Temperature-Sensitive Microgel Suspensions

Markus Stieger, Ingo Berndt, Nils Greinert, Walter Richtering, Jan Skov Pedersen, Peter Lindner; *Bunsentagung*, **Mai 2003**, Kiel
Temperature-Sensitive Microgel Suspensions: Smart Materials and Push me-Pull you Systems

Markus Stieger, Ingo Berndt, Nils Greinert, Walter Richtering, Jan Skov Pedersen, Peter Lindner; *77th American Chemical Society: Colloid and Surface Science Symposium*, **June 2003**, Atlanta, Georgia, USA
Temperature-Sensitive Microgel Suspensions: Smart Materials and Push me-Pull you Systems

Markus Stieger, Walter Richtering, Jan Skov Pedersen, Peter Lindner; *41st Biennial Meeting of the German Colloid Society*, **September 2003**, Bayreuth
Structural Changes in Temperature-Sensitive Microgel Suspensions at Rest and under Shear Flow

For Stacy

Acknowledgments

First of all I would like to express indebted gratitude to my supervisor Prof. Dr. Walter Richtering. He has always been extremely generous with his time, knowledge and allowed me great freedom in this research. His enthusiastic approach to research and his endless excitement for the chemistry and physics of colloids have made this thesis enjoyable and I am greatly appreciative.

I would also like to thank Prof. Dr. Jan Skov Pedersen very much for forming an important part of my supervisory panel, for many helpful and fruitful discussions, for establishing SANS modeling in the research group and for his depth knowledge of scattering methods. He was a constant source and a sounding board for many ideas.

I would like to thank Prof. Dr. Dr. h. c. Gerhard Lagaly for his advice as a member of my supervisory panel.

Special thanks I would like to express to all my colleagues who have collaborated with me at the Institute of Macromolecular Chemistry in Freiburg and the Institute of Physical Chemistry in Kiel. Most of them became valuable and close friends during this thesis. In detail, I would like to thank:

- Florian for being a partner in crime from the first days in Freiburg to the very end in Kiel
- Ingo for adding a shell to the core, shortening the sails whenever it was unnecessary and the unforgettable Wacken experience
- Matthias for his support during the Freiburg-Kiel move
- Holger, Frank and Johannes for introducing me to the double logarithmic world of rheology and scattering
- Edda for her commitment to the coffee breaks
- Nils for his declared intention to listen to peculiar audiobooks on the way to Freiburg
- David for his useful insights in the art of Italian cooking
- Liliana for her help during her project with her impressive relaxed attitude
- Stefanie for her encouragement during her lab class and her tasty cakes which would have been nothing without her famous coffee.

I am grateful to David Boyer and Dr. Peter Linder for their assistance during the experiments at the D11 beamline at the ILL in Grenoble even at unusual working hours.

I would also like to thank the many people who have contributed to various parts of this research, in particular to Prof. Dr. Jaro Ricka and Rene Nyffenegger for the possibility to use their lab and Mr. Rossel, Mr. Machutta, Mr. Eggers and Mr. Warns for their assistance with electronic and mechanical problems.

Especially, I would like to thank Stacy for coming to Kiel, contributing all the helpful discussions and “beautiful data” regarding the structure and dynamics of complex fluids and turning research conferences into marvelous trips. You have always been an unique source of moral feedback and emotional support. Sharing the time with the best chef ever made this time tremendously exciting. You are wonderful!

Last, but certainly not least, I am very grateful to my parents for their permanent support and essential aid during my entire education. Without you this would not have been possible.

Curriculum vitae

Name	Markus Stieger
Address	Holtenauerstraße 248 24106 Kiel phone: ++49 431 880 2829 stieger@phc.uni-kiel.de
Birth date	31.01.1973 in Wiesbaden, Germany
Family status	single
Nationality	German

Early Education

1979 - 1983	Primary school Idstein, Germany
1983 - 1985	Middle school Limesschule Idstein
1985 -1992	High school Pestalozzi-Gymnasium Idstein University-entrance diploma

Alternative civilian service

07/1992 - 09/1993	Cared for elderly and infirm citizens with the Mobile Social Service in Idstein

Higher Education

10/1993 - 09/1995	Pre-diploma study in Chemistry, *University of Freiburg*, Germany
10/1995 - 04/1996	Erasmus scholarship, *University of Sussex*, Brighton, England Research project with Prof. Dr. Harry Kroto: „Generation of Nanotubes by Pyrolysis of Acetylene
05/1996 - 08/1999	Diploma study in Chemistry, *University of Freiburg*, Germany Major in Polymer Chemistry Diploma thesis with Prof. Dr. Walter Richtering: „The Rheology of Temperature-Sensitive Polymers”

Graduate Studies and Professional Experience

09/1997 - 11/1997	Teaching assistant in Inorganic Chemistry, *University of Freiburg*
10/1999 - 10/2000	Start of Doctoral studies, *Institute of Polymer Chemistry University of Freiburg* with Prof. Dr. Walter Richtering: „Thermoresponsive Polymers at Rest and Under Shear“ Selected to participate in the interdisciplinary graduate course „Structure Formation in Macromolecular Systems“

Curriculum vitae

10/1999 - 10/2000	Teaching assistant for introductory Polymer Chemistry
11/2000 - Present	Continuation of Doctoral studies, *Institute of Physical Chemistry University of Kiel*, Germany
	Taught experimental techniques and theoretical background for advanced training courses in colloidal Chemistry with GDCh
	Teaching assistant for introductory Physical Chemistry
	Organized and supervised new laboratory course in colloidal Chemistry

Table of Contents

1 Introduction

1.1 Complex fluids and colloidal microgels

It has been known for a century or more that some condensed-phase materials are neither simple liquids nor simple crystalline solids. These “complex fluids” possess mechanical properties that are intermediate between ordinary liquids and ordinary solids. Complex fluids often reveal solid-like behavior on short time scales and liquid-like behavior on long time scales; hence, they are viscoelastic. The characteristic time to change from solid-like behavior to liquid-like behavior can vary from fractions of a second to years depending on the fluid. Examples of complex fluids include polymer solutions, micellar solutions, colloidal dispersions and liquid crystalline polymers.[1]

One interesting subset of complex fluids which reveal viscoelasticity in concentrated suspension are colloidal microgels. A microgel is a chemically cross-linked particle that is swollen by a good solvent, usually prepared by emulsion copolymerization techniques in aqueous media. Microgel particles have properties in common with soluble linear chain polymers, swollen macrogels and insoluble latex particles (see figure 1). As solutions of linear chain polymer, microgel properties depend on the subtle balance of polymer/polymer vs. polymer/solvent interactions. As macroscopic gels, colloidal microgels are characterized by a degree of swelling, a cross-linking density and characteristic time constants for swelling and shrinking. As hydrophobic polymer colloids, colloidal microgels can be prepared to have a monodisperse size distribution.[2] No special stabilization is needed to prevent aggregation of microgel suspensions due to its lyophilic character. A cross-linker is incorporated in the microgel network giving rise to a complex and inhomogeneous internal polymer network structure.[3]

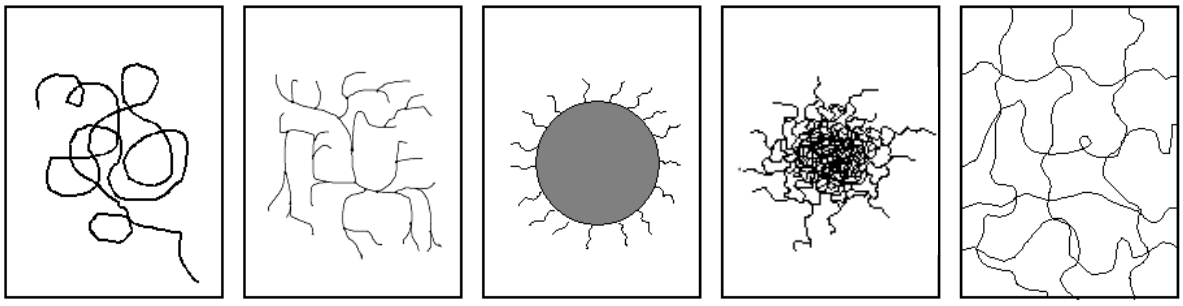

Figure 1: *Different molecular architectures for polymeric systems (from left to right): linear chain polymer, hyperbranched polymer, sterically stabilized colloid, microgel and macrogel*

Colloidal dispersions of aqueous microgels are an important part of water-borne polymer technologies since they are promising candidates for applications in various industries. Cosmetics, coatings and food industries employ aqueous microgels to modify rheological properties, to retain water and for many other reasons. Commodity microgels include those based on starch, cross-linked poly(sodium methacrylate) and a variety of gums. Microgels can also be used as model systems in soft condensed matter to investigate the structure and dynamics of concentrated colloidal suspensions. Since the interaction forces can be controlled by the properties of the particle, microgels are ideal systems to study the relation between the interaction potential and the fluid behavior.

1.2 Thermoresponsive poly(*N*-isopropylacrylamide) polymers

Over the past few years complex fluids composed of polymer solutions and colloidal dispersions gained great interest since they exhibit a unique set of characteristics. For many colloidal dispersions the physical state, e.g. the stability or phase behavior, can be altered dramatically by modest changes in composition. This behavior stems from the different forces that act among the particles, determining their spatial distribution. Colloidal dispersions can be flocculated by the addition of salt, since the increasing concentration of ions screens the surface charge, suppresses repulsion and allows fluctuation. Another type of transformation can occur when ions are removed from electrostatic stabilized systems. The absence of screening allows long-range repulsion to induce a disorder-order phase transition. The formation of colloid-crystals is observed. The crystals can be melted by subsequently applied shear flow.

An even more complex colloidal behavior can be achieved with thermoresponsive polymers whose properties can be controlled by temperature. A characteristic feature of many aqueous polymer solutions is that phase separation can occur upon heating. The temperature minimum of the miscibility gap is known as the lower critical solution temperature (LCST). Polymer solutions in organic solvents usually display an upper critical solution temperature (UCST) and demix upon cooling. Prominent examples for water-soluble polymers displaying inverse solubility upon heating (LCST) are poly(*N*-isopropylacrylamide) (PNiPAM),[4] methylhydroxypropyl cellulose (MHPC)[5] and poly(vinylcaprolactam) (PVCa)[6].

Temperature sensitive PNiPAM polymers gained interest particulary due to their potential use in many technological applications, including controlled drug delivery systems and biotechnology.[4,7,8] Figure 2 shows a flowchart for a PNiPAM microgel controlled drug release process. Essentially, if a collapsed microgel is placed into a an aqueous drug solution at T<LCST, the PNiPAM microgel particle will swell and small drug molecules will freely penetrate the pores of the polymer network. Subsequently, the drug-loaded microgel particle

can be easily removed by filtration or centrifugation leaving a more concentrated drug solution behind. The PNiPAM particle will squeeze out the encapsulated drug after the solution is heated up to T>LCST. The LCST of PNiPAM based microgels can be adjusted to near human body temperature by copolymerization or using additives.

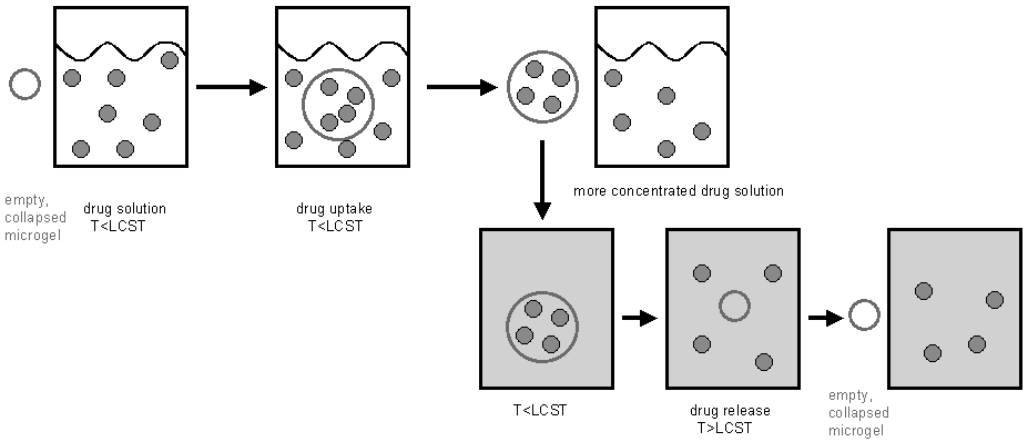

Figure 2: *Flowchart for a PNiPAM microgel based controlled drug release process*

PNiPAM is known to undergo a temperature induced phase transition in water at the LCST of 31-34 °C (see figure 3). The solvent quality changes from good to poor when the temperature is increased. The transition from hydrophilic to hydrophobic behavior eventually leads to phase separation in concentrated solution.

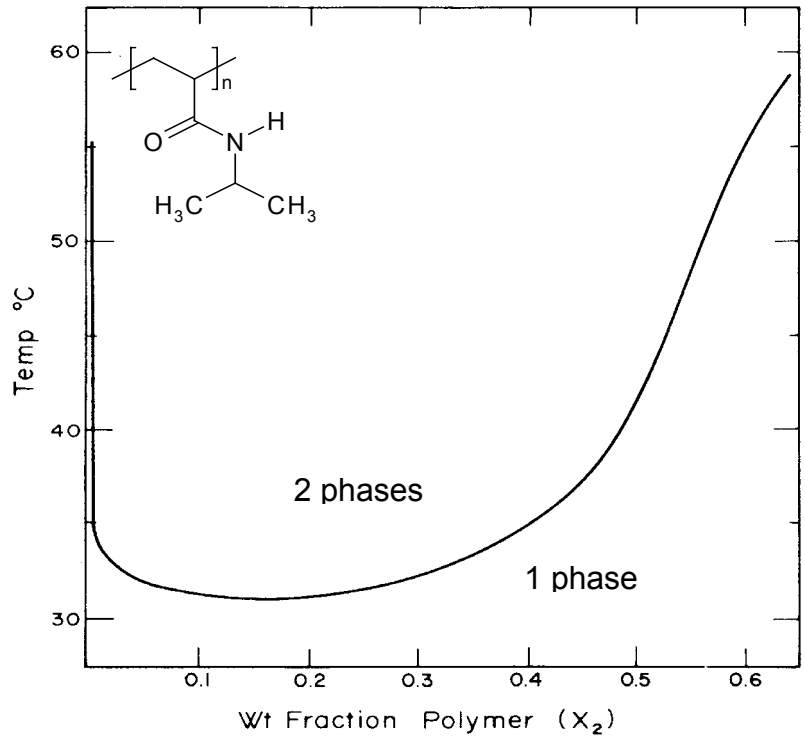

Figure 3: *Phase diagram and structural formula of linear chain poly(N-isopropylacrylamide) PNiPAM*

The phase transition was studied in great detail for polymers with different molecular architectures including solutions of linear chain PNiPAM, chemically cross-linked microgels and macroscopic gels employing various methods like static and dynamic light scattering, differential scanning calorimetry, viscometry and rheology.[4,8,9] For single linear PNiPAM, the flexible polymer chain contracts with increasing temperature and a coil-to-globule transition is observed. Water-swellable PNiPAM microgels are known to undergo a continuous temperature-induced volume phase transition when the LCST is approached. At temperatures below the LCST the spheres are highly swollen. Above the LCST water becomes a non-solvent leading to the collapse of the particles. Therefore the particle size decreases with increasing temperature which is shown in figure 4. Hence, a major advantage of thermoresponsive particles compared to suspensions of rigid hard spheres is that the effective volume fraction ϕ_{eff} can easily be controlled by simple temperature changes while the concentration c and thus the particle number density n are kept constant. Since the degree of swelling changes with temperature the rigidity of the particles depends on temperature as well.

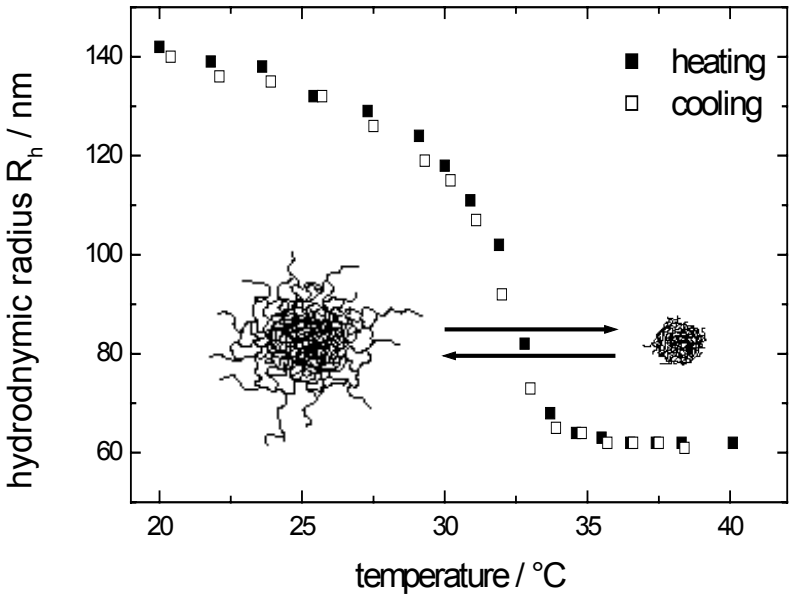

Figure 4: *Temperature-induced volume phase transition for PNiPAM microgels determined by dynamic light scattering in dilute solution*

It has been shown that the volume phase transition of poly(*N*-isopropylacrylamide) microgels can be induced not only by temperature but by pressure and solvent composition. In addition, the transition temperature can be altered by addition of salt[10] or surfactants[11], by variations in the solvent quality[12] or by copolymerization with charged monomers.[13]

1.3 Equilibrium colloidal phase behavior

Colloidal suspensions of hard spheres are often used as the simplest model systems to investigate the diffusion, equilibrium phase behavior and rheology of concentrated suspensions.[14,15,16,17,18] Model hard sphere suspensions consist of rigid particles dispersed in a Newtonian fluid that interact with a purely repulsive inter-particle interaction potential that becomes noticeable only when the particles are in contact. At larger distances the particles do not interact. Well established systems that display hard sphere like behavior consist of sterically stabilized colloids dispersed in an isorefractive non-solvent like poly-methylmethacrylate (PMMA) particles grafted with poly-12-hydroxystearic acid in cis-decalin or silica spheres grafted with octadecyl chains in cyclohexane.

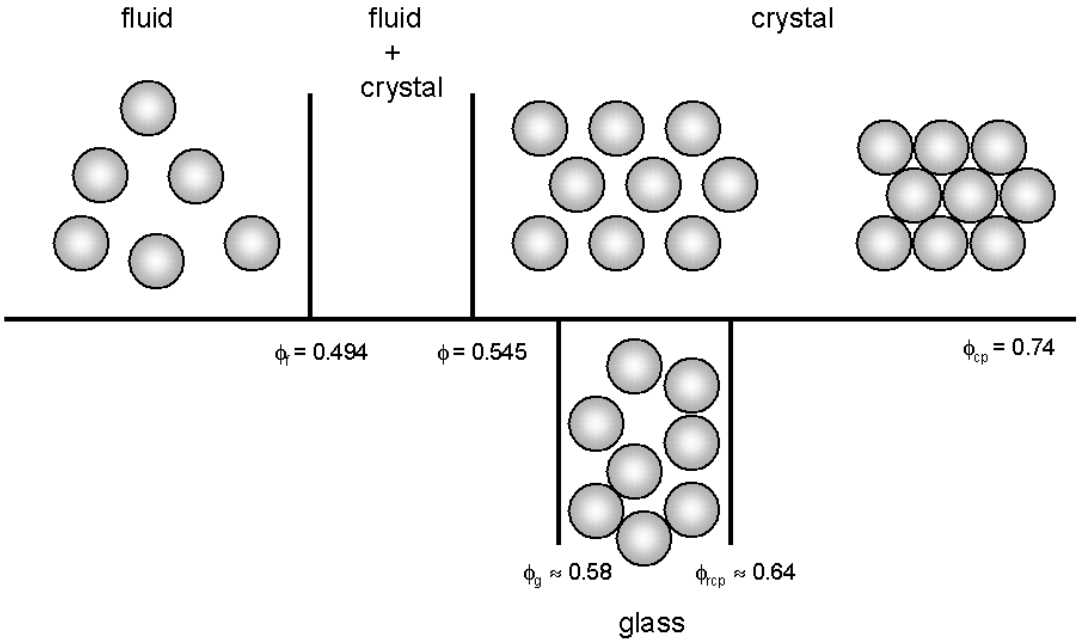

Figure 5: *The hard sphere phase diagram: With increasing volume fraction the transition from a disordered fluid to a highly ordered colloidal crystal and disordered glass is observed.*

The equilibrium phase diagram for hard spheres (see figure 5) has been determined by computer simulations and experiments on stable dispersions of monodisperse colloidal particles. At volume fractions below ϕ<0.49, the spheres are disordered in the liquid phase. At ϕ=0.49 the spheres begin to order into a macrocrystalline structure with close packing that can be considered a mixture of face-centered cubic and hexagonally close packed packings. Between ϕ=0.49 and ϕ=0.545 there is coexistence of the disordered phase with a colloidal crystalline phase. The colloidal crystalline phase is the equilibrium one up to the maximum close packing limit of ϕ=0.74. Nonequilibrium colloidal glassy behavior can also occur between ϕ=0.58 and the limit of random close packing at ϕ=0.64. Amazingly, the hard sphere

crystallization transition is driven by entropy. At high packing densities, the ordering of the spheres onto a regular lattice gives each sphere more space for positional fluctuations than would be the case for random packing at the same density, thus more than compensating for the entropic cost of ordering. In addition to the equilibrium phases (liquid and crystalline), there is a metastable glassy disordered state. This phase exists because at such high densities the long-range Brownian motions of the spheres are suppressed by the crowding or caging effect of neighboring spheres, which prevent rearrangement to a stable crystal.

As mentioned above, in contrast to conventional hard sphere dispersions microgels are swollen by a good solvent. The question has been raised whether microgels can be described with well-known hard sphere models or whether the swelling of the particles lead to softness and deformability. The rigidity of a sphere is expected to depend on the cross-linking density. A different particle-particle interaction potential results in significant differences in colloidal behavior. It was shown that concentrated microgel dispersions exhibit different phase behavior compared to hard spheres.[19]The phase behavior of concentrated PNiPAM microgel suspensions was studied by Senff et al.[20] A phase transition from the liquid to the crystalline and finally to the glassy state is observed with increasing volume fraction as shown in figure 6, but phase transitions in the PNiPAM microgels occur at very different volume fractions compared to model hard sphere suspensions. Crystallization starts at effective volume fraction of ϕ_{eff}=0.59 as compared to the freezing transition of ϕ_f=0.494 for hard spheres and the fluid-crystalline coexistence region is very narrow. The shift of the volume fraction when crystallization occurs towards higher volume fractions indicates the softness of the microgel particle. Thus, the experimental phase diagram reveals a soft sphere interaction potential at higher effective volume fractions ϕ_{eff}.

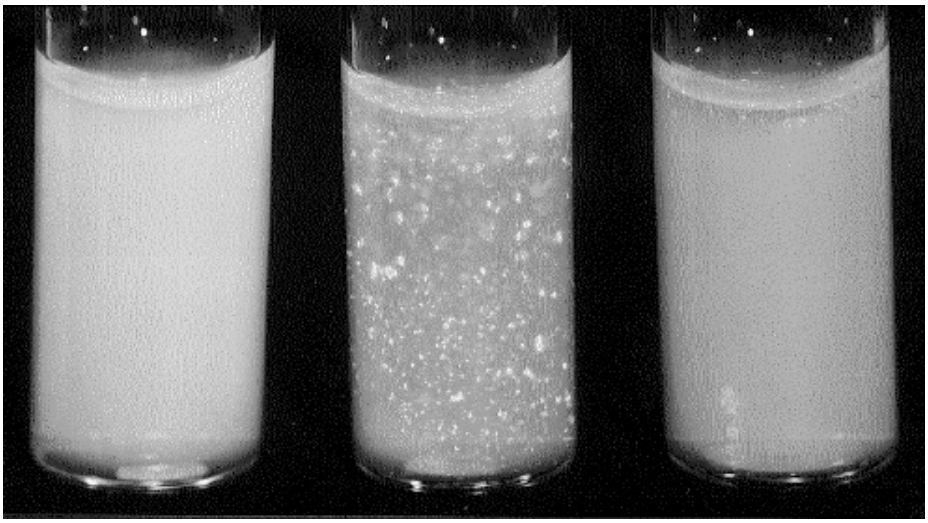

Figure 6: *Phase behavior of colloidal PNiPAM microgels: At ϕ_{eff}<0.59 the microgel particles are disordered in the fluid phase (left), crystallization starts at ϕ_{eff}=0.59 (middle) indicated by Bragg reflections of visible light and at high volume fractions the glassy state is reached (right).*

Hellweg et al. determined the structure of colloidal PNiPAM crystals using small angle neutron scattering (SANS).[21] A face-centred-cubic lattice was observed. Lyon and coworkers [22,23,24] report on the assembly of colloidal PNiPAM crystals with tunable optical properties. They observed by laser scanning confocal microscopy a compression of the soft microgel particles when they are closely packed in the crystal. Obviously, swollen microgel particles are not rigid and show soft-sphere behavior at higher concentrations.

1.4 Shear-induced structures in colloidal suspensions

Since colloidal dispersions play an important role in many different industrial applications, the rheological behavior and flow properties have been studied intensively.[25] Colloidal dispersions under shear reveal a large variety of distinct changes of the particle arrangement with shear rate (see figure 7). The shear-induced structures depend strongly on the particle-particle interaction potential. Various methods including light and small-angle neutron were employed to study the flow-induced structures in colloidal systems with different interaction potentials. The formation of different structures during flow have been predicted by non-equilibrium molecular dynamics simulations without hydrodynamic interaction[26] and by Stokesian dynamics simulations including hydrodynamic interactions.[27] For both purely repulsive hard spheres[28,29,30] as well as electrostatic stabilized particles,[31,32,33] shear thinning is often observed in concentrated dispersions. After application of shear flow a structural transition occurs from fluid-like particle ordering to two-dimensional hexagonal close-packed (2D hcp) layers which are arranged to minimize the resistance against flow. The shear thickening in hard sphere and electrostatic stabilized suspensions which occurs when high shear rates are applied can be attributed to the formation of jamming clusters bound together by hydrodynamic lubrication forces, often referred to as hydroclusters (see figure 7).[34]

The influence of shear flow on the structure of gel-forming sticky hard spheres was studied by Verduin et al.[35] At low shear rates the formation of larger structures aligned mainly along the flow direction was observed. At higher shear rates of the cloud point was shifted. Occasionally, shear flow in colloidal systems can also lead to aggregation or the formation of large-scale bundle ordering.[36] Shear-induced distortions of the microstructure in directions perpendicular to the flow were observed in near-critical suspensions of colloid-polymer mixtures under stationary shear flow.[37] Especially in the vicinity of the gas-liquid critical point the influence of shear flow on the concentration fluctuations was found to be substantial.[38]

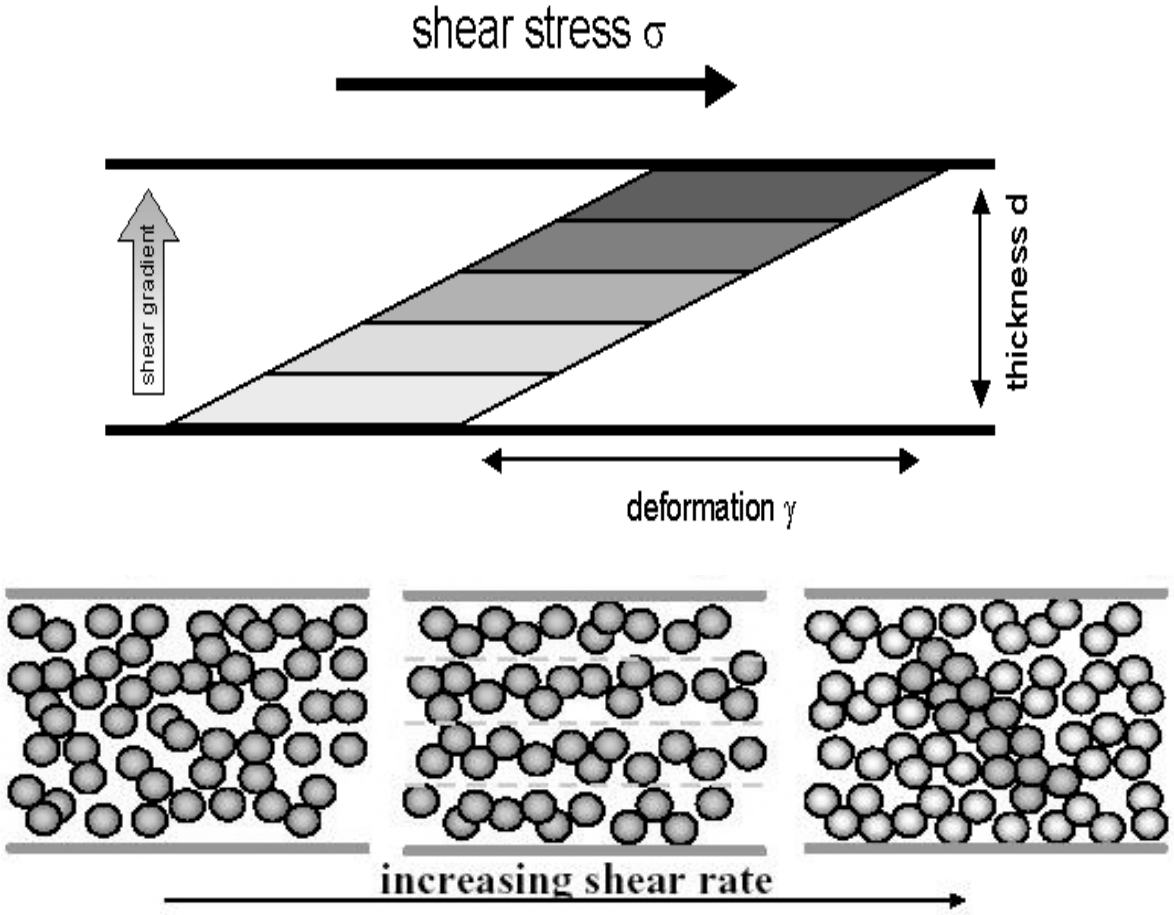

Figure 7: *Top: Shear flow is applied between parallel plates causing deformation of the sample. The shear gradient is perpendicular to the flow direction. Bottom left: A colloidal suspension in the liquid state at rest exhibits an unordered structure. Bottom middle: Shear flow induces the formation of a layered structure with layers that align along the flow direction giving rise to a decrease of the viscosity. Bottom right: At high shear rates the formation of rather large hydroclusters leads to shear thickening.*

To our knowledge very little is known about the influence of shear flow on the structure of suspensions of thermoresponsive microgels. Unlike suspensions of rigid spheres, the effective volume fraction ϕ_{eff} of microgel suspensions changes with temperature. The liquid-solid transition is shifted to higher concentrations with increasing temperature, due to particle collapse at temperatures above the LCST. Particle collapse occurs due to the changing interaction potential from repulsive to attractive which is in turn a result of decreasing solvent quality.

1.5 Structure formation under shear flow in polymer solutions

It is well known that shear flow can influence the phase separation of polymer solutions.[39] There are several reports on the behavior of poly(styrene) (PS) dissolved in dioctylphthalate (DOP) using different techniques to probe the demixing process including turbidity, dichroism, small angle light scattering (SALS) and small angle neutron scattering (SANS). Recent papers by Hashimoto and Boué et al. provide a thorough review of this system.[40,41,42] Often a so-called butterfly pattern in SALS and SANS is observed under shear flow indicating shear induced concentration fluctuations. The butterfly pattern is usually observed with semi-dilute solutions above the overlap concentration, indicating that entanglements are necessary for the enhancement of concentration fluctuations along the flow direction. Butterfly scattering patterns have also been observed with polymer networks and some colloidal systems.[43,44,45,46,47] It has been pointed out that viscoelastic properties, the first normal stress difference in particular, play an important role for the coupling between density fluctuations and shear stress[48]. The presence of an entanglement network appears to be unnecessary for the shear induced fluctuations, since experiments in dilute polymer solutions reveal that shear induced aggregation can occur.[49]

Much less is known about aqueous solutions where phase separation occurs upon heating. Recently Wolf and coworkers investigated aqueous solutions of hydrophobically modified ethyl hydroxyethyl cellulose, which also show LCST behavior.[50] Turbidity measurements revealed a strong influence of shear flow on the phase separation. With increasing shear rate the cloud temperature was shifted to higher values. It was concluded that the shear induced mixing is due to a destruction of intersegmental clusters, which are formed via the hydrophobic side chains. MHPC solutions demonstrate a very complex behavior, revealing shear induced mixing at low concentrations but demixing at higher concentrations.[51] Badiger et al.[52] observed shear induced demixing in aqueous solutions of high molecular weight PNiPAM solutions. Compared to the quiescent state the linear chain polymer solutions entered the two-phase region at lower temperatures when shear flow was applied. The authors attribute the shift of the cloud point temperature to the destruction of intersegmental clusters formed in the stagnant state. A stress overshoot is observed for concentrated solutions before the onset of steady shear flow, indicating the existence of clusters.

Most investigations employed solutions of linear chain macromolecules above the overlap concentration. Thus, the microstructure is characterized as a highly entangled polymer solution. Shear induced phase separation can be interpreted in different ways. Wolf suggested a general thermodynamic approach.[53] In addition to the usual Flory-Huggins-Gibbs energy of polymer solutions a second term is introduced, the stored elastic energy. In

the case of dilute polymer solutions the stored elasticity accounts for coil stretching. Other approaches describe the dynamic coupling between concentration fluctuations and stress.[54,55,56] Semi-dilute polymer solutions can be characterized by a typical correlation length and longest relaxation time of the entangled chains. In the strong shear regime of high shear rates, the stress can be released by squeezing solvent from the more entangled regions thus enhancing concentration fluctuations.

2 Motivation

The aim of this work was to gain an understanding of the influence of the polymer architecture on the structure formation of thermoresponsive polymers in the quiescent state and under shear flow. In the first section of this work, the internal structure of a PNiPAM microgel particle should be studied via small-angle neutron scattering (SANS) in dilute suspension. In addition, a modeling expression to describe the form of the particle should be introduced. The second section sought to encompass both the structure of a single microgel particle, and the larger, many-particle microstructure that is present in concentrated suspensions. A study of the influence of shear on both the internal particle structure and the particle-particle correlations should complete the characterization of the microgel suspensions. Finally, the corresponding studies should be carried out with solutions of linear chain PNiPAM to reveal the influence of the polymer architecture on the structure formation.

I) In order to gain a thorough understanding of the full range of PNiPAM microgel behaviors, first the structure of an individual particle in dilute solution should be characterized. A swollen microgel particle might exhibit a very different structure than a homogenous sphere due to inhomogeneous incorporation of a cross-linker. Scattering methods including small-angle neutron scattering (SANS), static and dynamic light scattering (SLS and DLS) are well suited to investigate the structure of PNiPAM microgels. From scattering in dilute solution a form factor can be obtained which describes the structure of microgel particles accounting for both the inhomogeneous internal network structure and the overall particle form. However, to our knowledge no such form factor has been published. Thus, a new model for the form factor which describes the structure of thermosensitive PNiPAM microgels with different cross-linking densities and particle sizes, in both the swollen and the collapsed state, and over a very broad q-range should be derived. Using this direct modeling approach, the structural changes induced by temperature, cross-link density and size should be revealed by the radial density profiles.

II) Once an expression has been derived to describe the structure of a single particle in dilute suspension, we should be able to answer the question of whether concentrated thermoresponsive PNiPAM microgels can be used as model systems for concentrated colloidal suspensions. Therefore, the structure formation of concentrated suspensions of PNiPAM microgels should be studied employing rheology and SANS. The following questions should be addressed:

a) How does the size of individual microgel particles change with concentration and temperature?
b) How can the interaction be described for highly concentrated microgel suspensions?
c) Do highly swollen microgel particles reveal hard sphere behavior?

For this purpose the above mentioned model expression for the particle form factor should be extended by a model structure factor that enables to fit the experimental data also at high concentrations. A new approach for calculating the average radial density profiles around a particle from the amplitude of the form factor and the structure factor should be derived. By this approach a direct description of the ordering in the neighborhood of a particle, which reveals the degree of particle-particle correlations, should be obtained. Again, concentrated microgel suspensions with different cross-linking densities and particle sizes should be compared at various temperatures. A broad concentration range should be investigated covering samples in the dilute and concentrated liquid phase as well as crystalline and glassy samples.

III) The differing colloidal properties of swollen PNiPAM microgels as compared to rigid spheres may give rise to different particle arrangements under shear flow. Since rigid colloidal behavior under shear has been well characterized, this comparison can be made only after study of microgels under shear. For large microgels, the main contribution to the overall scattering intensity arises from contributions of the particle form factor. Hence, detailed information about the influence of shear flow on the internal structure of an individual particle in concentrated suspension should be obtained from scattering experiments. In the case of small PNiPAM microgels, the scattering intensity distribution is dominated by contributions of the structure factor. Thus, studying small particles should lead to information about changes in the overall microstructure and shear-induced ordering. Therefore PNPAM microgels with different particle sizes should be studied at temperatures well below and close to the LCST to reveal the influence of the particle-particle interaction potential on the shear-induced structure formation. In addition, the rheological behavior and its connection to the observed microstructural phenomena should be investigated.

IV) The microstructures of colloidal and polymer solutions are very different and near the miscibility gap different properties can be anticipated. However, very little is known about the influence of the macromolecular architecture on the phase separation behavior under shear. Thus, the flow behavior and the viscoelastic properties of linear chain PNiPAM solutions as well as of concentrated PNiPAM microgel suspensions should be investigated for various temperatures. The influence of shear flow on the phase separation should be studied for both polymer architectures.

V) Whereas optical techniques as e.g. turbidity probe concentration fluctuations near the miscibility gap on a rather large length scale, small-angle neutron scattering (SANS) is an important technique to investigate spatial heterogeneities on a length scale of few nanometers. The influence of shear flow on the phase separation of concentrated aqueous solution of linear chain PNiPAM should also be investigated by means of small-angle neutron scattering. The scattering intensity distributions should be described with an established Ornstein-Zernike model in order to determine the influence of concentration, temperature and shear flow on the structure formation.

3 Structural changes in temperature sensitive microgel colloids

ABSTRACT: The structure of temperature sensitive poly(*N*-isopropylacrylamide) (PNiPAM) microgels in dilute suspension was investigated by means of small-angle neutron scattering (SANS). A direct modeling expression for the scattering intensity distribution was derived which describes very well the experimental data at all temperatures over an extensive *q*-range. The overall particle form as well as the internal structure of the microgel network are described by the model. The influence of temperature, cross-linking density and particle size on the structure were revealed by the radial density profiles and clearly showed that the segment density in the swollen state is not homogeneous but gradually decays at the surface. The density profile reveals a box profile only when the particles are collapsed at elevated temperatures. An increase of the cross-linking density resulted in both an increase of the polymer volume fraction in the inner region of the particle and a reduction of the smearing of the surface. The polymer volume fraction inside the colloid decreased with increasing particle size. The structural changes are in good agreement with the kinetics of the emulsion copolymerization used to prepare the microgel colloids.

3.1 Introduction

Over the past few years colloidal dispersions gained great interest as promising candidates for applications in the printing and pharmaceutical industries. Colloidal dispersions of microgel particles are discussed to have potential applications as controlled drug delivery systems. Microgels can also be used as model systems in soft condensed matter to investigate the structure and dynamics of concentrated colloidal suspensions.[19] Since the interaction forces can be controlled by the properties of the particle, microgels are ideal systems to study the relation between the interaction potential and the fluid behavior. A microgel particle is a chemically cross-linked latex sphere that is swollen by a good solvent, usually prepared by emulsion copolymerization techniques in aqueous media. A cross-linker is often incorporated in the microgel network giving rise to a complex and inhomogeneous internal structure.[3]

The most widely studied water-swellable microgel system is poly-*N*-isopropylacrylamide (PNiPAM). This temperature sensitive polymer displays inverse solubility upon heating. For PNiPAM microgels the transition from hydrophilic to hydrophobic behavior occurs when the

lower critical solution temperature (LCST) is passed. At the volume phase transition the size of the microgel particles decreases with increasing temperature. Above the LCST of ca. 34°C phase separation is observed for concentrated samples. The macroscopic volume phase transition has been thoroughly studied employing various methods including static and dynamic light scattering, differential scanning calorimetry, viscometry and rheology.[4,9]

Wu et al. were the first to study the kinetics of PNiPAM microgel particle formation during the emulsion copolymerization.[57] They observed that the cross-linker monomer *N,N´*-methylenbisacrylamide (BIS) was consumed faster than the monomer *N*-isopropylacrylamide (NiPAM) during the emulsion copolymerization. The average BIS content of the particles decreased with increasing conversion. They conclude that the different polymerization rates of NiPAM and BIS give rise to an inhomogeneous spatial distribution of the cross-linking density throughout the particle.

The structural inhomogeneities inside microgel particles consisting of poly-*N*-isopropylmethacrylamide (PNiPMAM) were studied by Guillermo et al. with nuclear magnetic resonance (NMR).[58] They distinguished different structural regions by their different proton mobilities detected through magnetic relaxation rates. A core-shell morphology of the PNiPMAM latex spheres was suggested.

Obviously, a swollen microgel particle exhibits a very different structure than a homogenous sphere. Scattering methods including small-angle neutron scattering (SANS), small-angle x-ray scattering (SAXS) and dynamic light scattering (DLS) are well suited to investigate thoroughly the structure of PNiPAM microgels. From scattering a form factor can be obtained which describes the structure of microgel particles accounting for both the inhomogeneous internal network structure and the overall particle form. However, to our knowledge no such form factor has been published. We present a new model for the form factor which describes the structure of thermosensitive PNiPAM microgels with different cross-linking densities and particle sizes, in both the swollen and the collapsed state, and over a very broad *q*-range.

Shibayama and coworkers[59,60,61] showed for PNiPAM macrogels that static inhomogeneities introduced into the network by chemical cross-links $I_{in}(q)$ as well as a fluctuation term originating from the chain statistics and the interchain interactions $I_{fluct}(q)$ contribute to the scattering intensity

$$I(q) = I_{in}(q) + I_{fluct}(q) \qquad (1)$$

where $q = (4\pi/\lambda) \sin(\theta/2)$ denotes the magnitude of the momentum transfer with wavelength λ and scattering angle θ. The static inhomogeneities of the network can be described assuming a Gaussian spatial distribution of the cross-links, while the fluctuations of the network arising from the chain statistics and the interchain interactions are described by a Lorentzian function.

Mears et al. investigated the local structure of PNiPAM microgels under a wide variety of different conditions.[62,63,64] To fit their SANS data they incorporated the form factor of the particle *P(q)* into their model expression and assumed that for particles with $R_g >> q^{-1}$ only the Porod region of *P(q)*, where scattering from a sharp interface is observed, contributes significantly to the scattering profile. The total scattering intensity of their model expression is given by a combination of a Porod function, reflecting scattering from the whole particle, and a Lorentzian function accounting for scattering from the fluctuations of the network. The latter is described by

$$I_{fluct}(q) = \frac{I_{fluct}(0)}{1+\xi^2 q^2} \tag{2}$$

where $I_{fluct}(0)$ denotes the intensity at q = 0 and ξ accounts for the correlation length of the fluctuations, which can be considered to be related to the blob or mesh size. Thus, equation (2) describes the ensemble average correlations in the network. In this way Mears et al. obtained for the scattering intensity distribution of microgels

$$I(q) = \frac{6\pi\phi_P \Delta\rho^2}{q^4 R}\left(1+\frac{1}{q^2 R^2}\right) + \frac{I_{fluct}(0)}{1+\xi^2 q^2} \tag{3}$$

where ϕ_P describes the volume fraction of the particles, $\Delta\rho$ is the difference in scattering length density between the particle and the solvent and R denotes the radius of the particle. This phenomenological approach neglects the contribution of the static inhomogeneities to the scattering intensity. The model describes well the intensity distribution in the q-range that was investigated in their studies ("high" q-regime with q = 0.01-0.1 Å^{-1}). However, this model would fail to describe scattering data obtained in the "low" q-regime (e.g. q = 0.001-0.01 Å^{-1}) where the form factor *P(q)* can not be approximated with a Porod expression.

Using fitting functions similar to equation (3), Kratz et al.[65,66] found that ξ decreased with increasing cross-linking density and can be compared with the corresponding lengths of PNiPAM macrogels. Above the LCST the scattering is dominated by interfacial Porod scattering ($I(q) \propto q^{-4}$). Slight deviations from ideal Porod behavior is interpreted in terms of surface roughness of the collapsed particles.

Fernandez-Barbero and co-workers proposed a core-shell structure for PNiPAM microgels characterized by different correlation lengths, ξ_{core} and ξ_{shell}, which were obtained by fitting different limited q-regimes of their SANS data with equation (2).[67]

Ballauff et al. studied the structure of colloidal core-shell particles composed of a compact, homogenous polystyrene core (PS) and a temperature sensitive PNiPAM shell.[68,69,70,71,72] They describe the scattering intensity of the core-shell colloids by including three contributions

$$I(q) = I_{CS}(q) + I_{network}(q) + I_{PS}(q) \tag{4}$$

where $I_{CS}(q)$ denotes the scattering from a particle composed of a homogeneous core and shell, $I_{network}(q)$ accounts for the static inhomogeneities and fluctuations of the polymeric shell network and $I_{PS}(q)$ describes the scattering caused by the density fluctuations of the solid PS core. The influence of the structure factor is limited to the "low" q-regime for small particle concentrations and is neglected ($S(q) = 1$). $I_{CS}(q)$ is given by $B^2(q)$ with the scattering amplitude $B(q)$ being defined as

$$B(q) = 4\pi \int_0^\infty [\rho(R) - \rho_s] \frac{\sin(qR)}{qR} R^2 \, dR \qquad (5)$$

with $\rho(R)$ denoting the radial scattering length density and ρ_s describing the scattering length density of the solvent. Equation (4) was extended to include particle size polydispersity. For $I_{network}(q)$ equation (2) is assumed and therefore the Gaussian term of equation (1) is neglected. The contribution of $I_{in}(q)$ is rather small unless the network was formed in a highly dilute state and furthermore appears in a q-range where the intensity is dominated by $I_{CS}(q)$. The scattering of the PS core $I_{PS}(q)$ was obtained from SAXS experiments with the core latex. $I_{PS}(q)$ was found to be small and subtracted from $I(q)$ of the core-shell particles. For the SANS data Ballauff and coworkers added a constant background to account for contributions from residual incoherent scattering. In their previous SAXS studies[68 69 70] a compact structure of the shell was assumed with a box profile for the radial density distribution. However, they pointed out that the SAXS scattering profiles do not provide clear evidence for the validity of the assumption since the data was from only one contrast and the q-range available was limited. Hence, the exact shape of the radial density profile of the core-shell particle could not be obtained. In more recent investigations Ballauff and coworkers[71] showed by SANS and SAXS using contrast variation that at temperatures above the phase transition a box profile can describe the collapsed core-shell particles quantitatively. In the shrunken state the PNiPAM network exhibits a rather compact structure. At temperatures below the phase transition the swollen core-shell particles can be best described with a polymer density profile that decreases slightly with increasing radial distance to the core surface assuming an affine deformation of the swollen shell network. The affine deformation of the shell does not lead to a strong radial variation of the polymer volume fraction in the shell.[72] A comparison of the SAXS and SANS data with DLS experiments revealed that a few polymer chains stick out of the particle contributing to the hydrodynamic size of the particles.

In the present paper we present a comprehensive investigation by SANS of the structure of temperature sensitive PNiPAM microgels. A new direct modeling expression for the scattering intensity distribution is presented which describes very well the experimental data at all temperatures and over a very broad q-range. The model expression includes both the overall particle form and the internal structure of the microgel network. Using this model, the

structure of microgels with different cross-linking densities and different particle sizes can be compared. The radial density profiles are calculated and they reveal the structural changes induced by temperature, cross-link density and size. In this paper we focus on the results obtained from dilute suspensions. The influence of particle-particle interactions at higher concentrations will be discussed elsewhere.

3.2 Experimental part

3.2.1 Preparation of the PNiPAM microgels

The PNiPAM microgel particles were prepared as described previously.[20,73] In order to adjust the particle radii and the degree of cross-linking, different quantities of the reagents were used and are summarized in table 1. SDS denotes the surfactant sodium dodecylsulfate and KPS the initiator potassium peroxodisulfate. The emulsion copolymerization was carried out in 1500 ml of pure water at 70°C in an inert gas atmosphere. The SDS concentration was always well below the critical micelle concentration. The degree of cross-linking is given as the molar ratio of BIS to NiPAM in mol%. The hydrodynamic radii at 25°C in heavy water R_h(25°C) as obtained from dynamic light scattering (DLS) experiments are indicated in nm as well. For the sake of clarity the degree of cross-linking and R_h(25°C) are summarized in the sample name omitting the units.

Tab. 1. *Reagent quantities used for the synthesis of the PNiPAM microgels. All syntheses were carried out in 1500 ml of pure water at 70°C in an inert gas atmosphere. The sample name represents the resulting cross-linking density given as the molar ratio of BIS to NiPAM in mol% and the hydrodynamic radius at 25°C in D_2O R_h(25°C) in nm. The units are omitted in the sample name for simplification.*

sample M-cross-linker/R_h(25°C)	*NiPAM*	*BIS*	*SDS*	*KPS*
/mol% /nm	/g	/g	/g	/g
M-5.5/115	27.167	2.027	0.567	1.138
M-1.4/141	27.555	0.533	0.525	1.012
M-1.5/353	23.188	0.483	0.014	0.962

3.2.2 Experimental details

Dynamic light scattering experiments were performed with an ALV goniometer and an ALV 5000 correlator at a wavelength of λ = 647 nm. The samples were highly diluted with D_2O ($c \leq 0.001$ wt%). The temperature was controlled to 0.05 K with an external heat bath (Lauda) and a calibrated Pt-100 temperature sensor. The samples were allowed to equilibrate for 20 min at each temperature. The scattered light was detected at an angle of θ = 90° with an integration time of 120 s. The hydrodynamic radii were calculated from the cumulant fits of the time correlation functions.

Solution densities were determined using a densitymeter DMA 5000 (Anton Paar, Graz), which uses the oscillating-tube technique. The density determination is based on measuring the period of oscillation of a vibrating U-shaped tube that is filled with the sample and using the relationship existing between the period of oscillation and the density. This relation holds as long as the sample is not too viscous, otherwise the density has to be corrected to take into account the modified elastic modulus of the U tube.[74] The densitymeter was calibrated daily at 20°C using air and water as reference samples. The sample volume needed was approximately 1.5 mL and concentrations of 1.0 - 1.5 wt% were employed. Each measurement was repeated at least twice in the same day with fresh sample. The temperature was increased from 20 to 40°C by steps of 1°C with an accuracy of 0.002°C. The measurements were run in the slow equilibrium time (about 15 minutes equilibration), in order to ensure the highest possible quality of data.

Small angle neutron scattering experiments (SANS) were performed at the instrument D11 of the Institute Laue-Langevin (ILL) in Grenoble, France. The neutron wavelength was λ = 6 Å or λ = 12 Å with a spread of $\Delta\lambda / \lambda$ = 9 %. The data were collected on a two-dimensional multidetector (64 x 64 elements of 1 x 1 cm^2) and corrected for background and empty cell scattering. Sample-detector distances of 36.7, 10.5 and 2.5 m were employed. The incoherent scattering of H_2O was used for absolute calibration according to standard procedures and software available at the ILL ($GRAS_{ans}P$ V. 3.25). H_2O calibration measurements were performed at sample-detector distances of 10.5 and 2.5m. The H_2O scattering obtained at 10.5m was used to calibrate the sample data measured at 36.7m since calibration by H_2O cannot realistically be performed with high accuracy for long sample-detector distances. Changes in the sample-detector distance and the collimation length modify the incident neutron flux at the sample position. Corrections for changes in the incident flux were made using the standard ILL database. Further processing was done by radially averaging to obtain a one-dimensional data set. All experiments were carried out at full contrast using D_2O as the solvent. The concentrations of all samples were in the range of 0.06 - 0.20 wt%.

3.3 Theory and Data analysis

SANS experiments yield information about an intensity distribution *I(q)* in reciprocal space as a function of momentum transfer *q*. In order to obtain the corresponding real space structure considerable effort must be invested in the SANS-data analysis.[75] In this contribution we present a direct modeling approach which involves least-square fitting. A convenient way to express *I(q)* is to introduce the differential scattering cross section $d\sigma(q)/d\Omega$ since it is independent of the transmission and the form of the sample. For a suspension of monodisperse particles with spherical symmetry the differential scattering cross section is given by

$$\frac{d\sigma(q)}{d\Omega} = n\Delta\rho^{2} V_{poly}^{2} P(q) S(q) \qquad (6)$$

where *n* denotes the number density of the particles, $\Delta\rho$ describes the difference in scattering length density between the polymer and the solvent and V_{poly} accounts for the volume of polymer in a particle. The (normalized) form factor *P(q)* describes the structure of a single particle and the structure factor *S(q)* accounts for the interference of scattering from different particles. The difference in scattering length density $\Delta\rho = \rho_{polymer} - \rho_{solvent}$ which corresponds to the scattering contrast was calculated for every microgel suspension accounting for the particle composition (fraction of cross-linking molecules) and the apparent specific density at a given temperature. The apparent specific density ascribes all density changes in the solution to the solute (polymer network), although changes in the solvent density in the neighborhood of the solute contribute to the measured solution density. The scattering length density of the particle or the solvent is given by

$$\rho = \frac{\rho_d}{M_w} N_A \sum_{i=1}^{m} b_i \qquad (7)$$

with the apparent specific density ρ_d, the molecular weight M_w, Avogardo´s Number N_A and the bound coherent scattering length of a nucleus b_i. The particles are swollen and contain solvent. The volume of a particle is $V(R) = 4/3\ \pi R^3$ and therefore the volume fraction of polymer in the particle is $\phi_{poly} = V_{poly}/V$. The number density of particles can be calculated as $n = c/(V_{poly}\ \rho_{poly})$, where *c* is the mass concentration of polymer in the sample and $V_{poly}\ \rho_{poly}$ is the mass of polymer in one particle. For *c* given as a weight fraction, one has to use $n = c/(V_{poly}\ \rho_{poly})/(c/\rho_{poly} + [1-c]/\rho_{D2O})$, where ρ_{D2O} is the density of D_2O.

For a homogeneous spherical particle with the radius *R*, the distribution of scattering material is uniform throughout the sphere. Therefore the radial scattering length density distribution is described by a box function and the form factor is:

$$P_{\mathrm{hom}}(q)=\left(\frac{3\left[\sin(qR)-qR\cos(qR)\right]}{(qR)^3}\right)^2 \tag{8}$$

For microgel particles a higher degree of cross-linking density is expected inside the particle than outside (see introduction). This leads to a fuzziness of the particle surface, which has to be included in the model. We assume that the fuzziness can be accounted for by convoluting the radial box profile with a Gaussian. In reciprocal space the convolution is just a product yielding the form factor $P_{inho}(q)$ that describes scattering from a monodisperse sphere with an interface that gradually decreases at the sphere surface as an error function. The form factor is

$$P_{inho}(q)=\left[\frac{3\left[\sin(qR)-qR\cos(qR)\right]}{(qR)^3}\exp\left(-\frac{(\sigma_{surf}\,q)^2}{2}\right)\right]^2 \tag{9}$$

where σ_{surf} denotes the width of the smeared particle surface. A similar approach was applied by Svaneborg et al.[76,77] to describe the scattering of block copolymer micelles. Figure 1 depicts the radial profile corresponding to $P_{inho}(q)$. The core of the microgel exhibits a higher degree of cross-linking density and is characterized by the radial box profile up to a radius of about $R_{box} = R - 2\sigma_{surf}$. The subsequent decrease in cross-linking density is described by σ_{surf} and the profile has decreased to half the core density at R. At $R_{SANS} = R + 2\sigma_{surf}$, the profile approaches zero and thus, the overall size of the particle obtained by SANS is approximately given by R_{SANS}. A small number of chains reaching outside the particle will contribute only to the hydrodynamics of the particle and therefore the size obtained by SANS is expected to be slightly smaller than the hydrodynamic radius R_h determined by DLS.

To consider size polydispersity of the particles we assume the number distribution with respect to the particle radius R to be a Gaussian function

$$D(R,\langle R\rangle,\sigma_{poly})=\frac{1}{\sqrt{2\pi\sigma_{poly}{}^2\langle R\rangle^2}}\exp\left(-\frac{(R-\langle R\rangle)^2}{2\,\sigma_{poly}{}^2\langle R\rangle^2}\right) \tag{10}$$

with $\langle R\rangle$ describing the average particle radius and σ_{poly} denoting the relative particle size polydispersity.

At infinite dilution colloidal systems reveal no position-position correlations. The influence of the structure factor $S(q)$ on the scattering distribution can be disregarded and $S(q) = 1$ can be assumed. At higher concentrations the interference of scattering from different particles cannot be neglected. Therefore, $S(q)$ needs to be included in the model expression for $I(q)$ providing information about the interaction of the particles. For monodisperse, spherical particles that interact with a spherically symmetric hard sphere interaction potential $S(q)$ is

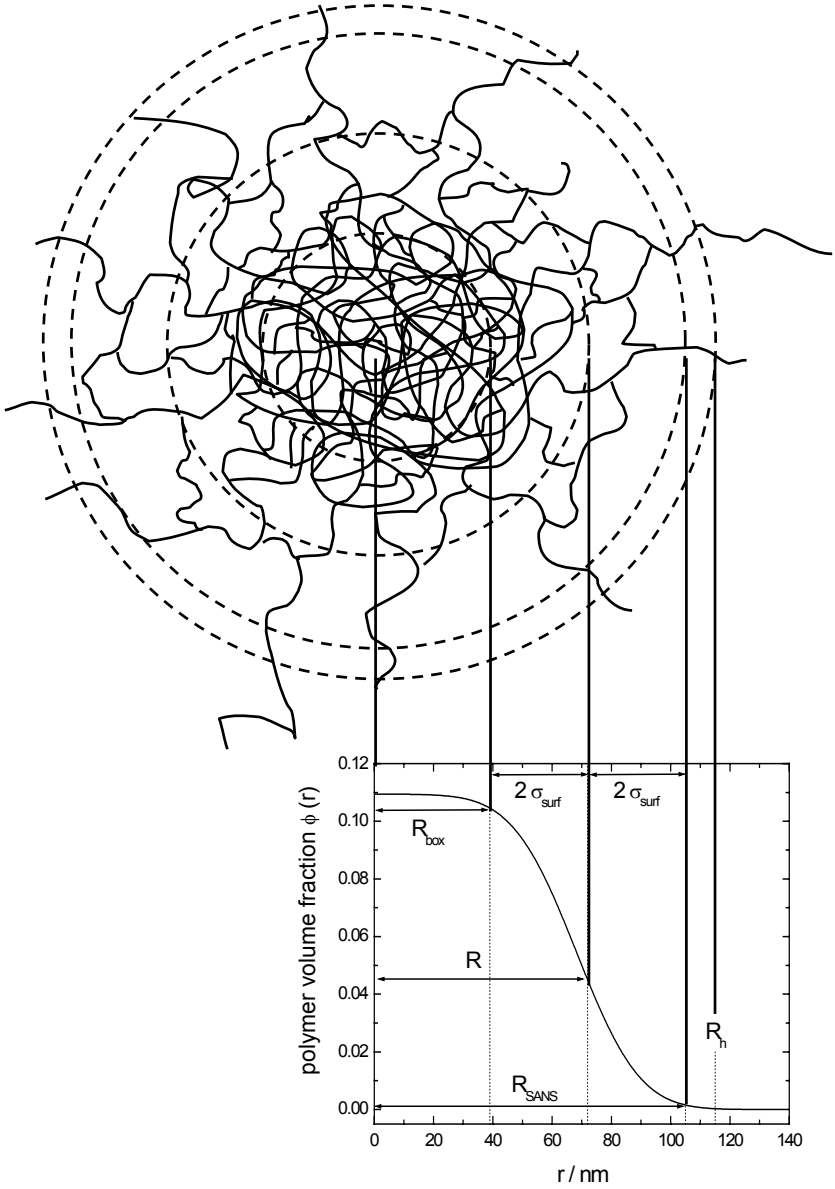

Fig 1. *The structure of PNiPAM microgels. A highly cross-linked core is characterized by a radial box profile up to* $R_{box} = R - 2\sigma_{surf}$*. The cross-linking density decreases with increasing distance to the core described by* σ_{surf}*. At R the profile has decreased to half the core density. The overall size obtained by SANS is approximately given by* $R_{SANS} = R + 2\sigma_{surf}$ *where the profile approaches zero.* R_{SANS} *is slightly smaller than the hydrodynamic radius* R_h *obtained by DLS.*

obtained from the liquid state theory employing the Percus-Yevick approximation for the closure relation.[78] *S(q)* depends only on the hard sphere volume fraction η_{HS} and the corresponding hard sphere radius R_{HS}. The data presented in this study were obtained from scattering experiments performed with samples in the concentration range of $c = 0.06$-

0.20 wt%. Although all samples were very dilute, the influence of *S(q)* on the intensity distribution cannot be neglected. Therefore *S(q)* was calculated using estimated values for η_{HS} and R_{HS}. The hard sphere volume fraction was approximated with $\eta_{HS} \approx c/[\rho_{poly}\phi_{poly}(0)]$ where $\phi_{poly}(0)$ describes the volume fraction of polymer in the particle center and the hard sphere radius with $R_{HS} \approx R_{SANS} = R + 2\sigma_{surf}$. Initial estimates for $\phi_{poly}(0)$, R and σ_{surf} were obtained by previous fits assuming $S(q)=1$. The estimated η_{HS} were in the range of η_{HS} = 0.003-0.025 depending on the sample concentration and temperature which was in good agreement with the effective volume fractions obtained by viscometry in dilute solution. The SANS data presented here does not provide sufficient information on *S(q)* to perform reliable and consistent free fits due to the small volume fractions. The structure factor of concentrated suspensions of PNiPAM microgels will be discussed more detailed in a following paper.

Thus, the differential scattering cross section

$$\frac{d\,\sigma(q)}{d\,\Omega} = n\,\Delta\rho^2\,S(q,\langle R\rangle)\int_0^\infty D(R,\langle R\rangle,\sigma_{poly})\,V_{poly}(R)^2\,P_{inho}(q,R)\,dR \qquad (11)$$

is obtained, where the structure factor effects are treated in the simple decoupling approximation. This approximation is valid for the present samples for which the size polydispersity is low. It has specifically been expressed that the structure factor $S(q,\langle R\rangle)$ is calculated for the average size. The influence of the polydispersity on the particle density *n* also has to be considered. One can calculate a number-average particle volume as

$$V_{av} = \phi_{poly}\int_0^\infty D(R,\langle R\rangle,\sigma_{poly})\,V(R)\,dR \qquad (12)$$

so that *n* in equation (11) is $n = c/(V_{av}\,\rho_{poly})/(c/\rho_{poly} + [1-c]/\rho_{D2O})$ for *c* given as weight fraction.

In order to describe the scattering contributions arising from fluctuations of the microgel network a Lorentzian function (see equation (2)) is added to the model expression. The ensemble average correlation length in the network is described by ξ. However, due to the incoherent background it is difficult to determine ξ with high accurancy as will be discussed in section 4.4.2. Finally, a constant background $const_{back}$ is added to account for residual incoherent scattering.

Experimental SANS data are always smeared by the instrument since a distribution of radiation with scattering vectors *q* around the nominal scattering vector $\langle q \rangle$ contributes. The distribution is due to the finite collimation of the beamline, the wavelength spread of the incoming neutrons and the finite spatial resolution of the detector. It was shown that all these three contributions can be approximated separately by Gaussian functions.[79] The combined

resolution function $R(\langle q\rangle, q)$ describes the distribution of scattering vectors q contributing to the scattering at the setting $\langle q\rangle$ as

$$R(\langle q\rangle, q) = \frac{q}{\sigma_{smear}^2} \exp\left[-\frac{1}{2}\left(q^2 + \frac{\langle q\rangle^2}{\sigma_{smear}^2}\right)\right] I_0\left(\frac{\langle q\rangle q}{\sigma_{smear}^2}\right) \tag{13}$$

where σ_{smear} denotes the width of the instrumental smearing, which is different for the different instrumental settings, and I_0 is a modified first kind and zeroth order Bessel function.[80] The contribution to σ_{smear} from wavelength smearing (9% FWHM) is included as well as the contributions from collimation and detector resolution. The latter can be determined by fitting the attenuated direct beam profile with a Gaussian. To account for instrumental smearing the resolution function is included in the model:

$$I^{\mathrm{mod}}(\langle q\rangle) = \int_0^\infty R(\langle q\rangle, q) \frac{d\sigma(q)}{d\Omega} dq \tag{14}$$

Finally, after incorporating all contributions the exhaustive model expression for the intensity distribution is found:

$$I^{\mathrm{mod}}(\langle q\rangle) = n\Delta\rho^2 \int_0^\infty \int_0^\infty R(\langle q\rangle, q) D(R, \langle R\rangle, \sigma_{poly}) V_{poly}(R)^2 P_{inho}(q,R) S(q, \langle R\rangle)\, dR\, dq + I_{fluct}(q) + const_{back} \tag{15}$$

After the model is fitted to the experimental data, the amplitude of the form factor can be calculated as the terms inside the square brackets in equation (9). A numerical Fourier transformation leads to the radial density profile of the particle providing useful information about the structure of the particle. It should be noted that the profile is easily normalized to the value of ϕ_{poly} at r = 0.

3.4 Results and Discussion

3.4.1 Characterization of the PNiPAM colloids by DLS and density measurements

Temperature sensitive PNiPAM microgels were prepared with different cross-linking density and different particle size by emulsion copolymerization. The sample name reflects the cross-linking density as the molar ratio of BIS to NiPAM in mol% and the hydrodynamic radius at 25°C in heavy water R_h(25°C) omitting its units. The overall size of the particle can be monitored employing DLS. For all microgels the hydrodynamic radii R_h decreased slightly with increasing temperature but when the LCST is approached at ≈ 34°C in D_2O a strong volume transition occurred. At all temperatures the M-1.5/353 microgel is explicitly larger

than the M-5.5/115 and M-1.4/141 samples since a smaller amount of surfactant was used in the synthesis. To compare the different cross-linking densities R_h(25°C) was normalized by the value of R_h(39°C).[81] As anticipated, the microgel with a higher degree of cross-linking density (M-5.5/115) is less swellable and R_h(25°C)/R_h(39°C) = 1.83 was found. The size of the microgel does not strongly influence the swelling behavior and for M-1.4/141 R_h(25°C)/R_h(39°C) = 2.31 and for M-1.5/353 R_h(25°C)/R_h(39°C) = 2.25 were obtained.

To account for changes in the SANS scattering contrast with temperature the apparent specific density ρ was investigated as a function of temperature (figure 2).

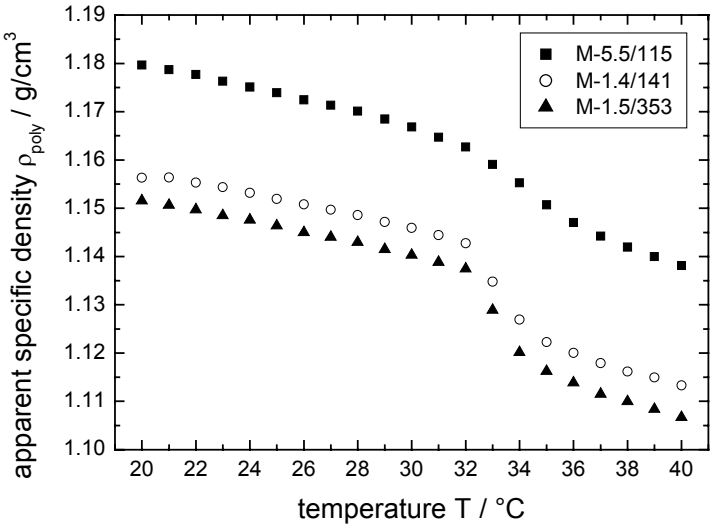

Fig. 2. *Apparent specific density ρ_{poly} as a function of temperature for the three PNiPAM microgels in D_2O. ρ_{poly} decreases continuously with increasing temperature and drops off when the LCST is reached.*

ρ ascribes all density changes in the solution to be associated with the solute, although changes in the solvent density contribute to the measured solution density. For all microgels the density decreases continuously with increasing temperature. When the LCST is reached, a drop off in the density is observed. The density of the highly cross-linked microgel (M-5.5/115) is larger compared to the two microgels with a lower cross-linking density (M-1.4/141 and M-1.5/353). The influence of the particle size on the density is small. The PNiPAM microgels with the same cross-linking density but different particle size (M-1.4/141 and M-1.5/353) reveal a similar temperature dependence of ρ. The temperature dependence of ρ was incorporated in the calculation of the SANS contrast according to equation (7).

3.4.2 Structural changes induced by temperature

In this study a broad *q*-range (q = 0.0007-0.15Å^{-1}) was employed and hence information about the local as well as the overall structure of the particles is present in the data. All parameters obtained from the fitting procedure are summarized in table 2.

Tab. 2. *Summary of the parameters obtained by fitting the experimental I(q) according to equation (15). The errors are obtained from the least-square fit. The error of $R_{h(DLS)}$ is estimated to 3%.*

sample	*T* /°C	*R* /nm	σ_{surf} /nm	σ_{poly} /%	$\phi_{poly}(0)$	$const_{scale}$	R_{SANS} /nm	$R_{h(DLS)}$ /nm
M-5.5/115	25 ± 0.1	72 ± 0.3	17 ± 0.2	9.9 ± 0.5	0.13 ± 0.001	1.16	106	115 ± 3
M-5.5/115	32 ± 0.1	60 ± 0.1	14 ± 0.1	9.9 ± 0.2	0.24 ± 0.001	1.16	88	97 ± 3
M-5.5/115	39 ± 0.1	54 ± 0.1	2 ± 0.1	9.5 ± 0.2	0.42 ± 0.002	1.16	58	63 ± 2
M-1.4/141	25 ± 0.1	94 ± 1.0	28 ± 1.0	9.7 ± 1.4	0.07 ± 0.001	1.16	150	141 ± 4
M-1.4/141	32 ± 0.1	70 ± 1.5	23 ± 1.1	13.5 ± 2.8	0.18 ± 0.008	1.16	116	115 ± 3
M-1.4/141	39 ± 0.1	53 ± 0.1	1 ± 1.2	9.6 ± 0.3	0.42 ± 0.002	1.16	55	61 ± 2
M-1.5/353	28 ± 0.1	242 ± 1.1	37 ± 1.0	5.9 ± 1.0	0.02 ± 0.0003	2.36	316	346 ±10
M-1.5/353	31 ± 0.1	220 ± 1.0	30 ± 1.0	6.7 ± 0.8	0.04 ± 0.0004	2.74	280	-
M-1.5/353	33 ± 0.1	150 ± 0.7	15 ± 0.6	2.6 ± 1.9	0.16 ± 0.002	1.88	180	-
M-1.5/353	39 ± 0.1	148 ± 1.2	1 ± 1.9	6.8 ± 0.9	0.40 ± 0.01	1.19	150	157 ± 5

Three scattering data sets measured at temperatures below, close to and above the LCST together with the curves from the data analysis according to equation (15) for the M-5.5/115 microgel are shown in figure 3.

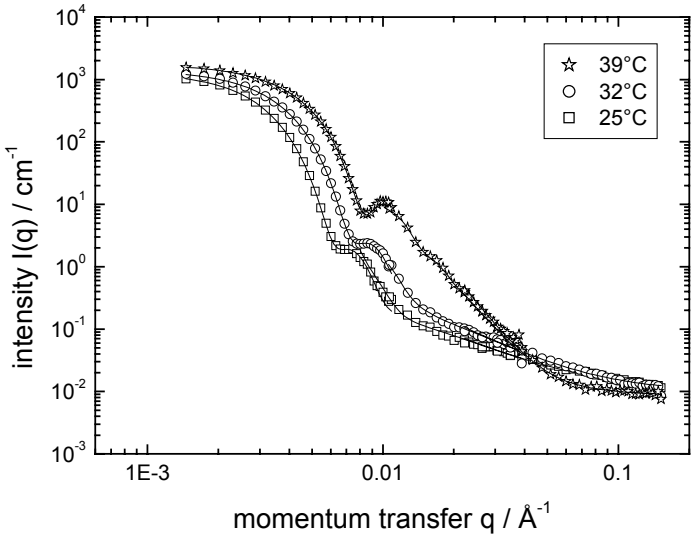

Fig. 3. *SANS scattering profiles of the M-5.5/115 microgel at a concentration of 0.20 wt% at 25°C, 32°C and 39°C. The lines represent fits according to equation(15). The shift of the form factor minima to higher q-values indicates the shrinkage of the particles with increasing temperature.*

The observation of form factor minima shows that the particle size polydispersity is small. From the fitting procedure σ_{poly} was determined to be nearly temperature independent and at 25°C σ_{poly} = 9.9 % and at 39°C σ_{poly} = 9.5 % were obtained (see table 2). The shift of the form factor minima to higher *q*-values with increasing temperature is directly related the shrinkage of the particle. At 39°C the particles are in the shrunken state. Porod scattering ($I \propto q^{-4}$) is observed in the "intermediate" *q*-range of *q* = 0.02-0.06 Å^{-1} indicating scattering from a sharp interface. Figure 4 displays the three corresponding radial polymer volume fraction profiles $\phi_{poly}(r)$. The polymer volume fraction inside the particle $\phi_{poly}(r)$ at r = 0 nm increases dramatically with increasing temperature and $\phi_{poly}(0)$ = 0.13 at 25°C and $\phi_{poly}(0)$ = 0.42 at 39°C are found. Those volume fractions are in good agreement with the average values reported by Ballauff et al. for PS-core-PNiPAM shell colloids.[72] The fuzziness of the particle surface described by σ_{surf} decreases when the temperature is raised (σ_{surf} (25°C) = 17 nm and σ_{surf} (32°C) = 14 nm). Above the LCST, the particle surface sharpens significantly and with σ_{surf} (39°C) = 2 nm the density profile resembles a box profile of a homogenous sphere. In contrast, only a slight decrease of *R* is observed when the temperature is changed from 32°C to 39°C (see table 2). Thus, the overall swelling behavior is basically dominated by the swelling of the outer regions of the particle. Since the inner regions of the microgel exhibit a higher cross-linking density than the outer regions the elasticity of the network is larger inside the particle and the swelling is less pronounced. It should be noted, that the dramatic

shrinkage of the outer regions of the particle at the volume phase transition was observed for all microgels independent of the cross-linking density and size. The overall particle size obtained by SANS (R_{SANS}) is smaller than the hydrodynamic radius R_h obtained by DLS. Clearly, a few dangling polymer chains that contribute to the hydrodynamics are attached to the particle surface. The concentration of those chains is not high enough to be detected by SANS (see figure 1).

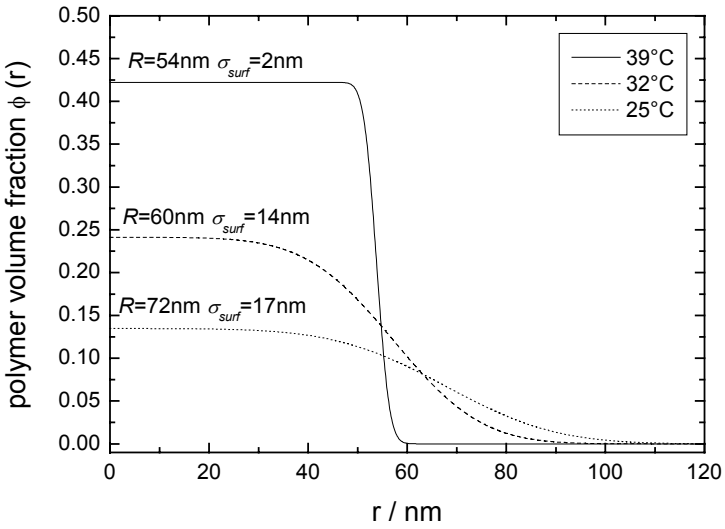

Fig. 4. *Radial density profiles of the M-5.5/115 microgel at a concentration of 0.20 wt% at 25°C, 32°C and 39°C. The amplitude of the form factor was calculated according to equation (9) and a numerical Fourier transformation lead to the profiles. A reduction of the fuzziness of the particle surface with increasing temperature is observed.*

The polymer mass of a particle m_{poly} is given by

$$m_{poly} = N_A \ \rho_{poly} \ V_{poly} = N_A \ \rho_{poly} \int_0^{R_{SANS}} \phi_{poly}(r) r^2 \, dr \qquad (16)$$

and should yield a constant value for all temperatures. The radial polymer mass distribution of a particle of the M-5.5/115 microgel is shown in figure 5. It is already apparent from $\phi_{poly}(r)$ that the integral at 39°C will be larger than those at 25°C and 32°C. m_{poly} was determined for all temperatures using equation (16) and normalized by m_{poly} at 39°C. An apparent decrease of m_{poly} by 22% at 25°C and by 18% at 32°C was observed. For a monodisperse system the forward scattering $I(0)$ at $q = 0$ is given by $I(0) \propto m_{poly}$. To obtain m_{poly} reliably, the forward scattering $I(0)$ needs to be precisely known. Consequently, the "low" q-data needs to be accurately transferred to an absolute scale. This data analysis is difficult for various reasons. Calibration measurements cannot be performed with high accuracy in the "low" q-regime (see experimental details) and were carried out in the

"intermediate" *q*-range instead. The overlap between the "low" and "intermediate" *q*-data sets (sample-detector distances of 36.7m and 10.5m, respectively) is very sensitive to the instrumental resolution as well as the slope of the scattering curve in the overlap region. The latter changes strongly with temperature for the PNiPAM microgels. The background subtraction of the "low" *q*-data sets is sensitive to small changes in experimental conditions. Errors in the background subtraction may occur either by under- or over-subtraction of the "low" *q*-data. For the aforementioned reasons it was difficult to transfer the "low" *q*-data sets precisely to an absolute scale. In order to improve the overlap between the "low" and "intermediate" *q*-range a scaling factor for the "low" *q*-data sets $const_{scale}$ was included in the fitting model. The same scaling factor ($const_{scale}$ = 1.16) was used for all fits of the scattering curves of M-5.5/115 and M-1.4/141. The M-1.5/353 microgel data at different temperatures were measured at different sessions at the ILL and their scale factors were less consistent. It turned out that different scaling factors ($const_{scale}$ = 1.19-2.74) had to be used for different temperatures for this sample. Consequently, $const_{scale}$ shifts *I(0)* which is directly related to $m_{poly} \propto \rho_{poly}\, \phi_{poly}(0)\, V_{poly}$. Therefore, only the results obtained from fits with the same $const_{scale}$ can be compared consistently, namely the M-5.5/115 and M-1.4/141 samples. The results obtained for the M-1.5/353 microgel will be discussed separately in section 4.4.4.

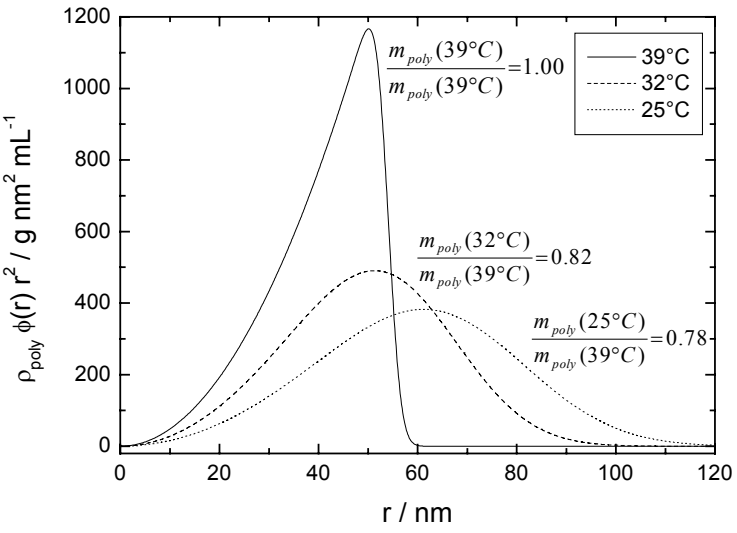

Fig. 5. *Radial polymer mass distribution of a particle of the M-5.5/115 microgel at a concentration of 0.20 wt% at 25°C, 32°C and 39°C. An apparent decrease of the polymer mass is observed with decreasing temperature.*

Dangling polymer chains are not detected by SANS at temperatures below the LCST when the particles are highly swollen, giving rise to an apparent smaller polymer concentration within one particle. In contrast, in the collapsed state above the LCST the well-

defined particle interface leads to a contribution of those chains to the overall scattering intensity. Additionally to the aforementioned, this explains why the apparent m_{poly} is different for different temperatures and gives further evidence for the assumed internal structure of the PNiPAM particle. It should be noted that an error function was chosen to describe the fuzziness of the particle surface. The missing contribution in the swollen state might have been picked up when a function with a longer and slower decay was chosen.

It has been shown in the literature that $I_{fluct}(q)$ contributes significantly to $I(q)$ only at "high" q-values.[72] In this q-range the incoherent background is large and the statistical error of the experimental data is rather big. It should be noted that Ballauff et al. were able to determine ξ solely from their SAXS data but not from SANS experiments. For some of the samples discussed here, SANS data in the "high" q-range were not collected. Therefore the correlation length ξ could not be extracted reliably from analysis of the SANS data.

3.4.3 Influence of cross-linking density on the particle structure

Senff et al. demostrated in a previous study that the particle interaction potential and the swelling ratio of PNiPAM microgels depend on the cross-linking density.[81] In order to investigate the influence of the cross-linking density on the structure of the microgels the scattering profile and the fits according to equation (15) of the M-1.4/141 microgel are presented in figure 6. A distinct form factor minimum was only observed when the particles were shrunken. σ_{poly} = 9.7% and σ_{poly} = 9.6 % were found at 25°C and 39°C, respectively, which are similar to the polydispersity found for M-5.5/115. The polymer volume fraction inside the particle at 25°C, $\phi_{poly}(0)$ = 0.07, is smaller than $\phi_{poly}(0)$ = 0.13 for M-5.5/115. This reflects a more pronounced ability to swell because of the lower cross-linking density (figure 7). In the swollen state at 25°C σ_{surf} = 28 nm is larger compared to the highly crosslinked M-5.5/115 (σ_{surf} = 17 nm). As mentioned earlier, the cross-linker BIS is consumed faster than the monomer NiPAM during emulsion copolymerization.[57] The reagent quantities employed in the preparation of M-5.5/115 and M-1.4/141 were nearly the same apart from the amount of BIS. Since less BIS was used in the preparation of M-1.4/141 the entire cross-linker must have been consumed at an earlier stage of the polymerization. Hence, more NiPAM is left to be polymerized without cross-linker yielding in a thicker fuzzy particle surface. The SANS data analysis strongly supports this. At 39°C, when the particles are collapsed, the structural differences between the microgels with different cross-linking density (M-5.5/115 and M-1.4/141) are barely observable. Both samples exhibit a sharp particle surface that nearly resemble a box profile with σ_{surf} = 2 nm for M-5.5/115 and σ_{surf} = 1 nm for M-1.4/141. A

polymer volume fraction inside the particle at 39°C of $\phi_{poly}(0) = 0.42$ is found for both samples.

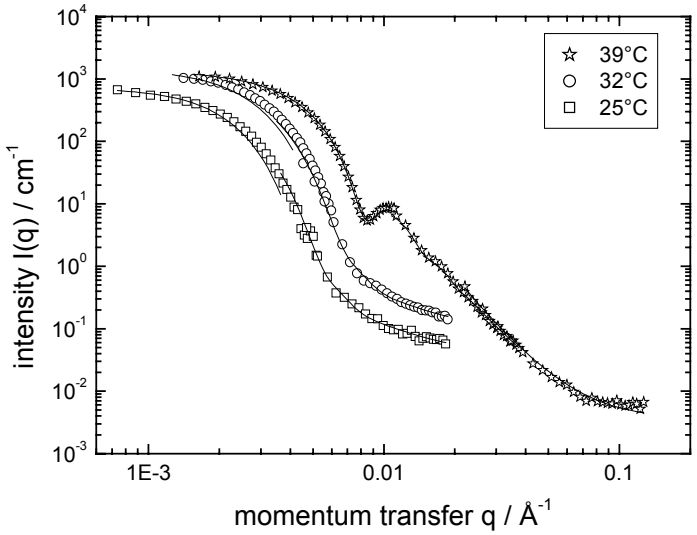

Fig. 6. *SANS scattering profiles of the M-1.4/141 microgel at a concentration of 0.10 wt% at 25°C and at a concentration of 0.16 wt% at 32°C and 39°C. The lines show the fits (equation (15)).*

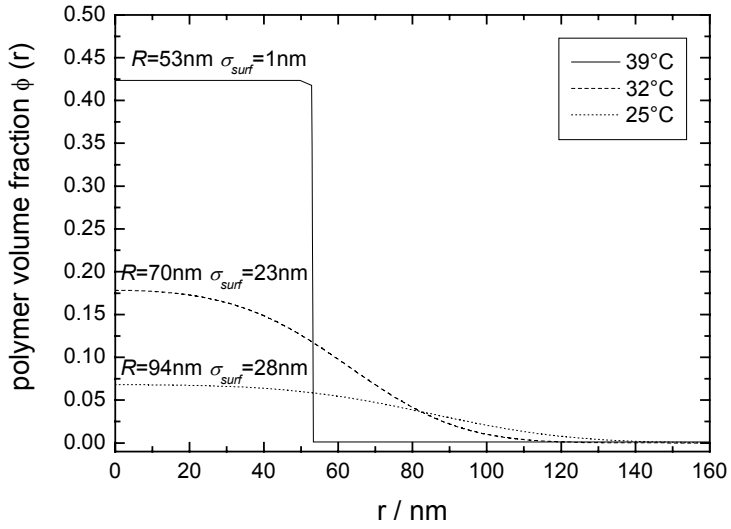

Fig. 7. *Radial density profiles of the M-1.4/141 microgel at a concentration of 0.10 wt% at 25°C and at a concentration of 0.16 wt% at 32°C and 39°C. The lower degree of cross-linking density compared to M-5.5/115 (figure 4) results in a fuzzier particle surface and a lower polymer volume fraction inside the particle.*

3.4.4 Comparison of microgels with different particle sizes

McPhee et al. have shown that the size of the PNiPAM particles can be controlled by variation of the surfactant concentration used in the emulsion copolymerization.[57,82] They have proposed that the microgel particles are formed by homogenous nucleaction. Initially, small precursor particles are formed which are colloidally unstable. The coagulative association with other precursor particles leads to the formation of larger stable primary particles. The surfactant adsorbs onto the surface of the precursor particles and enhances its colloidal stability. The size of the primary particles decreases and the concentration of the primary particles increases. Finally, a higher concentration of primary particles results in smaller PNiPAM microgels. To gain a detailed understanding of the structure of PNiPAM microgels with different particle sizes but similar cross-linking densities we will compare the M-1.4/141 and the M-1.5/353 samples. In contrast to the M-1.4/141 microgel the SANS experiments with the M-1.5/353 sample were performed at 28°C but not at 25°C. None of the microgels explicitly swells between these two temperatures. In the following we will therefore disregard the temperature difference and compare data obtained at 25°C with 28°C. A scaling factor of $const_{scale}$ = 1.16 was used for all fits of the scattering curves of M-1.4/141. In contrast, different scaling factors in the range of $const_{scale}$ = 1.19-2.74 had to be used for the fits of different temperatures for the M-1.5/353 microgel since the SANS data of M-1.5/353 were gathered at various sessions at the ILL. Consequently, the fitting results will not be discussed in terms of absolute values but rather as general trends. Careful tests of the influence of the scaling factor on the fitting results revealed that the conclusions made here are consistent and within the error of $const_{scale}$.

Figure 8 presents *I(q)* obtained from the M-1.5/353 microgel and the corresponding $\phi_{poly}(r)$ is shown in figure 9. The particle sizes obtained by SANS and DLS show that the reduction of the surfactant concentration in the emulsion copolymerization results in larger particles and R_{SANS} = 316 nm at 28°C for M-1.5/353 and R_{SANS} = 150 nm at 25°C for M-1.4/141 are obtained. The polydispersity of M-1.5/353 (e.g. σ_{poly} = 5.9 % at 28°C) was similar compared to the M-1.4/141. A polymer volume fraction inside the particle of $\phi_{poly}(0)$ = 0.02 at 28°C was found for the M-1.5/353 which is smaller than $\phi_{poly}(0)$ = 0.07 at 25°C for the M-1.4/141. The reduction of the surfactant concentration employed in the emulsion copolymerization might have decreased the rate of polymerization of the cross-linker BIS leading to a lower $\phi_{poly}(0)$. McPhee at al.[57,82] have reported that the reaction rates of the emulsion copolymerization are sensitive to the surfactant concentration, their conversion profiles reveal differences at the early stages of the copolymerization. At the beginning of the reaction, when the inner regions of the PNiPAM microgels are formed, a lower surfactant concentration gives rise to a lower conversion.

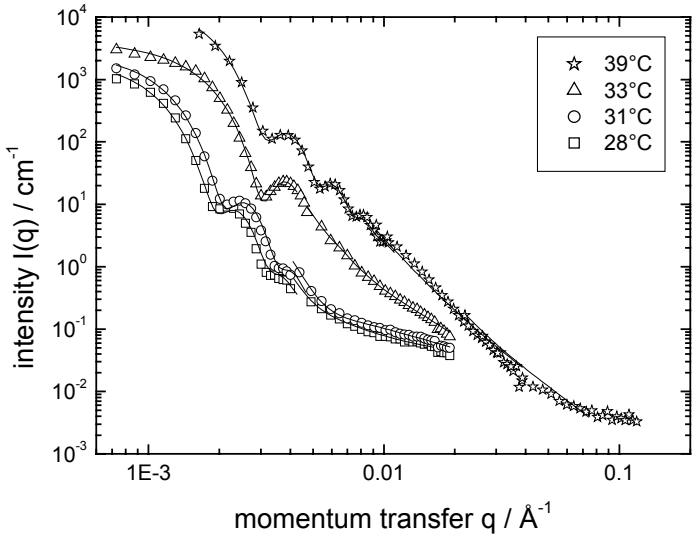

Fig. 8. *SANS scattering profiles and fits of the M-1.5/353 microgel at a concentration of 0.06 wt% at 28°C, 31°C and 33°C and at a concentration of 0.14 wt% at 39°C.*

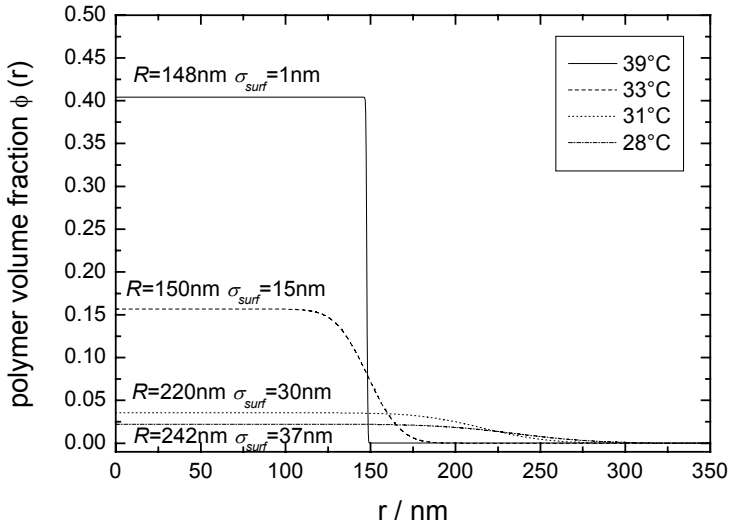

Fig. 9. *Radial density profiles of the M-1.5/353 microgel at a concentration of 0.06 wt% at 28°C, 31°C and 33°C and at a concentration of 0.14 wt% at 39°C. The larger PNiPAM particles reveal a lower polymer concentration inside the particle than smaller microgels (M-1.4/141 in figure 7) although the same amount of cross-linker was used in the emulsion copolymerization.*

3.5 Conclusions

The structure of temperature sensitive PNiPAM microgels has been studied by SANS in dilute suspension. A direct modeling expression for the scattering intensity distribution was derived which describes very well the experimental data at all temperatures over an extensive *q*-range. The overall particle form as well as the internal structure of the microgel network were included in the model expression. The inhomogeneous distribution of cross-linking density through a particle was accounted for with a radial density profile that decreased gradually at the sphere surface following an error function. The structural changes induced by temperature, cross-linking density and particle size were revealed by the density profiles. The polymer volume fraction inside the particle increased dramatically with increasing temperature accompanied by a decrease of the smearing of the particle surface. Above the LCST, the particle surface sharpened significantly and a radial profile with an almost box-shape was observed. The overall swelling behavior of the particle is dominated by the swelling of the outer, less cross-linked regions of the microgel at temperatures near the LCST. The overall particle size obtained by SANS was smaller than the hydrodynamic radius obtained by DLS. This is explained by a few dangling polymer chains attached to the particle surface contributing to the hydrodynamic radius. In the swollen state, an increase of the cross-linking density resulted in an increase of the polymer volume fraction in the inner region of the particle and a reduction of the fuzziness of the particle surface. The influence of the cross-linking densities on the structure of the PNiPAM microgels was explained with the kinetics of the emulsion copolymerization used to prepare the microgel colloids. A reduction of the surfactant concentration employed in the emulsion copolymerization lead to larger particles. A significant decrease of the polymer volume fraction inside the colloid was observed with increasing particle size.

Obviously, the structural inhomogeneities of microgels need to be considered when such systems are used as models for colloidal suspensions. The structure of concentrated PNiPAM suspensions studied by SANS will be subject of a future paper.

ACKNOWLEDGMENT. Financial support by the Deutsche Forschungsgemeinschaft, the Fonds der Chemischen Industrie and the Danish Natural Science Research Council is gratefully acknowledged. We thank Cornelia Sommer, University of Aarhus, Denmark, for performing the density measurements and for fruitful discussions.

4 Are Thermoresponsive Microgels Model Systems for Colloidal Suspensions?

ABSTRACT: The structure of concentrated temperature-sensitive poly(*N*-isopropylacrylamide) (PNiPAM) microgel suspensions has been investigated employing rheology and small-angle neutron scattering (SANS). A previously described model expression for the particle form factor $P_{inho}(q)$ was extended by a model hard sphere structure factor $S(q)$. The average radial density profiles $\phi(r)$ were calculated from the amplitude of the form factor $A(q)$ and the structure factor $S(q)$. By this procedure a direct real space description of the spatial ordering in the neighborhood of a single particle was obtained. The overall particle size and the correlation length ξ of the concentration fluctuations of the internal polymer network decreased with concentration revealing the increasing compression of the spheres. The particle form factor $P_{inho}(q)$ of the swollen PNiPAM microgels depended on concentration. The particle-particle interaction potential did not change significantly between 25°C and 32°C. Even approximately 1K below the LCST the experimental scattering intensity distributions $I(q)/c$ were described very well by the hard sphere structure factor when an equivalent hard sphere particle size R_{HS} and volume fraction η_{HS} were used. Microgels with different degrees of cross-linking and particle size resembled true hard sphere behavior up to effective volume fractions of ϕ_{eff}<0.35. At higher effective volume fractions ϕ_{eff}>0.35 strong deviations from true hard spheres were observed. Interpenetration of the outer, less cross-linked regions of the soft spheres as well as particle compression occurred at higher concentrations. In agreement with this, the equilibrium colloidal phase behavior and rheology also had some features of soft sphere systems. At temperatures well above the LCST the interaction potential became strongly attractive. The collapsed microgel spheres formed aggregates consisting of flocculated particles without significant long-range order. Hence, an attractive interaction potential in concentrated suspensions of PNiPAM microgels led to distinctively different structures as compared to attractive hard sphere colloids. When the above mentioned peculiar structural properties of the PNiPAM microgels are considered they can be used as model systems in colloidal science.

4.1 Introduction

Colloidal suspensions are often used as model systems in soft condensed matter science to study the structure and dynamics of concentrated dispersions. Especially diffusion, crystallisation and rheology of hard sphere suspensions have been thoroughly investigated.[14,15,16,17,18] Model hard sphere suspensions consist of rigid particles dispersed in a newtonian fluid that interact with a purely repulsive inter-particle interaction potential. Among the well established systems, that display hard sphere like behavior, are dispersions of sterically stabilized colloids. However, the particle-particle interactions of hard spheres can be altered from repulsive to weakly or strongly attractive by changing the solvent and temperature.[83,84,85] Attraction and phase separation can also be induced via the depletion effect by addition of free non-absorbing polymer to dispersions of hard spheres.[86]

Colloidal microgels, a further class of dispersions, have attracted interest as model systems for fundamental studies of e.g. the glass transition.[87,88] In contrast to conventional hard sphere dispersions, microgel particles are chemically cross-linked latex spheres that are swollen by a good solvent. The question has been raised whether microgels can be described with well-known hard sphere models or whether the swelling of the particles lead to softness and deformability.[19] The rigidity of a sphere is expected to depend on the cross-linking density.

An even more complex colloidal behavior can be achieved for thermoresponsive microgels, the properties of which can be controlled by external conditions.[4,9] Water-swellable microgels consisting of poly(*N*-isopropylacrylamide) (PNiPAM) are known to undergo a temperature induced volume-phase transition when the lower critical solution temperature (LCST) of ca. 33°C is approached. At temperatures below the LCST water is a good solvent and the spheres are highly swollen. At elevated temperatures the solvent quality changes and above the LCST water is a non-solvent leading to the collapse of the particles. The size of the particle decreases with increasing temperature. Hence, a major advantage of thermoresponsive particles is that the effective volume fraction ϕ_{eff} can easily be controlled by simple temperature changes while the mass concentration c and thus the particle number density n is kept constant. In concentrated suspension phase separation occurs at temperatures above the LCST. Since the degree of swelling changes with temperature the rigidity of the particles depends also on temperature.

In a previous study we have investigated the internal structure of PNiPAM microgels in dilute solution using small-angle neutron scattering (SANS).[89] A model expression for the particle form factor $P_{inho}(q)$ was introduced. The internal structure of the microgel network and the overall particle form were included in the model and the real space structure was described by radial density profiles. In the swollen state the polymer segment density of a

particle was found to be not homogeneously distributed but gradually decreasing at the surface. Only when the particles are collapsed at temperatures above the LCST the density profiles are described by a box profile like that of homogeneous hard spheres.

Once the internal structure of a microgel particle in dilute solution is known, the interaction between different particles in concentrated suspension can be investigated. Rheology and phase behavior of concentrated PNiPAM microgel suspensions were studied by Senff et al.[20] They were the first to report on the formation of colloidal crystals made of PNiPAM microgels. The relative zero shear viscosity $\eta_{0,rel}$ obtained in dilute suspension was employed to define an effective volume fraction ϕ_{eff} that is strongly temperature dependent. It was demonstrated that ϕ_{eff} allows to obtain temperature independent master curves over the entire concentration range for rheological properties and the colloidal phase behavior. At $\phi_{eff} < 0.5$ the viscosity data agreed well with that of hard sphere suspensions. At higher effective volume fractions, however, a soft sphere interaction potential was concluded from the experimental phase diagram and the power law concentration dependence of the plateau modulus G_P.

Hellweg et al. determined the structure of colloidal PNiPAM crystals using SANS.[21] A face-centred-cubic lattice was observed. The structure factor *S(q)* was extracted by dividing the intensity distribution of a concentrated sample $I_{conc}(q)$ (8.5 wt%) by the intensity distribution of a dilute sample $I_{dil}(q)$ (0.85 wt%). They assumed that the particle form factor *P(q)* is independent of concentration and that the effective volume fraction ϕ_{eff} of the dilute sample is small enough to neglect inter-particle correlations (*S(q)* = 1).

Lyon and coworkers [22,23,24] report on the assembly of colloidal PNiPAM crystals with tunable optical properties. They observed by laser scanning confocal microscopy a compression of the soft microgel particles when they are closely packed in the crystal. Obviously, swollen microgel particles are not rigid and show soft sphere behavior at higher concentrations.

Employing thermodynamic perturbation theory combined with static and dynamic light scattering (SLS and DLS) Wu et al. have shown that the particle-particle interaction potential alters strongly with temperature.[90] However, in their calculations they did not account for inhomogeneties in the internal particle structure.

In this contribution we present a study of the structure formation of concentrated suspensions of PNiPAM microgels using rheology and SANS. The following questions are addressed:

a) How does the size of individual microgel particles change with concentration?

b) How can the interaction be described for highly concentrated microgel suspensions at different temperatures?

c) Do highly swollen microgel particles display hard sphere behavior?

For this purpose the previously described model expression for the particle form factor $P_{inho}(q)$ is extended by a model structure factor $S(q)$ that enables to fit the experimental data also at high concentration. We introduce a new approach for calculating the average radial density profiles around a particle from the amplitude of the form factor $P_{inho}(q)$ and the structure factor $S(q)$. By this approach we obtain a direct description of the ordering in the neighborhood of a particle, which reveals the degree of particle-particle correlations. Concentrated microgel suspensions with different cross-linking densities and particle sizes will be compared at various temperatures. A broad concentration range will be presented covering samples in the dilute and concentrated liquid phase as well as crystalline and glassy samples (0.1 wt% - 13.9 wt%).

4.2 Experimental part

4.2.1 Synthesis of the PNiPAM microgels

As described previously the PNiPAM microgels were prepared in an emulsion copolymerization using *N*-isopropylacrylamide (NiPAM), *N,N´*-methylenbisacrylamide (BIS), sodium dodecylsulfate (SDS) and potassium peroxodisulfate (KPS).[89] The polymerization was carried out under stirring in an inert gas atmosphere at 70°C for 6 hours. After filtration and extensive dialysis against pure water, the microgel dispersion was freeze-dried. The characterization of the PNiPAM microgels is described elsewhere.[73] It should be noted, that the sample name denotes the degree of cross-linking given as the molar ratio of cross-linker to monomer and the hydrodynamic radius in nm at 25°C in heavy water obtained by dynamic light scattering. For example, the M-5.5/115 microgel exhibits a degree of cross-linking of 5.5 mol% BIS and a hydrodynamic radius of R_h(25°C) = 115 nm.

4.2.2 Experimental details

SANS experiments were performed at the instrument D11 of the Institute Laue-Langevin (ILL) in Grenoble, France. A neutron wavelength of λ = 6 Å or λ = 12 Å with a spread of $\Delta\lambda / \lambda$ = 9 % was employed. The data were collected on a two-dimensional multidetector (64 x 64 elements of 1 x 1 cm^2) and corrected for background and empty cell scattering. Sample-detector distances of 36.7, 10.5 and 2.5 m were used. The incoherent scattering of H_2O was used for absolute calibration according to standard procedures and software available at the ILL ($GRAS_{ans}P$ V. 3.25). H_2O calibration measurements were performed at sample-detector distances of 10.5 and 2.5m. Further data processing was done by radially averaging to obtain a one-dimensional data set. All experiments were carried out at full

contrast using D_2O as the solvent. The concentrations of the samples were in the range of 0.1 – 13.9 wt%.

Rheological properties of the concentrated PNIPAM dispersions were studied using a stress controlled Bohlin CVO-120 HR rheometer in cone/plate shear geometry (1°/40mm).

In addition, the effective volume fractions ϕ_{eff} of the microgel suspensions was determined as described previously[20] employing the relative viscosity η_{rel} which is related to ϕ_{eff} via an expression derived by Batchelor[91] ($\eta_{rel} = 1 + 2.5\ \phi_{eff} + 5.9\ \phi_{eff}^2$). The relative viscosity η_{rel} in dilute solution was measured with a computer controlled Lauda PVS-1/S5 capillary viscometer.

4.3 Theory and Data analysis

A detailed description of the model expression for the scattering intensity distribution *I(q)* of PNiPAM microgels in dilute solution was described previously.[89] The parameter *q* denotes the magnitude of the momentum transfer $q=4\pi/\lambda\ sin(\theta/2)$, where λ is the neutron wavelength and θ is the scattering angle. The internal and overall structures of the particles in dilute solution were successfully described by the form factor of an inhomogeneous sphere $P_{inho}(q)$. A model structure factor *S(q)* accounts for particle-particle correlations at finite concentration. A brief summary of the model expression will be given in the following section with special emphasis on the influence of the structure factor *S(q)* on the intensity distribution *I(q)*. In addition we describe a new approach for obtaining the average radial density around the center of a particle from the form factor amplitude and the structure factor *S(q)*.

Including both the (normalized) form factor *P(q)* to describe the structure of a single particle and the structure factor *S(q)* to account for the interference of scattering from different particles allows the model to describe more concentrated samples, which were studied in the present work. For a suspension of monodisperse centro-symmetric particles the differential scattering cross section $d\sigma(q)/d\Omega$ is given by:

$$\frac{d\sigma(q)}{d\Omega} = n\,\Delta\rho^{\,2}\,V_{poly}^{\,2}\,P(q)\,S(q) \qquad (1)$$

In addition to the form factor *P(q)* and structure factor *S(q)* of the particles, the number density of the particles *n*, the difference in scattering length density between the polymer and the solvent $\Delta\rho$ and the volume of polymer in a particle V_{poly} enter the differential scattering cross section $d\sigma(q)/d\Omega$. The difference in scattering length density $\Delta\rho$ which corresponds to the scattering contrast, must be calculated for each microgel suspension due to its dependence on the particle composition (fraction of cross-linking molecules) and the temperature dependent apparent specific density.

For PNiPAM particles a higher degree of cross-linking density is expected inside the particle than outside according to the polymerization kinetics.[57] The resulting inhomogeneous internal particle structure described by the form factor $P_{inho}(q)$ will be fuzzy rather than sharp. We convolute the radial scattering length density profile of a homogeneous sphere with a Gaussian to get a function with a gradual drop-off in scattering length density. These spheres with a fuzzy surface are described by the modified form factor $P_{inho}(q)$

$$P_{inho}(q)=\left[A(q)\right]^2 \text{ with } A(q)=\frac{3\left[\sin(qR)-qR\cos(qR)\right]}{(qR)^3}\exp\left(-\frac{(\sigma_{surf}\,q)^2}{2}\right) \quad (2)$$

where $A(q)$ defines the amplitude of the form factor $P_{inho}(q)$. R and σ_{surf} are the two adjustable parameters, representing the radius of the particle where the scattering length density profile decreased to half the core density and the width of the smeared particle surface, respectively. The inner regions of the microgel which exhibit a higher degree of cross-linking density are described by the radial box profile extending to a radius of about $R_{box} \approx R - 2\sigma_{surf}$. In dilute solution the profile approaches zero at $R_{SANS} \approx R + 2\sigma_{surf}$. Therefore, the overall size of the particle is approximated by the dilute solution radius R_{SANS}.

Thus far, the discussion has focused on monodisperse spheres. However, microgel particles may display a polydispersity. A Gaussian function describing the particle size distribution function $D(R,\langle R\rangle,\sigma_{poly})$ is assumed

$$D(R,\langle R\rangle,\sigma_{poly})=\frac{1}{\sqrt{2\pi\sigma_{poly}{}^2\langle R\rangle^2}}\exp\left(-\frac{(R-\langle R\rangle)^2}{2\,\sigma_{poly}{}^2\langle R\rangle^2}\right) \quad (3)$$

with $\langle R\rangle$ describing the average particle radius and σ_{poly} denoting the relative particle size polydispersity.

The structure factor $S(q)$ accounts for interference of scattering from different particles in concentrated suspensions. Because the structure factor $S(q)$ describes the relative particle-particle positions, it provides information about the interaction of the particles. For monodisperse particles that interact with a spherically symmetric hard sphere interaction potential, $S(q)$ is obtained from liquid state theory employing the Percus-Yevick approximation for the closure relation[78]

$$S(q)=\left(1+\frac{24\eta_{HS}\,G(2R_{HS}\,q)}{2R_{HS}\,q}\right)^{-1} \text{ with} \quad (4)$$

$$G(A)=\frac{\alpha\left(\sin A-A\cos A\right)}{A^2}+\frac{\beta\left(2A\sin A+\left(2-A^2\right)\cos A-2\right)}{A^3}+\frac{\gamma\left[-A^4\cos A+4\left\{\left(3A^2-6\right)\cos A+\left(A^3-6A\right)\sin A+6\right\}\right]}{A^5} \text{ and} \quad (5)$$

$$\alpha = \frac{(1+2\eta_{HS})^2}{(1-\eta_{HS})^4} \quad \beta = \frac{-6\eta_{HS}\left(1+\frac{\eta_{HS}}{2}\right)^2}{(1-\eta_{HS})^4} \quad \gamma = \frac{\eta_{HS}\alpha}{2} \tag{6}$$

The two adjustable parameters in *S(q)* are the hard sphere volume fraction η_{HS} and the corresponding hard sphere radius R_{HS}. The structure factor effects can be treated in a simple decoupling approximation when the particle size polydispersity is low. In this case the structure factor $S(q,\langle R\rangle)$ is calculated for the average size. Including all these factors, the differential scattering cross section can be written:

$$\frac{d\sigma(q)}{d\Omega} = n\Delta\rho^2\, S(q,\langle R\rangle)\int_0^\infty D(R,\langle R\rangle,\sigma_{poly})V_{poly}(R)^2\, P_{inho}(q,R)\, dR \tag{7}$$

The structure factor of hard spheres is the most simple one can think of. It has the further advantage that relatively simple analytical expressions are available for *S(q)*. The highly swollen PNiPAM microgels are quite soft and therefore one might suspect that the hard sphere potential does not work. However, there are numerous examples that it works quite well for other very soft systems, like block copolymer micelles with a highly swollen corona even up to quite high hard sphere volume fractions.[92,93] Thus, we started out with the hard sphere structure factor *S(q)* in the analysis of the PNiPAM microgels described in the present study, and it turned out that it worked very well. We therefore concluded that we did not have sufficient information in our scattering data to allow the use of a structure factor *S(q)* for a more sophisticated interaction potential. We note that some of the (effective) hard sphere volume fractions η_{HS} that we determine are quite high and in fact outside the expected validity range of the model and the Percus-Yevick approximation. Hence, these volume fractions have to be considered as just an empirical parameterization of the structure factor effects, which are present in our data. Consequently, one has to be careful with a physical interpretation of the values in the high concentration regime.

In addition scattering contributions arising from fluctuations of the microgel network are included in the model expression as a Lorentzian function

$$I_{fluct}(q) = \frac{I_{fluct}(0)}{1+\xi^2 q^2} \tag{8}$$

where $I_{fluct}(0)$ is the q = 0 limiting intensity and ξ represents the correlation length of the fluctuations, which can be considered to be related to the blob or mesh size. It should be noted, that the Lorentzian describes the ensemble average correlations in the polymer network.

Finally, the model expression accounts for instrumental smearing of the experimental SANS data. This work uses the approach of Pedersen et al. and includes a resolution function $R(\langle q\rangle, q)$ in the model.[79] Due to the finite collimation of the beam, the wavelength

spread of the incoming neutrons and the finite spatial resolution of the detector a distribution of radiation with scattering vectors *q* around the nominal scattering vector $\langle q \rangle$ also contribute to smearing. These three contributions can be approximated separately by Gaussian functions. The combined resolution function $R(\langle q \rangle, q)$ describing the distribution of scattering vectors *q* contributing to the scattering at the setting $\langle q \rangle$ is obtained

$$R(\langle q \rangle, q) = \frac{q}{\sigma_{smear}^2} \exp\left[-\frac{1}{2}\left(q^2 + \frac{\langle q \rangle^2}{\sigma_{smear}^2} \right) \right] I_0\left(\frac{\langle q \rangle q}{\sigma_{smear}^2} \right) \quad (9)$$

where σ_{smear} represents the width of the instrumental smearing and depends on the different instrumental settings, and I_0 is a modified first kind and zeroth order Bessel function.[80] This expression includes smearing contributions from wavelength smearing (9% FWHM), collimation and detector resolution.

The last factor in the model expression is a constant background $const_{back}$ to account for residual incoherent scattering. After incorporating all contributions the complete model expression for the intensity distribution can be fitted to the experimental data:

$$I^{\mathrm{mod}}(\langle q \rangle) = \int_0^\infty \frac{d\sigma(q)}{d\Omega} R(\langle q \rangle, q) dq \quad \text{with} \quad (10)$$

$$\frac{d\sigma(q)}{d\Omega} = n \Delta\rho^2 S(q, \langle R \rangle) \int_0^\infty D(R, \langle R \rangle, \sigma_{poly}) V_{poly}(R)^2 P_{inho}(q, R)\, dR + I_{fluct}(q) + const_{back} \quad (11)$$

We will now describe a new approach for calculating the average radial density distribution $\phi(r)$ around a particle from the scattering amplitude of the particles *A(q)* and the structure factor *S(q)* (see equation (2) and (4)). A numerical Fourier transformation of it provides the radial density profile of a single particle.

At very high concentrations the particles start to overlap. The overlapping volume fraction of the polymer constitutes a homogeneous component ϕ_{homo} which spans the entire sample. Our work and related studies show, that this contribution must be considered as part of the solvent.[94] The non-overlapping volume fraction of polymer can be regarded as an excess component ϕ_{excess}, which accounts for the modulation of the polymer density beyond the homogeneous component. Thus, the apparent polymer volume in the particle $V_{pol} = (\phi_{poly}\, 4\, \pi\, R^3)/3$ increases with concentration. The true total polymer volume in a particle was obtained from samples in dilute solution. For higher concentrations the fraction of polymer in the homogenous component ϕ_{homo} was calculated and used to correct the measured polymer volume fraction.

The Fourier transform of the structure factor *S(q)* gives the probability distribution of the centers of the particles *g(r)*. With a homogeneous contribution ϕ_{homo}, only the excess polymer

volume fraction ϕ_{excess} is described by *g(r)*. The probability distribution function *g(r)* is therefore normalized to approach ϕ_{excess} at long distances *r*. The total distribution of excess polymer around the center of a particle can be obtained by convoluting *g(r)* by the distribution around the center of a single particle and adding the single particle distribution $\phi_{poly}(r)$. The convolution is done by calculating [*S(q)*-1] *A(q)* and performing a numerical Fourier transformation. This gives a function proportional to $g_{poly}(r)-1$ which is related to the monomers in other particles. This function can easily be normalized leading to $g_{excess}(r)$ which approaches the excess polymer volume fraction ϕ_{excess} at large distances and is zero at short distances. When the single particle distribution $\phi_{poly}(r)$ and the homogeneous contribution is added to this function, it gives the average polymer volume fraction distribution $\phi(r)$ around the center of a particle.

4.4 Results and Discussion

4.4.1 Phase Behavior and Rheological Properties

Concentrated suspensions of the M-1.4/141 microgel form colloidal crystals. The transition from the liquid phase to a colloidal crystal started at an effective volume fraction of $\phi_{eff,f}$ =0.70 as compared to the freezing transition ϕ_f =0.494 for hard spheres. The shift of the freezing transition to higher volume fractions indicates a soft sphere interaction potential[95] which became noticeable at sufficient high concentrations.

Concentrated microgel suspensions are shear thinning. We determined the relative zero shear viscosity $\eta_{0,rel}$ for various temperatures and concentrations from the flow curves as described previously.[20] The relative zero shear viscosity $\eta_{0,rel}$ as a function of effective volume fraction ϕ_{eff} for the M-5.5/115 and M-1.4/141 microgel is shown in figure 1. A line representing $\eta_{0,rel}$ of model hard spheres as provided by Meeker et al.[15] is also plotted. Good agreement of our experimental data with the hard sphere data is obtained up to effective volume fraction of ϕ_{eff}<0.35 for both samples independent of the cross-linking density. At higher volume fractions ϕ_{eff}>0.35 strong deviations from hard sphere behavior are observed. The viscosity diverged for both particles at larger ϕ_{eff}. However, the viscosity master curve of the microgel with a higher cross-linking density (M-5.5/115) runs closer to the hard sphere line and exhibits a smaller ϕ_{max} than the less cross-linked M-1.4/141. The Dougherty-Krieger equation[96] ($\eta_{0,rel} = (1-\phi / \phi_{max})^{-[\eta]\phi max}$) describes the viscosity fairly well when $\phi_{eff,\,f}$ =0.70 was used as ϕ_{max} and the intrinsic viscosity [η]=2.98 for the M-1.4/141 sample. It should be noted, that the particle size polydispersities σ_{poly} which were obtained from the SANS scattering

profiles in dilute solution were similar for both microgels.[89] A polydispersity of σ_{poly}=9.9 % for M-5.5/115 and σ_{poly}=9.7 % for M-1.4/141 was found at 25°C.

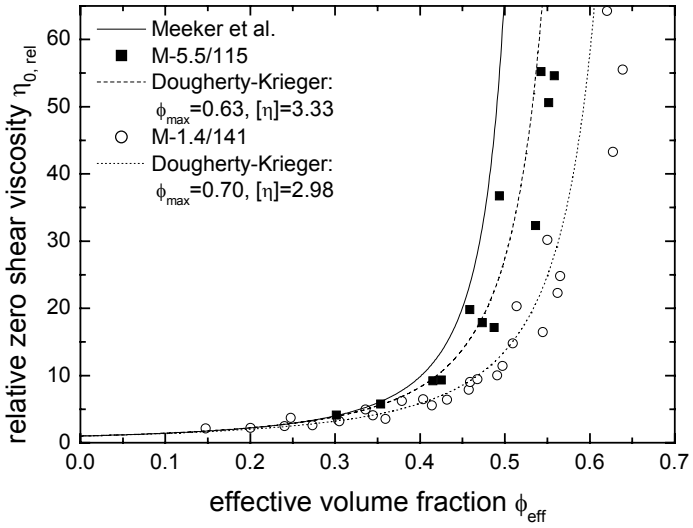

Fig. 1. *Relative zero shear viscosity $\eta_{0,rel}$ vs effective volume ϕ_{eff} fraction for the M-5.5/115 and the M-1.4/141 microgel. The solid line represents model hard sphere data provided by Meeker et al.*

At high concentrations the samples became viscoelastic and were characterized with low amplitude oscillatory shear experiments. The frequency dependence of the storage modulus *G´* and loss modulus *G´´* was investigated and the frequency independent plateau modulus G_P was determined. Figure 2 shows the plateau modulus G_P vs the effective volume fraction ϕ_{eff} for two microgels with different cross-linking density. A mastercurve was obtained for both samples. G_P can be related to the interaction potential $\psi(r) \propto 1/r^n$ and the pair correlation function using an expression given by Zwanzig and Mountain.[97] When a lattice like microstructure is assumed where the particles are arranged at well defined distances one obtains $G_P \propto (1/r)\,(\delta^2\psi / \delta r^2)$.[98] We note, that Wagner has pointed out that hydrodynamic interactions are neglected in this simple approach.[99] The exponent of the interaction potential *n* can be related to the slope of the mastercurve via *m=1+n/3* and *n*=21.9 for M-5.5/115 and *n*=9.5 for M-1.4/141 were obtained. Thus, both particles reveal soft sphere behaviour but the higher cross-linking density of M-5.5/115 leads to a harder interaction potential. A similar influence of the cross-linking density on the interaction potential has been reported by Senff et al.[81]

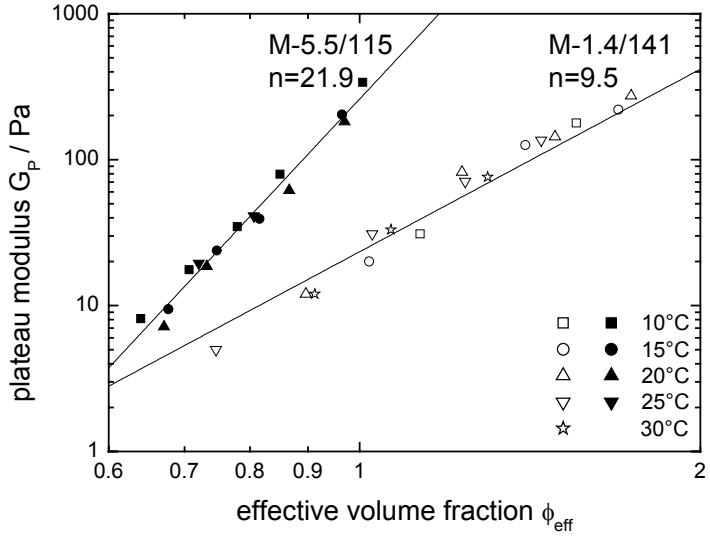

Fig. 2. *Plateau modulus G_P vs effective volume fraction ϕ_{eff} for the M-5.5/115 and the M-1.4/141 microgel. The exponents of the interaction potential n are indicated.*

4.4.2 Structural changes induced by temperature and concentration below the LCST

Figure 3 shows the scattering intensity distribution normalized by the concentration *I(q)/c* for the M-5.5/115 microgel at 25°C for different concentrations. The normalized scattering profiles *I(q)/c* for the same sample but at different temperatures are shown in figure 4. For the sake of clarity some of the data sets were multiplied by constant factors as indicated in the diagrams. The lines represent fits according to equation (10). The model describes very well the experimental data at all concentrations and temperatures over the entire *q*-range.

At 25°C, well below the LCST the main contribution to the overall scattering intensity *I(q)* in the low *q*-regime (ca. 0.0014 $Å^{-1}$<*q*<0.0055 $Å^{-1}$) arises from the structure factor *S(q)*. The evolution of the structure factor peak with concentration can be nicely traced in the low *q*-regime. Already at a mass concentration of *c*=2.0 wt% which corresponds to an effective volume fraction of ϕ_{eff}=0.20 a broad maximum in the scattering profile is observed. This indicates that the contribution of the structure factor *S(q)* to the overall scattering intensity *I(q)* must be considered and the correlations between different particles can not be neglected although the mass concentration is fairly low. With increasing concentration a decrease of the width of the structure factor peak is observed which is accompanied by an increase of the peak height. A shift of the structure factor peak towards larger *q*-values with increasing concentrations reveals a decrease of the average particle-particle distance.

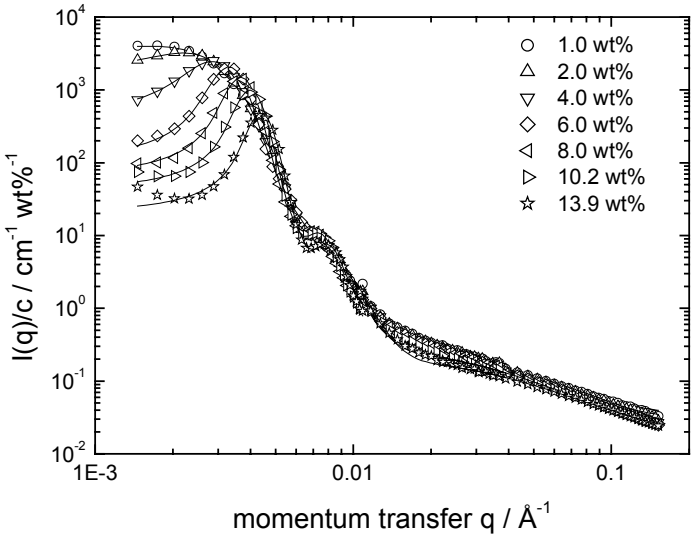

Fig. 3. *Intensity distribution normalized on concentration I(q)/c vs momentum transfer q for various concentrations of the M-5.5/115 microgel at 25°C. The lines represent fits according to equation (10).*

The forward scattering intensity *I(q)* for $q \rightarrow 0$ is reduced by a factor of ca. 80 when the concentration is raised. At high concentrations (10.2 and 13.9 wt%) *I(q)* does not reach a constant value for $q \rightarrow 0$ but increases. Those highly concentrated samples reached the glass state. The slowing down of the particle dynamics due to the cage effect in the glass state becomes more efficient with increasing concentration. Eventually, structural relaxation freezes and the structural inhomogeneties of the glassy dispersion can be observed on large length scales. This leads to an increase of *I(q)* for $q \rightarrow 0$.

In the intermediate *q*-range (ca. 0.0055 $Å^{-1} < q < 0.03\ Å^{-1}$) the main contribution to the overall scattering intensity *I(q)* arises from the form factor $P_{inho}(q)$. Changes of the course of the scattering profiles as well as a shift of the form factor minimum towards higher *q*-values are observed with increasing concentration (figure 3 and figure 4). This indicates the compression of the particles at high concentrations. In contrast to rigid hard spheres the particle form factor $P_{inho}(q)$ of the swollen PNiPAM microgel spheres obviously depends on concentration.

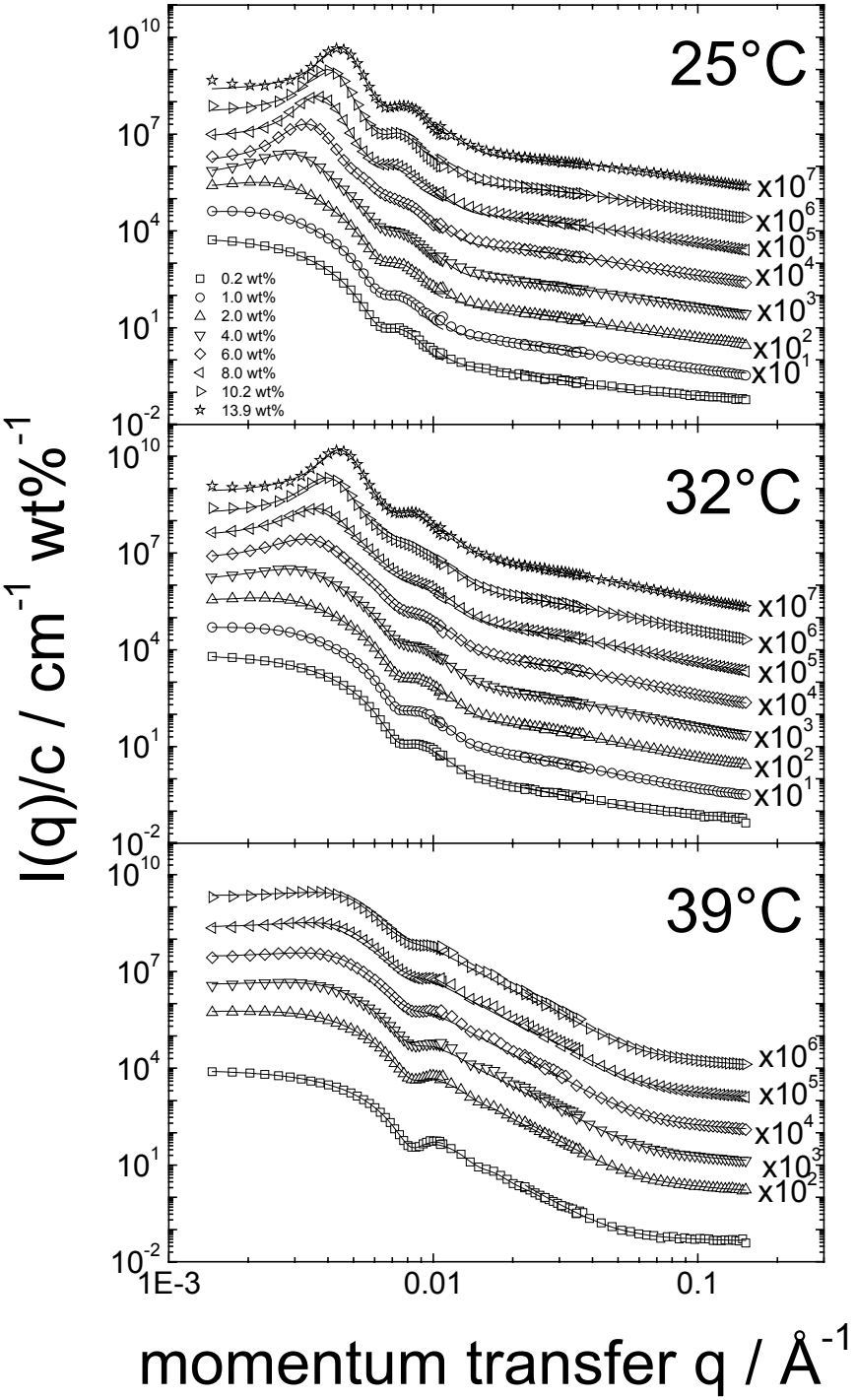

Fig. 4. *Intensity distribution normalized on concentration I(q)/c vs momentum transfer q for various concentrations of the M-5.5/115 microgel at 25°C, 32°C and 39°C. For the sake of clarity some of the data sets were multiplied by constant factors as indicated. The lines represent fits according to equation (10).*

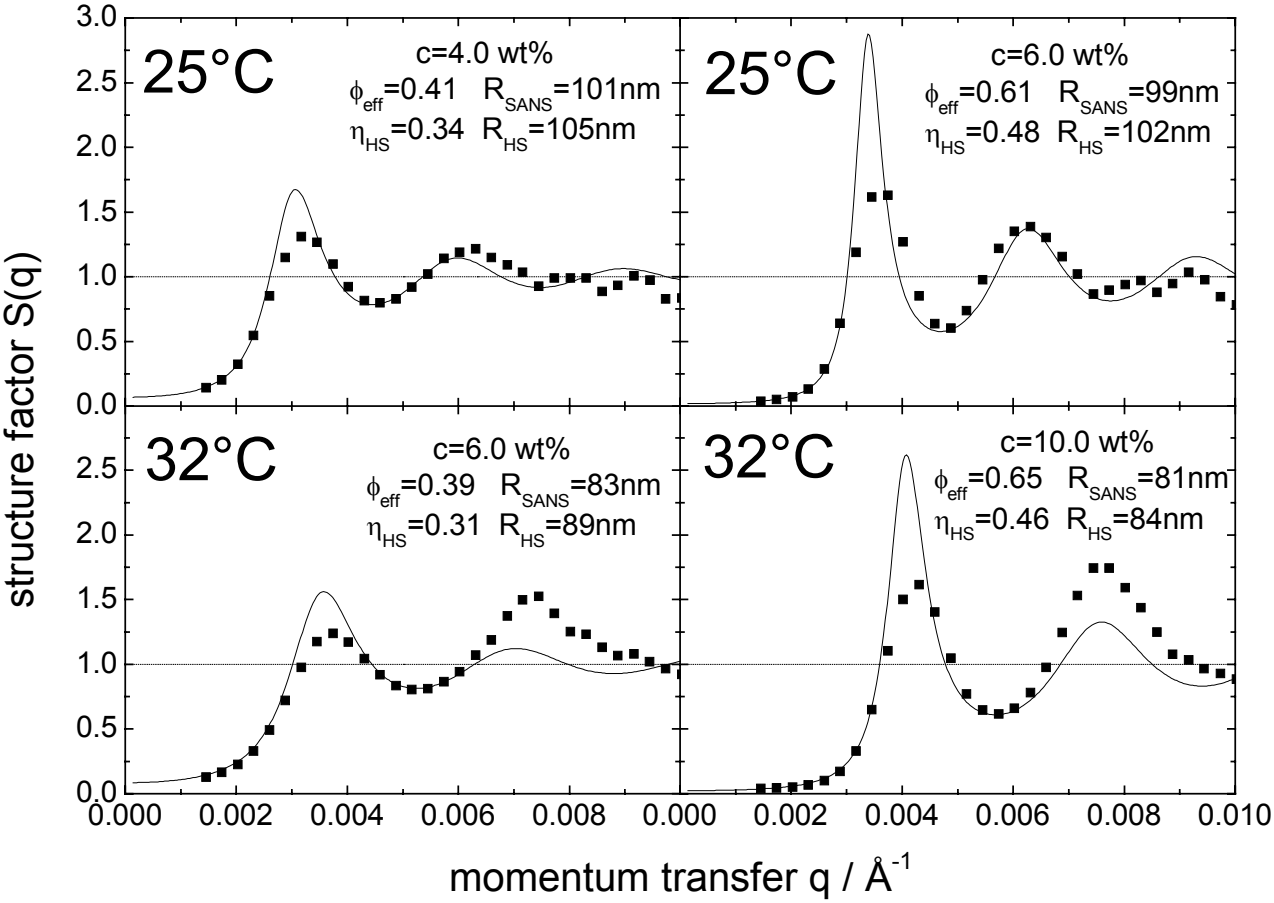

Fig. 5. *Comparison of the structure factor S(q) obtained from the fitting procedure (line) taking the concentration dependence of the form factor $P_{inho}(q)$ into account and obtained by division of $[I_{conc}(q)/c_{conc}]/[I_{dil}(q)/c_{dil}]$ assuming a concentration independent $P_{inho}(q)$ (symbol).*

Figure 5 compares the structure factor *S(q)* obtained by two different methods: the lines represent the structure factor *S(q)* obtained from the direct modeling and thus taking the concentration dependence of the form factor $P_{inho}(q)$ into account by performing simultaneously a free fit of $P_{inho}(q)$ and *S(q)*. It should be noted, that the quality of the fits is very good (see for example figure 4). The fits obtained by the full fitting procedure have reduced χ^2-values in the range of $5 < \chi^2 < 50$. Therefore, the structure factors *S(q)* derived by this procedure are quite reliable. In figure 5 the symbols denote the structure factor *S(q)* obtained by dividing the normalized scattering intensity distribution of a concentrated sample by the profile of a dilute sample $[I_{conc}(q)/c_{conc}]/[I_{dil}(q)/c_{dil}]$ assuming that the particle form factor $P_{inho}(q)$ remains unchanged with concentration. At 25°C the differences between the structure factors *S(q)* obtained from the fitting procedure and the division of the experimental intensity distributions $[I_{conc}(q)/c_{conc}]/[I_{dil}(q)/c_{dil}]$ are fairly small. In contrast, at 32°C significant

deviations between the structure factors *S(q)* obtained by the two approaches are observed. At 32°C the second peak of *S(q)* obtained by the dividing procedure is even higher than the first peak clearly indicating the error made by neglecting the concentration dependence of the form factor. The cross-linking density of the PNiPAM particles decreases gradually with increasing distance to the particle center. The elasticity of the polymer network is expected to be smaller at the outer regions of the particle than the inner. Therefore the outer regions can be compressed easier. An estimate of the relative contributions of the less cross-linked outer regions to the overall particle size is provided by the ratio of the width of the smeared particle surface σ_{surf} to the overall particle size R_{SANS}. When the temperature is altered from 25°C to 32°C a slight increase of σ_{surf}/R_{SANS} is observed.[89] Hence, the compression of the particles is more efficient at the higher temperature. When a concentration independent particle form factor $P_{inho}(q)$ is assumed, the compression of the particles is entirely neglected. The resulting error in the calculation of the structure factor *S(q)* according to $[I_{conc}(q)/c_{conc}]/[I_{dil}(q)/c_{dil}]$ is thus larger at 32°C than at 25°C which is in good agreement with the data shown in figure 5.

Next the high *q*-regime (ca. 0.03 $Å^{-1}<q<0.16$ $Å^{-1}$) will be discussed where the main contribution to the overall scattering intensity arises from concentration fluctuations of the polymer network which can be described by a Lorentzian (equation (8)). The correlation length ξ can be considered to be related to the blob size describing the ensemble average correlations of the polymer network. Due to the high incoherent background and the rather large statistical error of the experimental data in the high *q*-regime it was not possible to obtain ξ from dilute PNiPAM suspensions with high accuracy.[70,71,72,89] However, the statistics of the SANS data discussed in the present work was significantly better since the samples were more concentrated. The correlation length ξ was obtained reliably from the fitting procedure and the effective volume fraction ϕ_{eff} dependence of ξ for the M-5.5/115 microgel at 25°C can be seen in figure 6. A decrease of ξ is observed with increasing effective volume fraction ϕ_{eff}. Thus, the network fluctuations are restricted to smaller length scales at high effective volume fractions ϕ_{eff}. Apparently, the above observed compression of the particle with increasing concentration also leads to changes in the internal network structure indicating that the entire particle is compressed and not only the fuzzy surface.

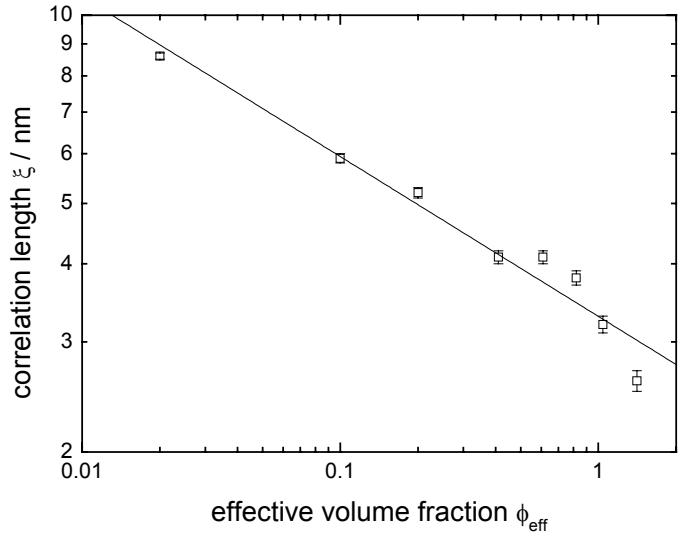

Fig. 6. *Correlation length of the network fluctuations ξ vs effective volume fraction ϕ_{eff} for the M-5.5/115 microgel at 25°C. A power law behavior is observed $\xi \propto \phi_{eff}^{-0.26}$.*

The normalized scattering intensity distributions *I(q)/c* of the larger particles M-1.5/353 obtained at various concentrations and temperatures are shown in figure 7. Compared to the M-5.5/115 sample which has a higher degree of cross-linking density and smaller particle size both the form factor minima and the structure factor peaks are shifted towards lower *q*-values.

The thermoresponsive PNiPAM particles shrink when the temperature is raised. The temperature induced deswelling leads to a decrease of the effective volume fraction ϕ_{eff} while the mass concentration *c* and the particle number density *n* is not changed. By the temperature variation, scattering profiles *I(q)/c* obtained at different effective volume fractions ϕ_{eff} can be compared without changing the concentration *c*. When the temperature is raised, the form factor minima shift to higher *q*-values for the M-5.5/115 and M-1.5/353 microgel (figure 4 and figure 7). In contrast, the position of the structure factor peak remains unchanged upon heating at a given concentration *c*. The shift of the form factor minima indicate the temperature induced shrinkage of an individual particle whereas the unchanged position of the structure factor peak demonstrates that the average particle-particle distance is not altered. The center to center distance between different particles depends only on the particle number density *n* but is independent of the size of an individual particle.

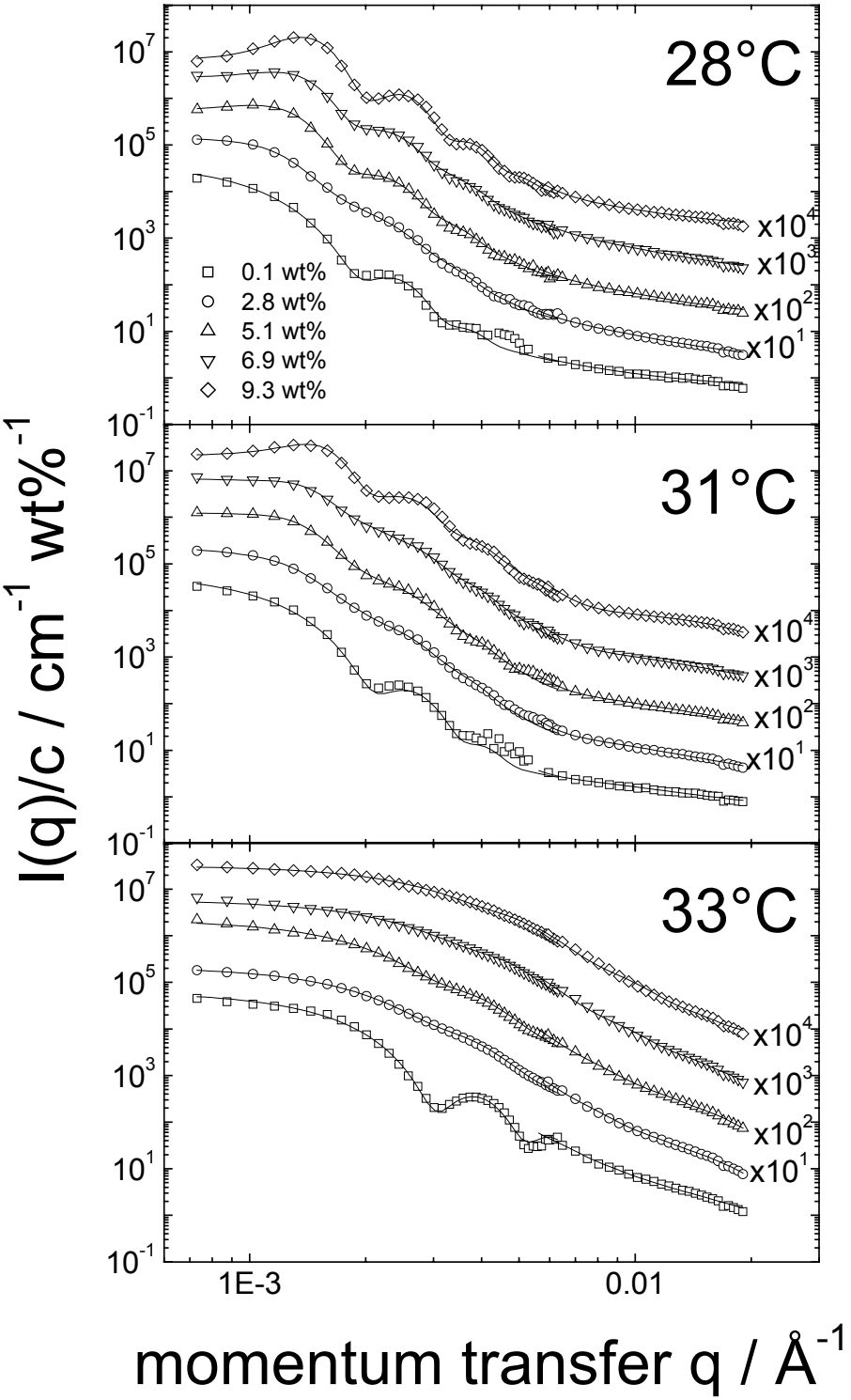

Fig. 7. *Intensity distribution normalized on concentration I(q)/c vs momentum transfer q for various concentrations of the M-1.5/353 microgel at 28°C, 31°C and 33°C. For the sake of clarity some of the data sets were multiplied by constant factors as indicated. The lines represent fits according to equation (10).*

The real space structures of the M-5.5/115 microgel at different concentrations and temperatures are revealed by the polymer volume fraction profiles $\phi(r)$ which are shown in figure 8. The higher the concentration the more maxima in the density profiles $\phi(r)$ are observed. The maxima in $\phi(r)$ indicate the position of the surrounding neighbors of a particle. The shift of the position of the maxima in the polymer volume fraction profiles $\phi(r)$ to smaller distances r clearly reveals the increasing compression of the particles with increasing concentration. At high concentrations the volume fraction profiles $\phi(r)$ do not approach zero anymore indicating the increasing overlap of the particles. A certain volume fraction of the polymer constitute a homogeneous component ϕ_{homo} which spans the entire sample. The polymer volume fraction in the center of a particle $\phi(0)$ increases slightly with concentration. The overlap of the particles is restricted to the outer regions of the sphere which exhibit a lower degree of cross-linking density. The inner regions of the particle which are characterized by the box profiles up to a distance of R_{box} do not interpenetrate. At large distances r the density profiles $\phi(r)$ approach the average polymer volume fraction which is given by the mass concentration.

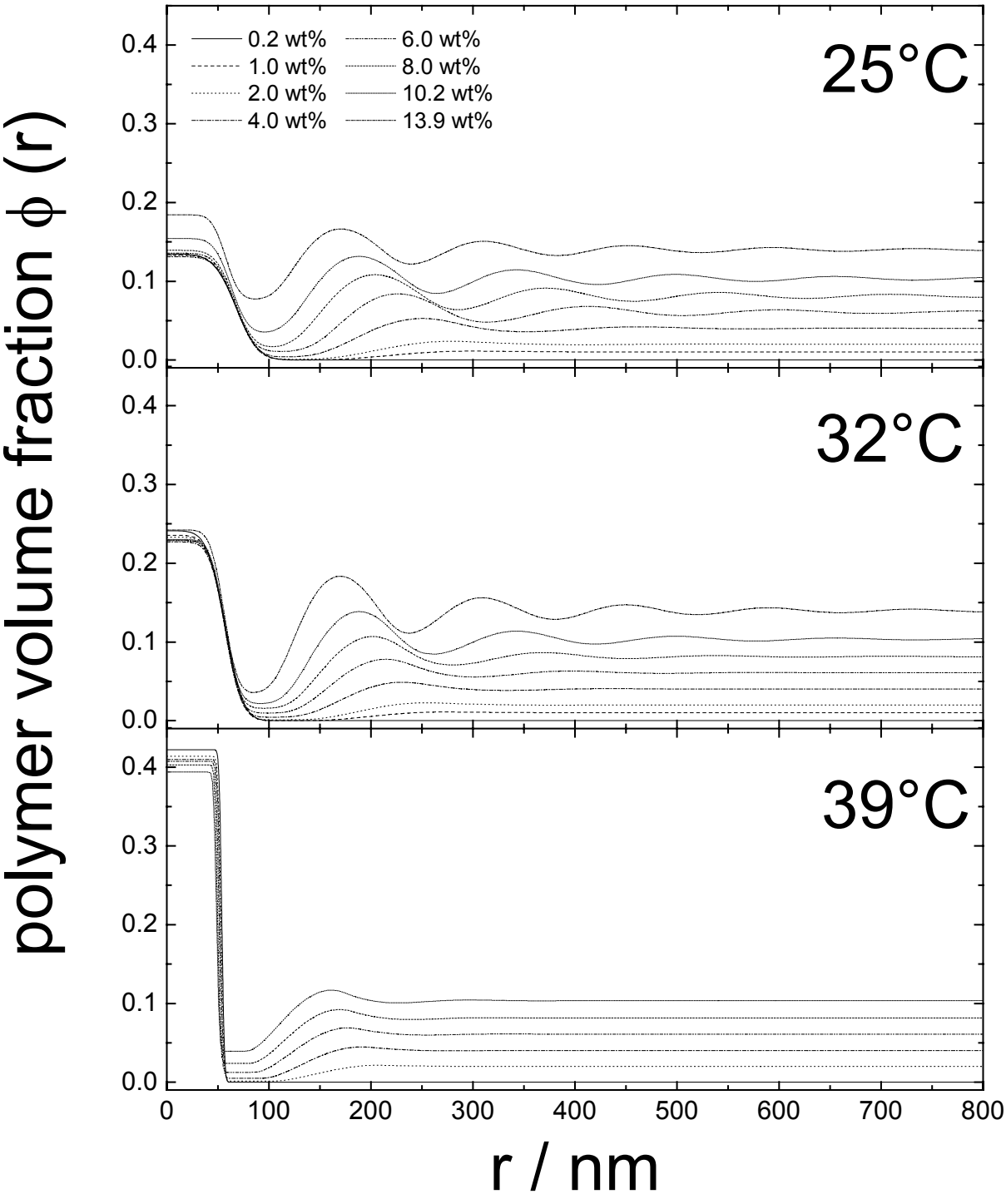

Fig. 8. *Radial polymer volume fraction profiles $\phi(r)$ for different concentrations of M-5.5/115 at 25°C, 32°C and 39°C.*

With increasing temperature the polymer volume fraction in the center of the particle $\phi(0)$ increases significantly. The observation of well-defined maxima in the density profiles $\phi(r)$ at 32°C reveal a long-ranged ordered structure although the temperature is only approximately 1K below the LCST.

To obtain information about temperature induced changes in the interaction potential, figure 9 compares the normalized polymer volume fraction profiles $\phi(r)/c$ vs $r/R_{SANS(dilute)}$ at different temperatures for similar effective volume fractions ϕ_{eff}. The normalized polymer volume fraction profiles $\phi(r)/c$ at 25°C and 32°C coincide on a single curve for all effective volume fractions ϕ_{eff}. The structure formation depends only on the effective volume fraction ϕ_{eff}. Thus, the particle-particle interaction potential does not change significantly between 25°C and 32°C. Even approximately 1K below the LCST the experimental scattering intensity distributions $I(q)/c$ are described very well by the hard sphere structure factor $S(q)$ (see figure 4). This might indicate that the interaction potential is still repulsive at 32°C. An attractive interaction potential would eventually lead to aggregation of the particles giving rise to an increase of the scattering intensity $I(q)/c$ in the very low q-regime (0.001 $Å^{-1} < q$) which was not investigated in our experiments.

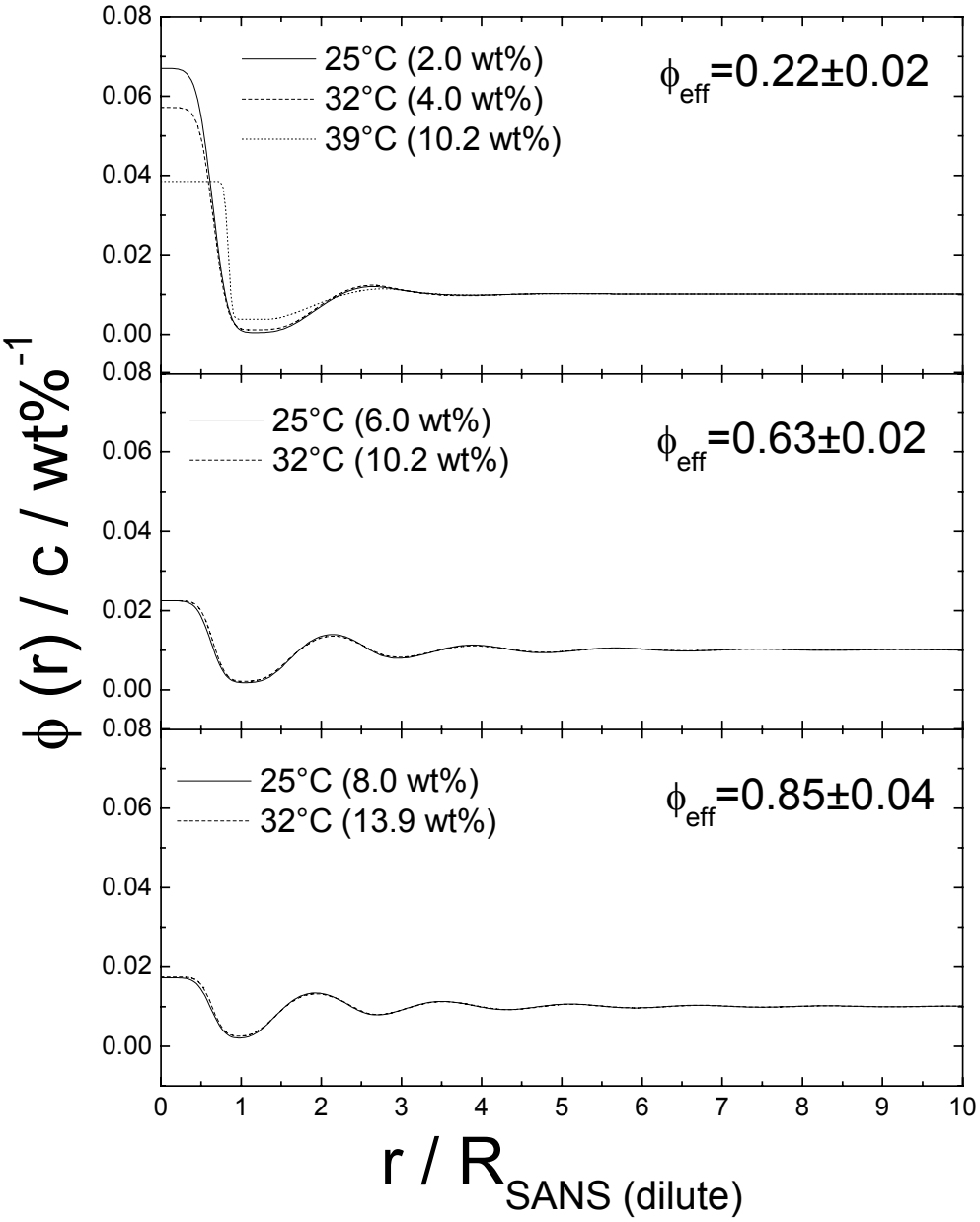

Fig. 9. *Normalized radial polymer volume fraction profiles $\phi(r)/c$ vs $r/R_{SANS(dilute)}$ for M-5.5/115 at 25°C and 32°C for similar volume fractions but different concentrations.*

As mentioned previously (section IV.A), concentrated suspensions of the M-1.4/141 microgel form colloidal crystals. The temperature induced phase transition from a colloidal crystal to a liquid was investigated by SANS and the normalized intensity distributions *I(q)/c* are shown in figure 10. First, second and third order Bragg peaks are observed at 26°C indicating a highly ordered crystal lattice structure. Upon heating the effective volume fraction ϕ_{eff} decreases and the crystal melts. The Bragg peaks of higher order vanish but, again, the

position of the structure factor peak does not change with temperature since the particle number density *n* was not altered.

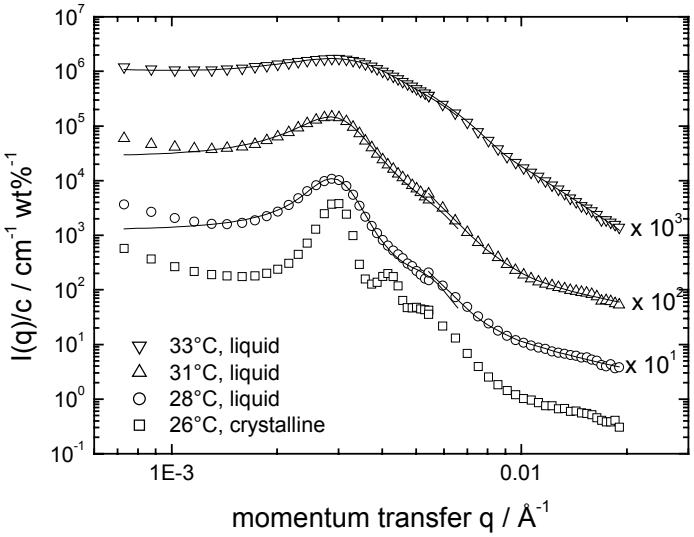

Fig. 10. *Temperature induced crystalline-liquid phase transition for M-1.4/141 at a concentration of c= 3.6 wt% seen by SANS. The lines represent fits according to equation (10).*

4.4.3 Structure formation at temperatures above the LCST

At temperatures above the LCST macroscopic phase separation occurs in concentrated PNiPAM microgel suspensions. The structure factor peaks which were observed for the M-5.5/115 and M-1.5/353 microgel at temperatures below the LCST almost vanished for all concentrations at 39°C (figure 4 and figure 7). The corresponding polymer volume fraction profiles $\phi(r)$ obtained for the M-5.5/115 at 39°C are shown in figure 8. The polymer volume fraction in the center of a particle $\phi(0)$ is almost independent of concentration. Even in the collapsed state the particles still contain more than 55% water. The particle surface sharpened dramatically compared to temperatures below the LCST. Only one broad maximum is observed in the density profiles $\phi(r)$ at high concentrations indicating only one well-defined layer of surrounding neighbour particles. At 39°C, which is well above the LCST, the collapsed particles have obviously formed a structure without any long-range order. The strongly attractive interaction potential led to an aggregation of the spheres. The aggregates comprise of polymer particles that are flocculated together and interpenetrate strongly. Actually, this effect is used for film formation in microgel based polymer coatings. Thus, the structure formation of the PNiPAM microgels at temperatures above the LCST is distinctively different compared to attractive hard sphere colloids. An attractive interaction potential in

suspensions of rigid hard spheres should not lead to random polymer-like flocs but to the formation of aggregates with a higher degree of long-range order.

4.4.4 Comparison of PNiPAM microgels with different cross-linking densities and particle sizes

Figure 11 compares the effective volume fraction ϕ_{eff} obtained from viscometry in dilute solution with the hard sphere volume fraction η_{HS} determined from the fitting procedure of the experimental scattering curves. Data for the three microgels at various temperatures and concentrations is presented together with a line representing hard sphere behavior e.g. $\phi_{eff} = \eta_{HS}$. Independent of the cross-linking density or size all microgels reveal hard sphere behavior up to $\phi_{eff} \approx 0.35$. At higher effective volume fractions $\phi_{eff} > 0.35$ the softness of the particles is revealed and strong deviations from the hard sphere behavior occur. It should be noted again, that the Percus-Yevick hard sphere model agrees with simulations of hard spheres up to volume fractions of about $\eta_{HS} \approx 0.45$. At higher volume fractions η_{HS} the Percus-Yevick model is not expected to be valid, resulting in an underestimation of concentration effects. Thus, caution must be taken interpreting the results obtained from the fits of the highly concentrated samples.

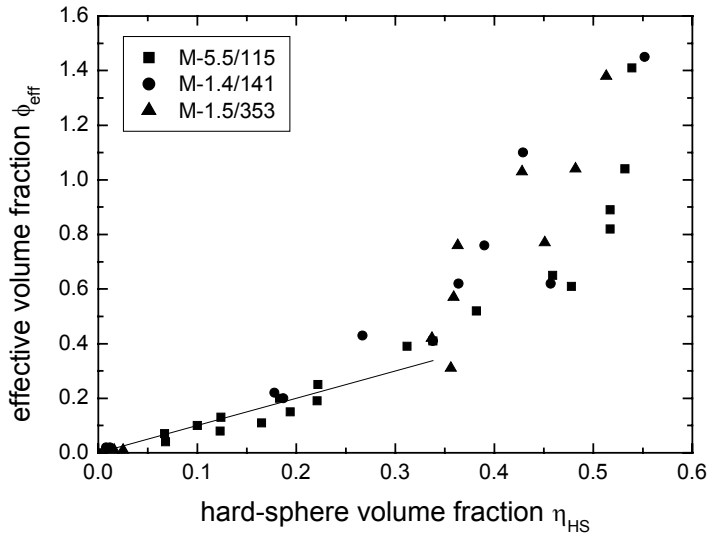

Fig. 11. *Effective volume fraction ϕ_{eff} vs hard sphere volume fraction η_{HS} for all microgels at all temperatures. The line represents hard sphere behavior ($\phi_{eff} = \eta_{HS}$).*

The particle radius R_{SANS} determined from the fits of the form factor $P_{inho}(q)$ and the hard sphere radius R_{HS} obtained from the structure factor $S(q)$ fit are displayed as a function of the

effective volume fraction ϕ_{eff} in figure 12 for the M-5.5/115 and M-1.4/141 microgel. At all temperatures a gradual decrease of both R_{SANS} and R_{HS} with increasing effective volume fraction ϕ_{eff} is observed. The strong decrease at high effective volume fractions ϕ_{eff} is caused by compression of the soft PNiPAM particles as discussed in section IV.B.. Surprisingly, already at rather small effective volume fractions ϕ_{eff}<0.35 a decrease of both radii is observed which can not be caused by interpenetration of the particles. This effect might be due to a form of excluded volume screening. For the individual particle, a slight shrinkage leads to a loss of configurational entropy of the polymer strands inside the particle. On the other hand, the microgel particle gains translational entropy. At higher concentrations, the overlap of the particles that we consider as part of a flat solvent background (see section III.) will make the particles smaller even at small effective volume fractions ϕ_{eff}. In fact, the particle is considered only to be the contribution which is above the background.

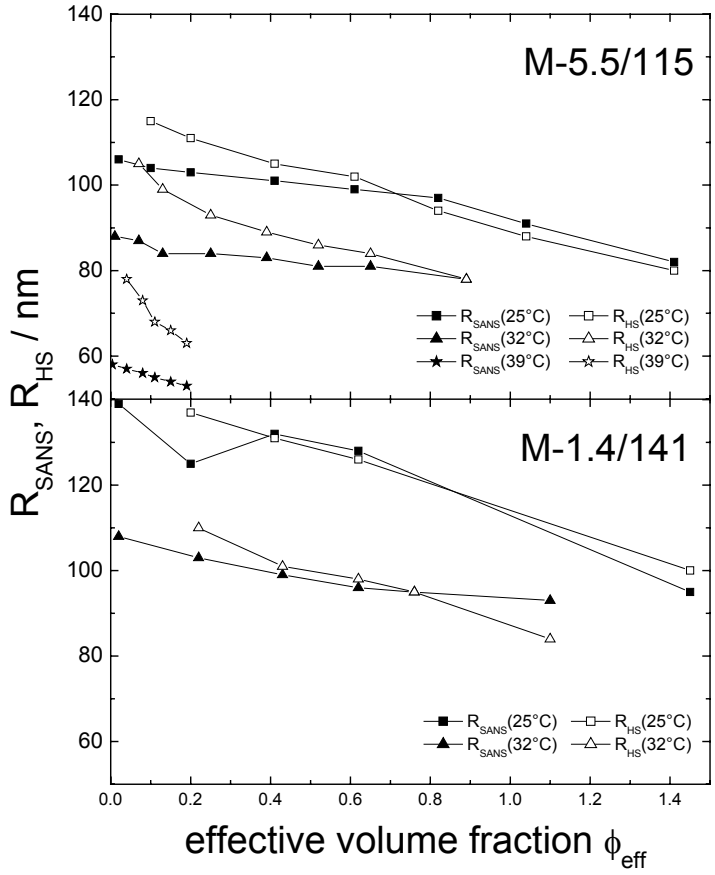

Fig. 12. *Radii obtained from the analysis of the form factor R_{SANS} and structure factor R_{HS} vs effective volume fraction ϕ_{eff} for the M-5.5/115 and M-1.4/141 microgels.*

4.5 Conclusions

We address the question whether thermoresponsive PNiPAM microgels can be used as model systems for concentrated colloidal suspensions. A previously described model expression for the particle form factor $P_{inho}(q)$ is extended by a model hard sphere structure factor $S(q)$ in order to describe experimental data at high concentration. The particle form factor $P_{inho}(q)$ accounts for the inhomogeneous distribution of the polymer segment density throughout an individual particle whereas the Percus-Yevick hard sphere structure factor $S(q)$ describes the correlations between different particles. Average radial density profiles $\phi(r)$ are calculated from the amplitude of the form factor $A(q)$ and the structure factor $S(q)$. By this procedure a direct real space description of the spatial ordering in the neighborhood of a single particle is obtained. The model expression describes the experimental scattering intensity distributions $I(q)$ very well over the entire q-regime for a broad range of concentrations at temperatures below as well as above the LCST. The main conclusions are:

a) The overall particle size and the correlation length ξ of the concentration fluctuations of the internal polymer network decrease with concentration revealing the increasing compression of the spheres. In contrast to suspensions of rigid hard spheres, the concentration dependence of the particle form factor $P_{inho}(q)$ of the swollen PNiPAM microgels needs to be accounted for when structure factors $S(q)$ of concentrated suspensions are discussed.

b) The particle-particle interaction potential does not change significantly between 25°C and 32°C. Even approximately 1K below the LCST the experimental scattering intensity distributions $I(q)/c$ are described very well by the hard sphere structure factor $S(q)$ by using an equivalent hard sphere particle size R_{HS} and volume fraction η_{HS}. The hard sphere parameters $R_{HS}(c)$ and $\eta_{HS}(c)$ differ from R_{SANS} and the effective volume fraction ϕ_{eff}. At 39°C, which is well above the LCST, the interaction potential becomes strongly attractive leading to macroscopic phase separation. The collapsed microgel spheres form aggregates consisting of flocculated particles without significant long-range order. Instead only one well-defined layer of surrounding neighbour particles is observed. Hence, an attractive interaction potential in concentrated suspensions of PNiPAM microgels leads to distinctively different structures as compared to attractive hard sphere colloids.

c) As mentioned above, concentrated suspensions of PNiPAM microgel particles can be described within the frame work of a hard sphere structure factor $S(q)$ when equivalent hard sphere parameters R_{HS} and η_{HS} are employed. Microgels with different degrees of cross-linking and particle size resemble true hard sphere behavior up to effective volume fractions of $\phi_{eff}<0.35$. At higher effective volume fractions $\phi_{eff}>0.35$ strong deviations from true hard spheres are observed. Interpenetration of the outer, less cross-linked regions of the soft

spheres as well as particle compression occur at higher concentrations. The equilibrium colloidal phase behavior also reveals a soft sphere behavior as indicated by the shift of the freezing transition ϕ_f towards higher effective volume fractions. The divergence of the relative zero shear viscosity $\eta_{0,rel}$ occurs at higher effective volume fractions ϕ_{eff} as well and the power law concentration dependence of the plateau modulus G_P reveals typical soft sphere behavior.

Thermoresponsive PNiPAM microgels can be considered a model system in colloidal science when the above mentioned properties are taken into account. The temperature sensitivity leads to several advantages over other systems: i) The preparation of concentrated samples at low temperatures is facilitated since the suspensions can be prepared at elevated temperatures with low viscosity and cooling will lead to homogeneous particle swelling. ii) The liquid-solid transition (crystallization and glass transition) can be investigated both as a function of concentration at constant temperature and as a function of temperature at a constant particle number density. iii) The aggregation behavior near the LCST can be used to study the onset of film formation.

ACKNOWLEDGMENTS. Financial support by the Deutsche Forschungsgemeinschaft and the Danish Natural Science Research Council is gratefully acknowledged.

5 Structure Formation in Microgel Suspensions Under Shear Flow

ABSTRACT: Shear-induced structures of concentrated temperature-sensitive poly(*N*-isopropylacrylamide) (PNiPAM) microgel suspensions have been studied employing small angle neutron scattering (rheo-SANS). The interaction potential of swollen PNiPAM microgels could be varied from repulsive at temperatures below the lower critical solution temperature (LCST) to attractive at temperatures above the LCST. In contrast to suspensions of rigid spheres, the effective volume fraction could be changed by temperature while the mass concentration and particle number density were kept constant. Thus, aqueous PNiPAM microgels are interesting model systems with unique colloidal properties. Complementary information about shear-induced changes of both the internal particle structure and the overall microstructural phenomena were obtained from rheo-SANS experiments with PNiPAM microgels with different particle sizes. The shear-induced particle arrangements strongly depended on the particle-particle interaction potential. When the interaction potential was repulsive at temperatures below the LCST, no significant deformation of the swollen PNiPAM particles was observed even at high shear rates. Shear-induced ordering was found at high shear rates resulting in the formation of two dimensional hexagonal close packed layers that aligned along the flow direction giving rise to shear thinning. The formation of sliding hexagonal close packed layers under shear flow is therefore proposed to be a general property of colloidal dispersion independent of the internal structure of the particle. At temperatures near the LCST, when the particle interaction potential is not yet strongly attractive, shear flow induces the collapse of an individual particle in concentrated suspension at high shear rates. A so-called butterfly scattering pattern indicates the shear-induced enhancement of concentration fluctuations along the flow direction leading to solvent being squeezed out of the particles until phase separation occurs finally.

5.1 Introduction

Colloidal microgels have attracted great interest as model systems in soft condensed matter science to study the structure and dynamics of concentrated suspensions.[3] In particular, the equilibrium phase behavior and rheology have been thoroughly investigated.[87,88] Usually, microgels are prepared by emulsion polymerization techniques. Microgels can be considered intermediates between sterically stabilized colloids and macroscopic polymer gels. Like colloids, spherical microgels are usually limited to

mesoscopic dimensions ranging from several nanometers to a few microns. But in contrast to conventional latex dispersions, microgels are chemically cross-linked particles that are swollen by a good solvent and due to their lyophilic character no special stabilization is needed to avoid aggregation. The internal structure of a microgel is that of a swollen polymer network and can be compared with macroscopic gels.

Thermoresponsive microgels facilitate control of a large variety of colloidal properties by temperature. Water-swellable microgels consisting of poly(*N*-isopropylacrylamide) (PNiPAM) are known to undergo a temperature-induced volume phase transition when the lower critical solution temperature (LCST) of ca. 33°C is approached. At temperatures below the LCST water is a good solvent and the particles are highly swollen. At elevated temperatures the solvent quality changes and above the LCST water is a non-solvent leading to the collapse of the particles and eventually phase separation in concentrated suspension. Thus, a major advantage of thermoresponsive PNiPAM microgels is that the particle-particle interaction potential can be controlled by temperature.[2,4,9] The interaction potential is repulsive at temperatures well below the LCST and does not change significantly up to approximately 1K below the LCST. At temperatures above the LCST, the interaction potential becomes attractive. The size of the particle decreases with increasing temperature. Hence, an additional interesting property of PNiPAM microgels is that the effective volume fraction ϕ_{eff} can easily be controlled by simple temperature changes while the mass concentration c and thus the particle number density n are kept constant. The degree of swelling changes with temperature and the rigidity of the particles is expected to depend on temperature as well.

Since colloidal dispersions play an important role in many different industrial applications, the rheological behavior and flow properties have been studied intensively.[25] Colloidal dispersions under shear reveal a large variety of distinct changes of the particle arrangement with shear rate. The shear-induced structures depend strongly on the particle-particle interaction potential. Various methods including light and small-angle neutron were employed to study the flow-induced structures in colloidal systems with different interaction potentials. The formation of different structures during flow have been predicted by non-equilibrium molecular dynamics simulations without hydrodynamic interaction[26] and by Stokesian dynamics simulations including hydrodynamic interactions.[27] For both purely repulsive hard spheres[28,29,30] as well as electrostatic stabilized particles,[31,32,33] shear thinning is often observed in concentrated dispersions. After application of shear flow a structural transition from fluid-like particle ordering to two-dimensional hexagonal close-packed (2D hcp) layers occurs which are arranged to minimize the resistance against flow.[28,29,30,31,32,33] The shear thickening in hard sphere and electrostatic stabilized suspensions which occurs when high shear rates are applied can be attributed to the formation of jamming clusters bound together by hydrodynamic lubrication forces, often referred to as hydroclusters.[34] The influence of

shear flow on the structure of gel-forming sticky hard spheres was studied by Verduin et al.[35] At low shear rates the formation of larger structures aligned mainly along the flow direction was observed. At higher shear rates of the cloud point was shifted. Occasionally, shear flow in colloidal systems can also lead to aggregation or the formation of large-scale bundle ordering.[36] Shear-induced distortions of the microstructure in directions perpendicular to the flow were observed in near-critical suspensions of colloid-polymer mixtures under stationary shear flow.[37] Especially in the vicinity of the gas-liquid critical point the influence of shear flow on the concentration fluctuations was found to be substantial.[38]

To our knowledge very little is known about the influence of shear flow on the structure of suspensions of thermoresponsive microgels. Unlike suspensions of rigid spheres, the effective volume fraction ϕ_{eff} of microgel suspensions changes with temperature. The liquid-solid transition is shifted to higher concentrations with increasing temperature, due to particle collapse at temperatures above the LCST. Particle collapse occurs due to the changing interaction potential from repulsive to attractive which is in turn a result of decreasing solvent quality. Previously, we observed shear-induced phase separation for aqueous suspensions of PNiPAM microgels.[73] Changes in the cloud curve under shear flow were present when the particle density was sufficiently high to be above the liquid-solid transition. The solvent squeezing mechanism, which describes the dynamic coupling between concentration fluctuations and stress, seems to describe this phenomenon.[56]

In this contribution we address the question of whether the differing colloidal properties of PNiPAM microgels as compared to rigid spheres give rise to different particle arrangements under shear flow. Two PNiPAM microgels with different particle sizes but similar cross-linking density (M-1.4/141 and M-1.5/353) were investigated by means of small-angle neutron scattering under various shear conditions (rheo-SANS). The scattering intensity distributions *I(q)* were obtained in the *q*-regime of ca. $0.0008\ \text{Å}^{-1} < q < 0.006\ \text{Å}^{-1}$ where *q* denotes the magnitude of the momentum transfer. For the large particles (M-1.5/353), the main contribution to the overall scattering intensity *I(q)* in this *q*-regime arises from contributions of the particle form factor *P(q)*. Hence, detailed information about the influence of shear flow on the internal structure of an individual particle in concentrated suspension is obtained from scattering experiments with the M-1.5/353 sample. Under shear the highly swollen particles might be deformed. In the case of the small PNiPAM particles (M-1.4/141), the scattering intensity distribution *I(q)* in this *q*-regime is dominated by contributions of the structure factor *S(q)*. Thus, studying the small M-1.4/141 particles leads to information about changes in the overall microstructure and shear-induced ordering. Both microgels were studied at temperatures well below and close to the LCST to reveal the influence of the particle-particle interaction potential on the shear-induced structure formation. In addition, the rheological behavior will be presented.

5.2 Experimental part

Synthesis and characterization of the PNiPAM microgels has been described elsewhere.[20,73,81,89,105] In this work, a standard naming procedure for the PNiPAM microgels is followed: the two numbers in the sample name refer to the degree of cross-linking as the molar ratio of cross-linker to monomer, and to the hydrodynamic radius in nm at 25°C in heavy water obtained by dynamic light scattering. For example, the M-1.4/141 microgel exhibits a cross-linking density of 1.4 mol % cross-linker *N*,*N´*-methylenbisacrylamide and a hydrodynamic radius of R_h(25°C) = 141 nm.

Small angle neutron scattering experiments under shear (rheo-SANS) were performed at the instrument D11 of the Institute Laue-Langevin (ILL) in Grenoble, France. The neutron wavelength was λ = 6 Å or λ = 12 Å with a spread of $\Delta\lambda / \lambda$ = 9 %. The data were collected on a two-dimensional multidetector (64 x 64 elements of 1 x 1 cm^2) at a sample-detector distance of 36.7 m. The data were corrected for background and empty cell scattering. A Bohlin CVO-120-HR rheometer was adjusted to the D11 beamline. Measurements were performed using a Searle shear cell of quartz cylinders with a gap of 1 mm. The scattering experiments were performed in the radial position yielding information in the plane formed by the flow and vorticity directions. To obtain a one-dimensional data set *I(q)*, further processing of the two-dimensional SANS pattern was done by radially averaging in the flow and vorticity directions employing a radial sector analysis with an opening angle of $\Delta\varphi$ = 10° and using software available at the ILL ($GRAS_{ans}P$ V. 3.25). Azimuthal intensity distributions $I(\varphi)$ were obtained by averaging in a 270° or 360° sector with an angular bin of 4° or 6° covering different *q*-regimes as indicated. All experiments were carried out at full contrast using D_2O as the solvent.

5.3 Results and Discussion

5.3.1 Shear-induced structures at temperatures well below the LCST

The first aspect of this work is to describe the behavior of swollen PNiPAM microgels under shear at temperatures well below the LCST. Results from 25.0°C and 28.5°C will be presented. At those temperatures, the interaction potential is purely repulsive. We first present data on the internal structure of the particles, then the flow-induced microstructural changes. Since the M-1.5/353 microgel particles are rather large, the main contribution to the overall scattering intensity distribution with this sample in the investigated *q*-regime

arises from contributions of the form factor *P(q)*. The scattering intensity distributions *I(q)* obtained from the large microgel at a concentration of 8.0 wt% at rest (filled symbols) and under sheared conditions (open symbols) are presented in figure 1. The two dimensional scattering patterns were averaged radially along the flow (squares) and neutral (stars) direction.

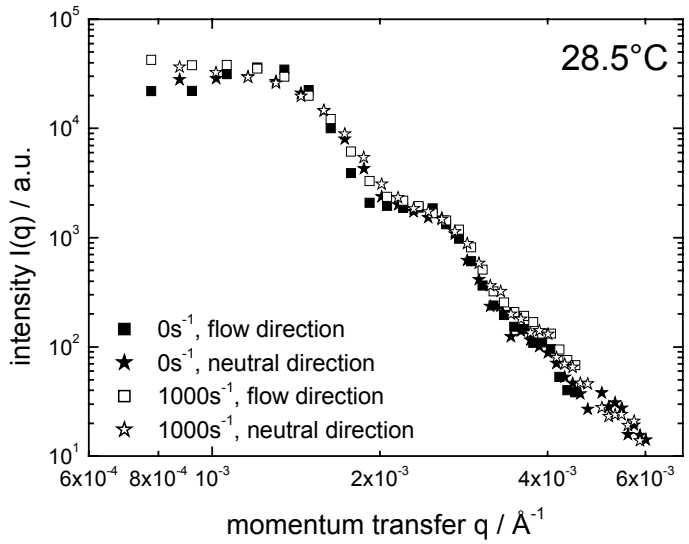

Figure 1. *Scattering intensity distribution I(q) for the M-1.5/353 at T = 28.5°C and a concentration of 8.0 wt%. The filled symbols represent data obtained at rest and the open symbols the data obtained under shear flow. The squares show the data along the flow direction, the stars represent the neutral direction.*

No significant changes were observed in *I(q)* obtained from averaging procedure along both directions when shear flow was applied. The sample was shear thinning, but the scattering patterns remained isotropic even at high shear rates. In the quiescent state and under shear the scattered intensity *I(q)* exhibits pronounced form factor minima at similar *q*-values. This indicates that no significant deformation of an individual, highly swollen microgel particle occurs in concentrated suspension after application of shear flow.

Since the 2D SANS patterns of the large M-1.5/353 were isotropic, experimental intensity distributions *I(q)* with small statistical errors could be obtained from radial averaging procedures over the entire spectra. The previously established model expression for the particle form factor *P(q)* and structure factor *S(q)* for concentrated PNiPAM microgel suspensions described the experimental data at rest and under shear *I(q)* well.[73] Since the *q*-range investigated under shear was limited compared to our previous studies in the quiescent state, the fitting parameters obtained under shear must be interpreted cautiously. However, the particle radius *R*, the width of the smeared particle

surface σ_{suf}, the particle size polydispersity σ_{poly} and the polymer volume fraction in the center of a particle $\phi(r=0)$ determined under shear were generally in fairly good agreement with the data obtained at rest. The SANS data obtained at a concentration of 8.0 wt% of the M-1.5/353 microgel are similar to the previously described scattering profiles *I(q)* of a 10.0 wt% sample of the same microgel.

In contrast to the larger M-1.5/353 microgel, the main contribution to the overall scattering intensity of the small M-1.4/141 sample in the low *q*-regime arises from the structure factor *S(q)*. Thus, information about shear-induced changes in the overall microstructure can be gained from scattering experiments with the small PNiPAM microgels. 2D SANS patterns of the small microgel in combination with the flow curve at 25.0°C under various sheared conditions at a concentration of 3.6 wt% are shown in figure 2.

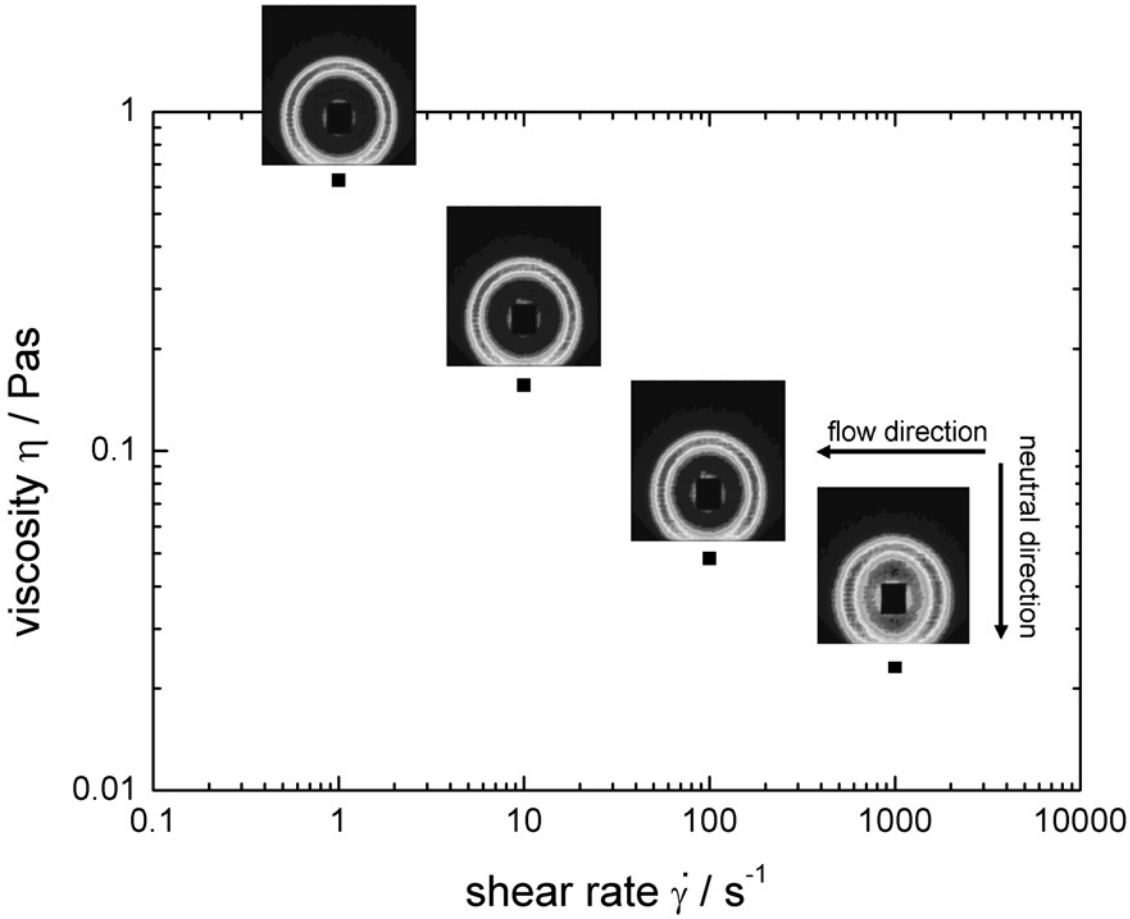

Figure 2. *2D SANS patterns and viscosity vs. shear rate for the M-1.4/141 at 25°C and a concentration of 3.6 wt%.*

This microgel sample formed colloidal crystals in the quiescent state at this temperature and concentration. Shear thinning is observed and the viscosity η decreased by a factor of

40 when the shear rate was increased from $\dot{\gamma}=1s^{-1}$ to 1000 s^{-1}. The 2D SANS patterns reveal the maximum of the structure factor *S(q)* as a ring. At low shear rates ($\dot{\gamma}=1s^{-1}$ and 10 s^{-1}) the scattering patterns are isotropic but at higher shear rates ($\dot{\gamma}=100s^{-1}$ and 1000 s^{-1}) an anisotropy of the pattern evolves, which is quantified by the averaged intensity distributions *I(q)* along the neutral and flow direction that are shown in figure 3. A broadening of the structure factor peak is observed in both the neutral and flow direction with increasing shear rate. When shear flow is applied, the maximum of the structure factor determined along the flow direction is shifted towards smaller *q*-values, whereas the peak position obtained along the neutral direction remains unchanged at a position of approximately *q*=0.0029 $Å^{-1}$. This indicates that the average particle-particle distance along the flow direction increases at high shear rates without changing the distance along the neutral direction.

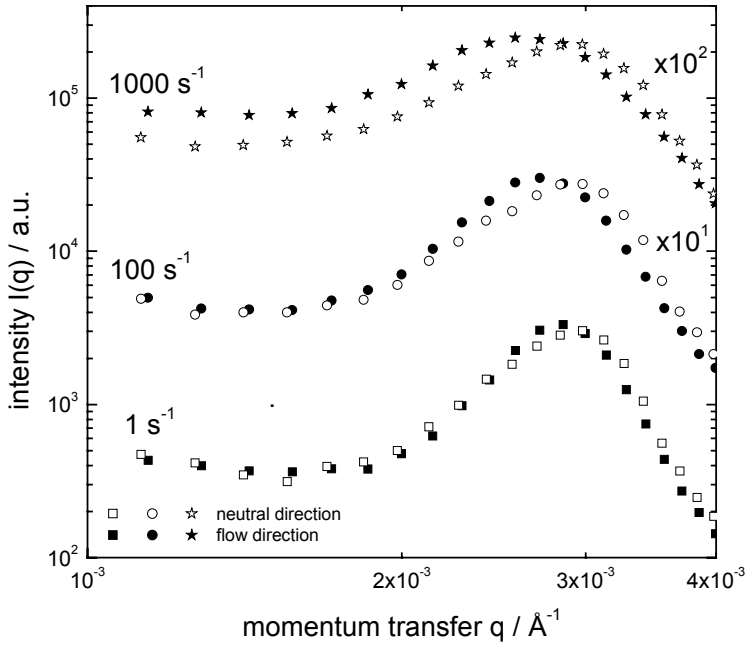

Figure 3. *Scattering intensity distribution I(q) for the M-1.4/141 at 25°C and a concentration of 3.6 wt% at various shear rates. The open symbols represent data obtained along the neutral direction, the filled symbols represent the flow direction. For the sake of clarity some of the data sets were multiplied by constant factors.*

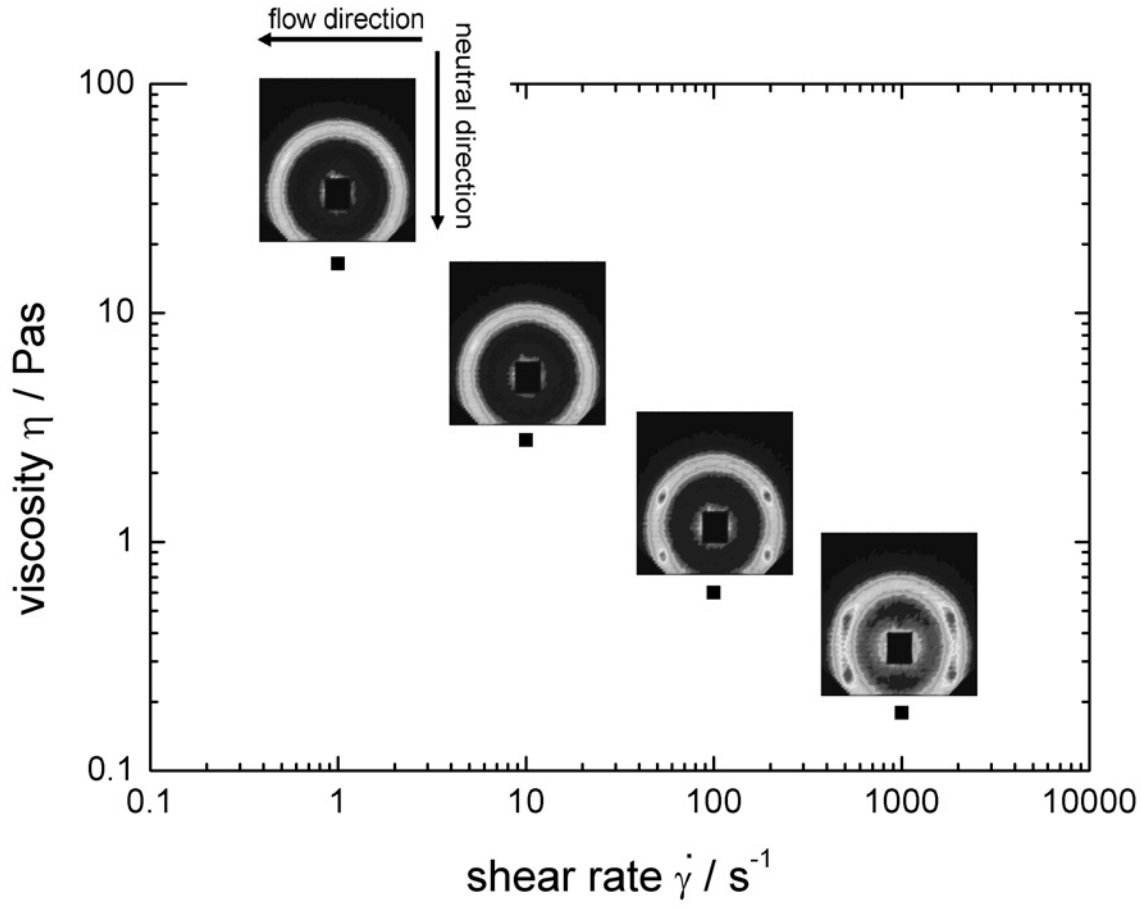

Figure 4. *2D SANS patterns and viscosity vs. shear rate for the M-1.4/141 at 25°C and a concentration of 7.0 wt%.*

The 2D SANS patterns accompanied by the flow curve for a more concentrated suspension of the small M-1.4/141 microgel are shown in figure 4. The microgel suspension was in the glassy state at 25.0°C at a concentration of 7.0 wt%. At high concentrations shear thinning is more pronounced and a decrease of the viscosity η by a factor of ca. 100 is found when the shear rate was increased from $\dot{\gamma} = 1 s^{-1}$ to 1000 s^{-1}. As for the less concentrated sample, broadening of the structure factor maximum and shift of the peak position along the flow direction towards smaller *q*-values is observed. In addition, a highly ordered superstructure is observed at a shear rate of $\dot{\gamma} = 100 s^{-1}$ indicated by four sharp Bragg peaks at the (1$\underline{1}$), (01), (0$\underline{1}$) and ($\underline{1}$1) position.[31,32] This clearly indicates a sliding layer motion of two-dimensional hexagonal close packed (2D hcp) layers, which gives rise to a significant decrease of viscosity η with increasing shear rate. The experimentally observed 2D SANS patterns are in good agreement with calculated scattering patterns.[100] Similar shear-induced structures have been observed by different

groups in suspensions of hard spheres[29] and electrostatic stabilized latices[31,32] at various shear rates in the shear thinning regime. We therefore conclude that the formation of sliding hexagonal close packed layers under shear flow is a general property of colloidal dispersions independent of the internal structure of the particle. The corresponding azimuthal averaged intensity distributions $I(\varphi)$ are depicted for different shear rates in figure 5. At $\dot{\gamma} = 1000\,s^{-1}$ the sliding motion of the hcp layers is slightly distorted in favor of a more liquid-like structure which can be seen by a broadening of the Bragg peaks. The positions of the Bragg peaks do not change significantly with increasing shear rate and are observed at angles of approximately φ = 60° and 120°.

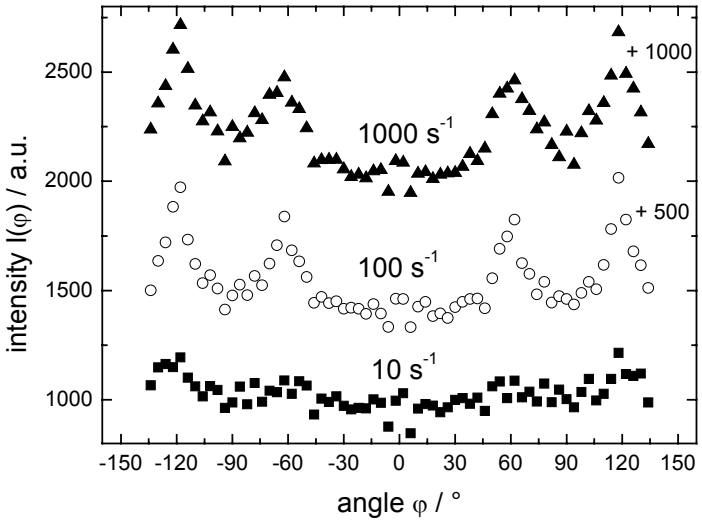

Figure 5. *Azimuthal intensity distribution $I(\varphi)$ for the M-1.4/141 at 25°C and a concentration of 7.0 wt% at various shear rates. $I(\varphi)$ was obtained by averaging in a 270° sector with an angular bin of 4° covering the q-range from 0.0026 Å^{-1} < q < 0.0041 Å^{-1}. For the sake of clarity constants were added to some of the data sets as indicated.*

The anisotropic scattering intensity distributions *I(q)* of the small M-1.4/141 microgel presented in this contribution could not be reasonably be described with the previously established model for the structure factor *S(q)*, since the model expression does not account for anisotropy of the scattering intensity *I(q)*. The volume fractions of the M-1.4/141 suspensions studied under flow were outside the expected validity range of the Percus-Yevick approximation for the structure factor, which was used in the model.

5.3.2 Structure formation under flow at temperatures near the LCST

The second aspect of this work is to investigate the influence of shear flow on the behavior of PNiPAM microgels at temperatures near the LCST. Data obtained at 32.0°C and 32.5°C will be presented. At those temperatures, the interaction potential at rest is not yet strongly attractive, but can no longer be said to be purely repulsive. First data of the internal structure and then changes of the microstructure are discussed. Figure 6 shows the scattering intensity *I(q)* obtained from a 8.0 wt% suspension of the large M-1.5/353 microgel at rest (filled symbols) and under shear (open symbols).

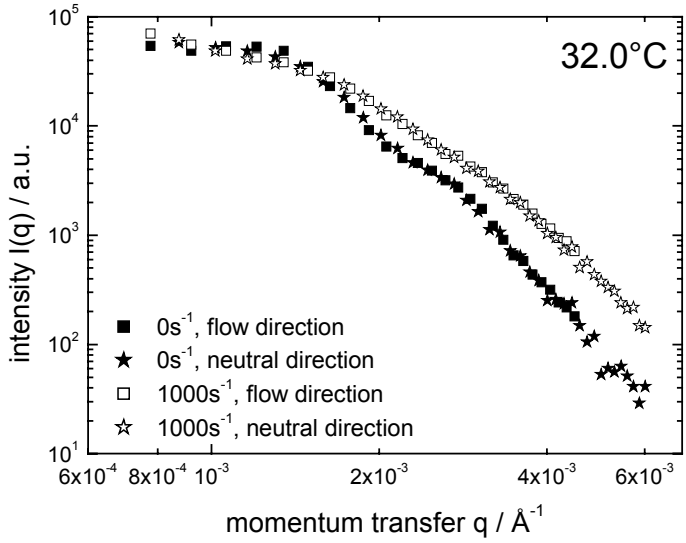

Figure 6. *Scattering intensity distribution I(q) for the M-1.5/353 at T = 32.0°C and a concentration of 8.0 wt%. The filled symbols represent data obtained at rest and the open symbols the data obtained under shear flow. The squares show the data along the flow direction, the stars represent the neutral direction.*

Again, the scattering patterns revealed no anisotropy even at high shear rates and the data obtained in flow and neutral direction fell on a single curve. The individual microgel particles reveal no significant deformation under shear, but a strong increase of *I(q)* in the high *q*-regime of 0.002 Å^{-1} < *q* < 0.006 Å^{-1} is observed when the suspension is sheared. The minima of the form factor *P(q)* observed at rest vanish when shear flow is applied. Experimental intensity distributions *I(q)* with small statistical errors were obtained from radial averaging procedures over the entire spectra, then described at rest and under shear by the previously established model expression.89 As mentioned before, due to the limited *q*-range investigated under shear, care must be taken discussing the absolute values obtained from the fitting procedures under shear. However, compared to the quiescent state shear flow

provoked a decrease of the particle radius from $R_{32°C}(\dot{\gamma}=0s^{-1})$ = 298 nm to $R_{32°C}(\dot{\gamma}=1000s^{-1})$ = 167 nm and an increase of the polymer volume fraction in the center of a particle from $\phi_{32°C}(r=0,\dot{\gamma}=0s^{-1})$ = 0.04 to $\phi_{32°C}(r=0,\dot{\gamma}=1000s^{-1})$ = 0.09 accompanied by a dramatic sharpening of the width of the smeared particle surface from $\sigma_{suf,32°C}(\dot{\gamma}=0s^{-1})$ = 23 nm to $\sigma_{suf,32°C}(\dot{\gamma}=1000s^{-1})$ = 3 nm. This reveals the shear-induced collapse of individual particles in concentrated suspension. We emphasize that results determined at a shear rate of $\dot{\gamma}=1000s^{-1}$ approximately 1K below the LCST agree qualitatively with the data obtained previously in the quiescent state at temperatures above the LCST. This demonstrates nicely that the influence of shear flow on the phase separation process near the miscibility gap is similar to a temperature increase. This is in good agreement with the SANS data obtained recently at a concentration of 10.0 wt% for the M-1.5/353.[101]

The rheo-SANS experiments provide information about the internal structure of a single particle in concentrated suspension. Apparently, shear flow induces the particle collapse at temperatures near the LCST. However, previously described rheo-turbidity experiments revealed no shift of the cloud point temperature under shear flow for this concentration. A shear-induced shift of the cloud point temperature was found only for concentrations of 10.0 wt% or higher. The rheo-turbidity measurements reveal the macroscopic shear-induced phase separation. Shear-induced demixing was only observed when the concentration of the microgel suspension was so high that the sample had dominant elastic properties at temperatures near the LCST. This may indicate that the demixing process starts at a local, microscopic level on small length scales which is detected by rheo-SANS before it is observed macroscopically in rheo-turbidity experiments.

The flow curve in combination with the 2D SANS patterns at 32.0°C and 32.5°C for the 7.0 wt% suspension of the small M-1.4/141 microgel is shown in figure 7 and shear thinning is observed again. At high shear rates of $\dot{\gamma}=100s^{-1}$ and 1000 s^{-1} an anisotropy evolves in the low *q*-regime. The increase in scattering intensity *I(q)* along the flow direction relative to the neutral direction under shear is shown in figure 8 for both temperatures. In addition, the peak of the structure factor that is visible at rest and small shear rates vanished almost entirely after application of shear flow. This can be compared with SANS experiments performed with concentrated thermoresponsive PNiPAM microgels at rest. In the quiescent state, particle collapse is induced when the temperature is raised above the LCST.[101] The peak of the structure factor which was observed at temperatures below the LCST vanished at elevated temperatures.

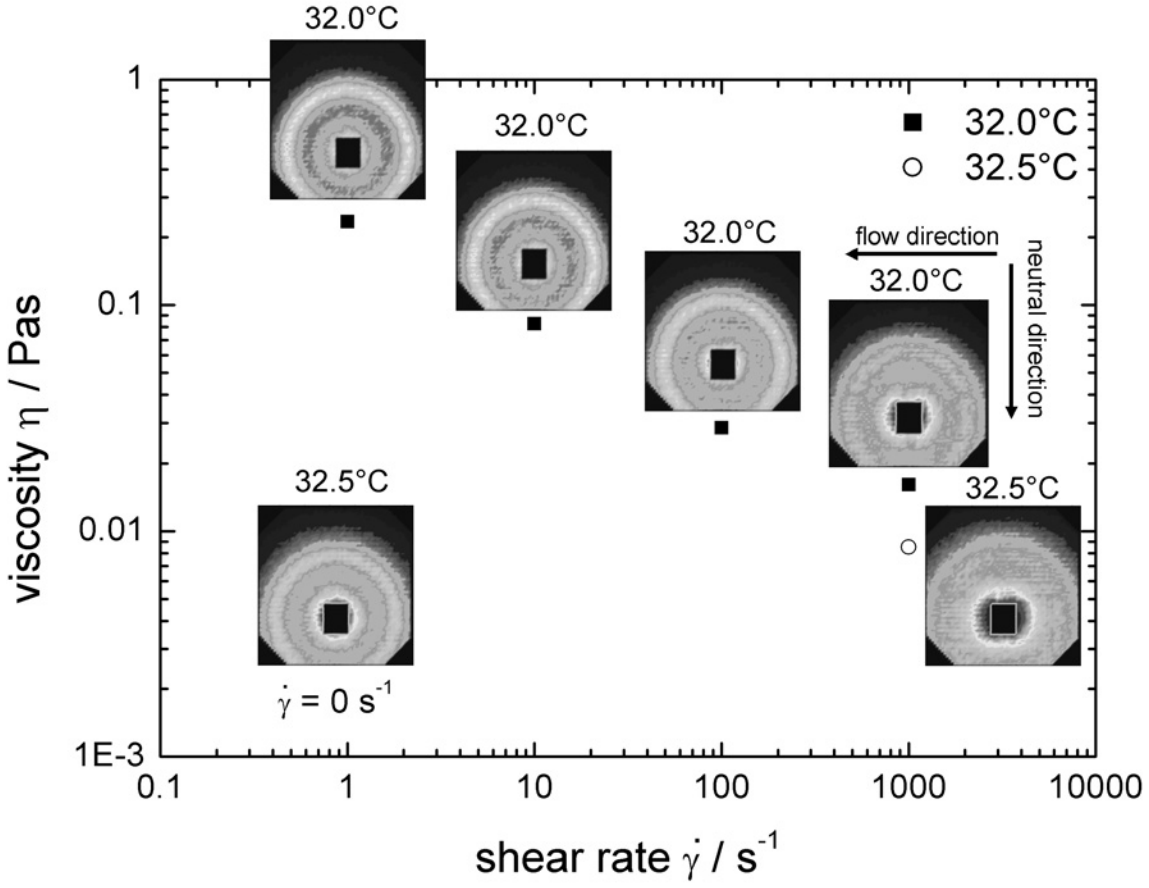

Figure 7. *2D SANS patterns and viscosity vs. shear rate for the M-1.4/141 at 32.0°C and 32.5°C at a concentration of 7.0 wt%.*

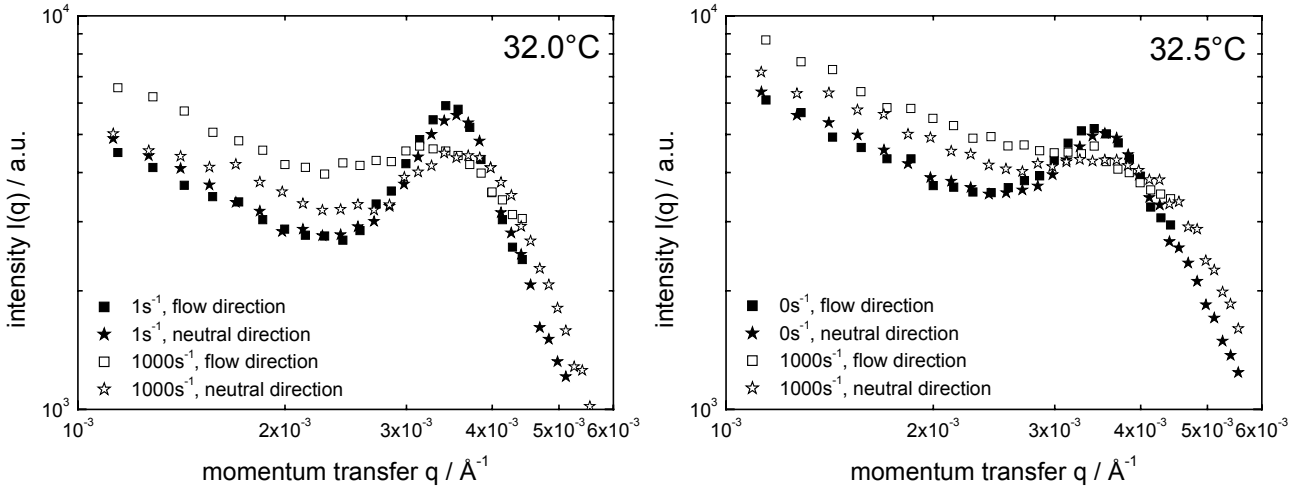

Figure 8. *Scattering intensity distribution I(q) for the M-1.4/141 at 32.0°C (left) and 32.5°C (right) and a concentration of 7.0 wt% at different shear rates. The filled symbols represent data obtained at rest or very small shear rates and the open symbols the data obtained at high shear rates. The squares show the data along the flow direction, the stars represent the neutral direction.*

This demonstrates again that shear flow induced phase separation. However, the scattering patterns obtained at rest were always isotropic. The anisotropy in the scattering intensity in the low *q*-regime provoked by high shear rates is depicted in more detail in the azimuthal averaged intensity distributions *I(φ)* which are shown in figure 9. At rest and small shear rates of $\dot{\gamma} = 10\,s^{-1}$ the patterns are entirely isotropic. At high shear rates of $\dot{\gamma} = 1000\,s^{-1}$ a two-fold symmetric intensity distribution *I(φ)* indicated the presence of a so-called butterfly pattern in the low *q*-regime consisting of two lobes along the flow direction. The application of shear flow apparently led to an enhancement of concentration fluctuations along the flow direction indicated by the butterfly pattern. A solvent squeezing mechanism may therefore be responsible for the shear-induced demixing at high concentrations. When the particles are densely packed stress relaxation via particle diffusion is hindered. The coupling between concentration fluctuations and shear stress can result in squeezing solvent out of the particle giving rise to an enhancement of concentrations fluctuations and turbidity eventually leading to shear-induced phase separation.

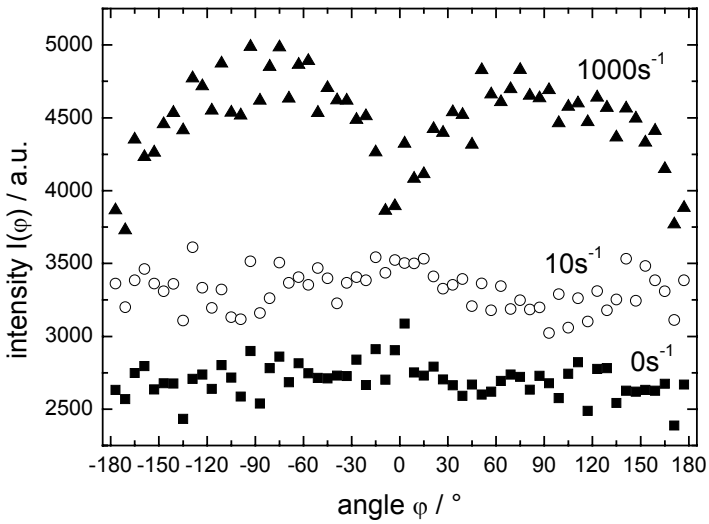

Figure 9. *Azimuthal intensity distribution I(φ) for the M-1.4/141 at 32°C and a concentration of 7.0 wt% at various shear rates. I(φ) was obtained by averaging in a 360° sector covering the q-range from 0.0015 Å^{-1} < q < 0.002 Å^{-1} with an angular bin of 6°.*

5.4 Conclusions

Thermoresponsive PNiPAM microgels are interesting model systems for concentrated suspensions with unique colloidal properties. The interaction potential of thermoresponsive PNiPAM microgels can be varied from repulsive at temperatures below the LCST to attractive at temperatures above the LCST. In contrast to suspensions of rigid spheres, the effective volume fraction can be changed by temperature while the mass concentration and particle number density are kept constant. Above the LCST the microgel particles eventually collapse.

Investigating PNiPAM microgels with different particle sizes in the same *q*-regime provides complementary information about shear-induced changes of both the internal particle structure as well as the overall microstructural phenomena. The shear-induced particle arrangements strongly depend on the interaction potential. When the interaction potential is repulsive at temperatures below the LCST, individual swollen PNiPAM particles in concentrated suspension are not deformed significantly even at high shear rates. Shear-induced ordering is observed at high shear rates resulting in the formation of two dimensional hexagonal close packed layers that align along the flow direction giving rise to shear thinning. The formation of sliding hexagonal close packed layers under shear flow is therefore proposed to be a general property of colloidal dispersion independent of the internal structure of the particle. At temperatures near the LCST, when the particle interaction potential is not yet strongly attractive, shear flow induces the collapse of an individual particle in concentrated suspension at high shear rates. A so-called butterfly scattering pattern indicates the shear-induced enhancement of concentration fluctuations along the flow direction and phase separation occurs finally. Shear-induced demixing has also been observed in aqueous solutions of linear chain PNiPAM by rheo-SANS and rheo-turbidity.[102]

ACKNOWLEDGMENTS We are gratefully indebted to Jan Skov Pedersen, University of Aarhus, Denmark, for his contributions to the development of the model for the scattering intensity and rewarding discussions. Financial support by the Deutsche Forschungsgemeinschaft is gratefully acknowledged.

6 Shear induced phase separation in aqueous polymer solutions

ABSTRACT: The influence of shear flow on the phase separation of aqueous poly(*N*-isopropyl acryamide) (PNiPAM) microgel suspensions was investigated by means of rheo-turbidity and rheo-small angle neutron scattering (rheo-SANS) and compared to the behavior of linear PNiPAM macromolecules. The rheological behavior of concentrated microgel suspensions depends strongly on temperature, but flow and viscoelastic properties of concentrated solutions of the linear polymer are not significantly affected by temperature changes. Shear induced phase separation was observed for both polymer architectures, although the viscoelastic properties of the two systems have different structural origins. Shear induced demixing was found with a microgel with a cross-linking density of 1.5 mol% only at high concentrations when the sample behaved as a viscoelastic solid near the equilibrium demixing temperature. No influence of shear flow on the miscibility gap was observed for a PNiPAM microgel with a higher cross-linking density (5.5 mol%). This indicates that a coupling of shear stress with the concentration fluctuations leading to solvent squeezing is only possible when the particles are densely packed and sufficiently soft.

6.1 Introduction

A characteristic feature of many aqueous polymer solutions is that phase separation can occur upon heating. The temperature minimum of the miscibility gap is known as the lower critical solution temperature (LCST). Polymer solutions in organic solvents usually display an upper critical solution temperature (UCST) and demix upon cooling. Prominent examples for water-soluble polymers displaying a LCST are poly(*N*-isopropylacrylamide) (PNiPAM),[4] methylhydroxypropyl cellulose (MHPC)[5] and poly(vinylcaprolactam) (PVCa)[6].

Temperature sensitive PNiPAM polymers gained great interest due to their potential use in many technological applications, including drug delivery systems and biotechnology.[7] PNiPAM is known to undergo a temperature induced phase transition in water at the LCST of 31-34 °C. The solvent quality changes from good to poor when the temperature is increased, eventually leading to phase separation. The phase transition was studied in great detail for polymers with different molecular architectures including solutions of linear chain PNiPAM, chemically cross-linked microgels and macroscopic gels.[8,9] For single linear PNiPAM, the

flexible polymer chain contracts with increasing temperature and a coil-to-globule transition is observed. Cross-linked microgels and macrogels exhibit a volume phase transition from a highly swollen to a collapsed state at elevated temperatures. It has been shown that the volume phase transition can be induced by temperature, pressure and solvent composition. The transition temperature can be altered by addition of salt[10] or surfactants[11], by variations in the solvent quality[12] or by copolymerization with charged monomers.[13]

It is well known that shear flow can influence the phase separation of polymer solutions.[39] There are several reports on the behavior of poly(styrene) (PS) dissolved in dioctylphthalate (DOP) using different techniques to probe the demixing process including turbidity, dichroism, small angle light scattering (SALS) and small angle neutron scattering (SANS). Recent papers by Hashimoto and Boué et al. provide a thorough review of this system.[40,41,42] Often a so-called butterfly pattern in SALS and SANS is observed under shear flow indicating shear induced concentration fluctuations. The butterfly pattern is usually observed with semi-dilute solutions above the overlap concentration, indicating that entanglements are necessary for the enhancement of concentration fluctuations along the flow direction. Butterfly scattering patterns have also been observed with polymer networks and some colloidal systems.[43,44,45,46,47] It has been pointed out that viscoelastic properties, the first normal stress difference in particular, play an important role for the coupling between density fluctuations and shear stress[48]. The presence of an entanglement network appears to be unnecessary for the shear induced fluctuations, since experiments in dilute polymer solutions reveal that shear induced aggregation can occur.[49]

Much less is known about aqueous solutions where phase separation occurs upon heating. Recently Wolf and coworkers investigated aqueous solutions of hydrophobically modified ethyl hydroxyethyl cellulose, which also show LCST behavior.[50] Turbidity measurements revealed a strong influence of shear flow on the phase separation. With increasing shear rate the cloud temperature was shifted to higher values. It was concluded that the shear induced mixing is due to a destruction of intersegmental clusters, which are formed via the hydrophobic side chains. MHPC solutions demonstrate a very complex behavior, revealing shear induced mixing at low concentrations but demixing at higher concentrations.[51] Badiger et al.[52] observed shear induced demixing in aqueous solutions of high molecular weight PNiPAM solutions. Compared to the quiescent state the linear chain polymer solutions entered the two-phase region at lower temperatures when shear flow was applied. The authors attribute the shift of the cloud point temperature to the destruction of intersegmental clusters formed in the stagnant state. A stress overshoot is observed for concentrated solutions before the onset of steady shear flow, indicating the existence of clusters.

Most investigations employed solutions of linear chain macromolecules above the overlap concentration. Thus, the microstructure is characterized as a highly entangled polymer solution. Shear induced phase separation can be interpreted in different ways. Wolf suggested a general thermodynamic approach.[53] In addition to the usual Flory-Huggins-Gibbs energy of polymer solutions a second term is introduced, the stored elastic energy. In the case of dilute polymer solutions the stored elasticity accounts for coil stretching. Other approaches describe the dynamic coupling between concentration fluctuations and stress.[54,55,56] Semi-dilute polymer solutions can be characterized by a typical correlation length and longest relaxation time of the entangled chains. In the strong shear regime of high shear rates, the stress can be released by squeezing solvent from the more entangled regions thus enhancing concentration fluctuations. In colloidal systems shear flow can also lead to aggregation and flocculation and different structures for example the formation of large scale bundle ordering has been observed.[36]

The microstructures of colloidal and polymer solutions are very different. Thus, different properties near the miscibility gap can be anticipated. However, very little is known about the influence of the macromolecular architecture on the phase separation behavior under shear. In the present study we investigated the flow behavior and the viscoelastic properties of linear chain PNiPAM solutions as well as of concentrated PNiPAM microgel suspensions for various temperatures. The influence of shear flow on the phase separation was studied for both polymer architectures. Phase separation was monitored by rheo-turbidity measurements. Cloud point temperature curves will be presented for both polymer architectures at rest and under sheared conditions. Small angle neutron scattering experiments under shear (rheo-SANS) were performed in order to determine the flow induced structures. Preliminary results of the rheo-SANS investigations are included in this contribution.

6.2 Experimental part

6.2.1 Synthesis of the linear chain PNiPAM

The preparation of the linear chain PNiPAM is based on the procedure described by Meewes et al.[103,104] The monomer *N*-isopropylacryamide NiPAM (204.0 g, Aldrich) was purified by recrystallization from a 50 wt% benzene-hexane solution (324.0 g). An aqueous solution of hydrogen peroxide H_2O_2 (30 wt%, Merck), argon (99.998 %) and pure methanol were used as received. NiPAM (100.0 g) was dissolved in 2000 ml of pure water at 25 °C. The polymerization vessel was evacuated and filled with argon. The H_2O_2 (1 ml) was added and the reaction mixture was degassed again. The polymerization was started by opening

the shutter of the UV lamp (Osram mercury vapor lamp Hg-10) and stopped after 35 minutes by closing the shutter and aerating the solution. The reaction mixture was poured into cold methanol and was heated up slowly to room temperature. A fine precipitate of PNiPAM was decanted. For further purification the polymer was dissolved in methanol and cold water was added. The precipitate was decanted and another purification cycle was performed. Finally, the polymer was dissolved in water and isolated by freeze-drying.

6.2.2 Synthesis of the crosslinked PNiPAM microgel

The PNiPAM microgel particles were prepared as described previously,[20] but different quantities of the reagents were employed for this study in order to obtain particles with larger radii. All chemicals were reagent grade and used without further purification. NiPAM (23.19 g), *N,N´*-methylenbisacrylamide (0.48 g, Fluka) and sodium dodecylsulfate (0.014 g, Merck) were dissolved in 1500 ml pure water (Millipore). The synthesis was performed in an inert gas atmosphere at 70 °C. Potassium peroxodisulfate (0.96 g, Merck) was dissolved in water and added to the solution. The polymerization was proceeded for 6 hours and thereafter the dispersion was cooled to room temperature under continued stirring. For purification the dispersion was filtered followed by extensive dialysis against pure water for 20 days. Finally, the microgel dispersion was freeze dried.

6.2.3 Experimental details

Differential scanning calorimetry measurements (DSC) were carried out with a Perkin Elmer Pyris 7 calorimeter over temperatures from 10 °C to 40 °C, and at a heating and cooling rate of 0.5 K/min. The concentration of the samples was typically 6 wt% and the positions of the peak maxima were used to determine the phase transition temperatures. Unless otherwise stated all concentrations are denoted as the ratio of the mass of the polymer to the mass of the solution (wt%).

Static light scattering experiments (SLS) were performed using a computer controlled modified FICA goniometer with a helium-neon ion laser at a wavelength of λ_0 = 632.8 nm. The polymer solutions were filtered (MembraPure, pore size 0.2 μm) and diluted resulting in concentrations ranging from 0.05 mg/ml to 0.5 mg/ml. The intensity of the scattered light was monitored from 30° to 145° in steps of 5°. For the refractive index increment at 25 °C *dn/dc* = 0.162 ml/g was used at λ_0 = 632.8 nm[105].

The rheological experiments were performed with a Bohlin CS-10 rheometer using a cone and plate shear geometry (1°/40 mm) made of aluminum.

For the rheo-optical experiments a modified Bohlin CVO-120-HR rheometer was used with a cone and plane shear geometry (1°/40 mm) made of quartz glass. The light of a HeNe-Laser (λ = 632.8 nm) passes through the sample along the velocity gradient direction and the transmitted intensity is measured by a photo diode. The signal of the photo diode is amplified and recorded by a computer. The temperature and shear rate dependent transmitted intensity, I_t, was normalized by the intensity at low temperatures, I_0, when the sample was in the stable one-phase region. The turbidity α was obtained from the ratio of the normalized intensities and the sample thickness L = 0.3 mm as α = (-1/L) ln (I_t/I_0). A detailed description of the apparatus is provided in the literature.[106]

Small angle neutron scattering experiments under shear were performed at the instrument D11 of the Institute Laue-Langevin (ILL) in Grenoble, France. The neutron wavelength was λ = 12 Å with a spread of $\Delta\lambda / \lambda$ = 9 %. The data were collected on a two-dimensional multidetector (64 x 64 elements of 1 x 1 cm^2) and corrected for background and empty cell scattering. The incoherent scattering of H_2O was used for absolute calibration according to standard procedures and software available at the ILL. Further analysis was done by radially averaging. A Bohlin CVO-120-HR rheometer was adjusted to the D11 beamline. Measurements were performed using a Searle shear cell consisting of quartz cylinders with a gap of 1 mm. The scattering experiments were performed in the radial position yielding information in the plane formed by flow and vorticity direction.

6.3 Results and discussion

6.3.1 Static light scattering of the linear chain PNiPAM and the PNiPAM microgel

The coil-to-globule transition of very dilute solutions of linear chain PNiPAM in water has been studied intensely. Kubota and coworkers[107] studied various molecular parameters characterizing the solution properties in a broad range of molecular weights. They describe the temperature dependence of the second virial coefficient A_2 in the range from 20 °C to 30.6 °C for a high molecular weight polymer (weight average molar mass M_w = 9.1 $\times$ 10^6 g/mol) and show that the molecule behaves like a flexible coil. Wu[108] reports on the observation of the thermodynamically stable collapsed single-chain globule at elevated temperatures. The temperature dependence of the radius of gyration R_g and the hydrodynamic radius R_h is presented for two high molecular weight PNiPAM samples (M_w = 10.8 $\times$ 10^6 and 12.1 $\times$ 10^6 g/mol). The ρ-parameter $\rho = R_g/R_h$ first decreases linearly with increasing temperature and then drops before reaching the two-phase region. They attribute the linear decrease of the ρ-parameter to a chain crumpling process. At elevated

temperatures in the two-phase region they report a plateau value of $\rho = 0.62$ indicating that the density of the globule is higher in the centre. They conclude that the coil-to-globule transition is not an "all-or-nothing" process.

In order to determine molecular weight M_w, radius of gyration $R_g = \langle s^2 \rangle_z^{0.5}$ and second virial coefficient A_2, static light scattering experiments in dilute solution were performed with the linear chain PNiPAM. From the extrapolation of *Kc/R(q)* to zero angle and zero concentration in the Zimm plots R_g and A_2 were determined. The weight average molar mass $M_w = 3.9 \times 10^6$ g/mol was obtained and the overlap concentration c^* given by $c^* = (3\, M_w / 4\, \pi\, R_g^3\, N_L)$ was calculated. The temperature dependence of A_2, R_g and c^* is summarized in table 1.

Table 1. *Radius of gyration R_g, second virial coefficient A_2 and overlap concentration c^* for solutions of linear chain PNiPAM at different temperatures determined by SLS*

T / °C	R_g / nm	A_2 / mol × cm^3/g^2	c^* / wt%
22.2	115 ± 3	$1.4 \times 10^{-4} \pm 8 \times 10^{-6}$	0.1
25.8	114 ± 1	$1.2 \times 10^{-4} \pm 3 \times 10^{-6}$	0.1
30.3	97 ± 2	$5.0 \times 10^{-5} \pm 4 \times 10^{-6}$	0.1
33.7	89 ± 2	$1.8 \times 10^{-5} \pm 4 \times 10^{-6}$	0.2
35.8	78 ± 2	$-9.3 \times 10^{-7} \pm 2 \times 10^{-8}$	0.3
36.5	65 ± 3	$-1.0 \times 10^{-6} \pm 2 \times 10^{-8}$	0.6

A_2 and R_g remain nearly unchanged in the temperature range between 22 °C to 26 °C. At temperatures above 26 °C, A_2 and R_g decrease with increasing temperature due to the changes in solvent quality from good to poor. At temperatures above the θ-temperature negative values for the second virial coefficient are found and the radius of gyration declined dramatically. The overlap concentration c^* increases slightly with increasing temperature. From the SLS experiments the θ-temperature corresponding to $A_2 = 0$ is found to be in the range of 33.7 °C < θ < 35.8 °C. In order to compare the results obtained by SLS the transition temperature was determined employing DSC measurements with a 6 wt% solution. A transition temperature of 33.9 °C in H_2O was found. Hence, the transition temperatures determined by SLS and DSC are in fairly good agreement.

Figure 1 shows the static light scattering intensity obtained from very dilute suspensions of the PNiPAM microgel (0.0126 wt%) at four temperatures.

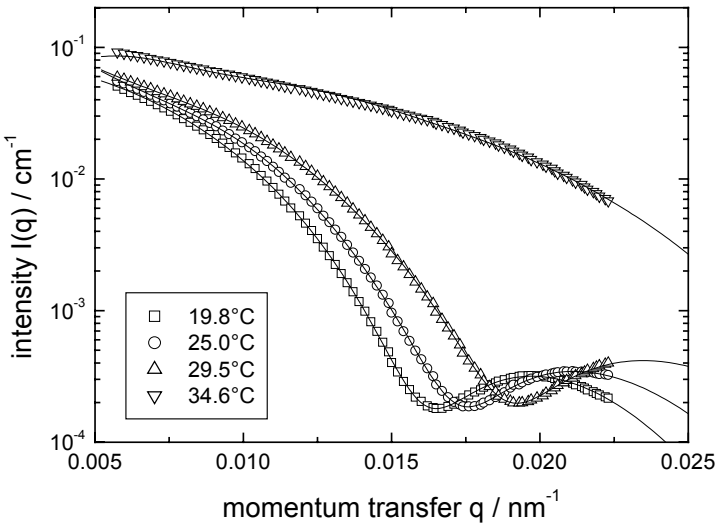

Figure 1. *Static light scattering intensity from the PNiPAM microgel at a concentration of 0.126 g/l in D_2O at different temperatures. The shrinkage of the particles with increasing temperature is indicated by the shift of the form factor minima to higher q-values. The lines represent fits with a form factor model of a sphere with an scattering length distribution that gradually decreases at the sphere interface.*

A shift of the form factor minima to higher q-values and the decrease of the initial slope of the scattering profiles in the low-q regime confirm the apparent shrinkage of the particles with rising temperature. From SLS experiments the particle radius and the size distribution can be obtained by fitting the intensity profile with a model expression of the form factor. For a homogenous sphere with a box shaped radial scattering length density distribution the form factor did not describe the experimental data at temperatures below the LCST.[109] Obviously, the polymer network of the cross-linked microgel particles exhibits inhomogeneous segment density in the highly swollen state which have to be included in the model expression. The form factor of a sphere with an scattering length distribution that gradually decreases at the sphere interface following a half gaussian distribution[89] fitted the experimental data very well for all temperatures. In this manner particle radii of R (19.8 °C) = 355 nm, R (25.0 °C) = 325 nm, R (29.5 °C) = 279 nm, R (34.6 °C) = 155 nm and a relative particle size polydispersity of 9 % at 25 °C was found.

6.3.2 Rheology of concentrated solutions of linear chain PNiPAM

Unless otherwise stated all rheological investigations were carried out using heavy water (D_2O) as a solvent for the linear polymer and the microgels to facilitate comparison to SANS. First results of SANS experiments on the influence of shear on the miscibility gap will be presented in this article. A detailed analysis of the rheo-SANS investigations will be discussed in another work. Shirota and coworkers[110] report that the phase transition temperature is shifted by 1 K to higher temperatures when D_2O is used as a solvent instead of H_2O. This shift can be contributed to the difference in the polymer-solvent interaction introduced by the deuterium isotope effect.

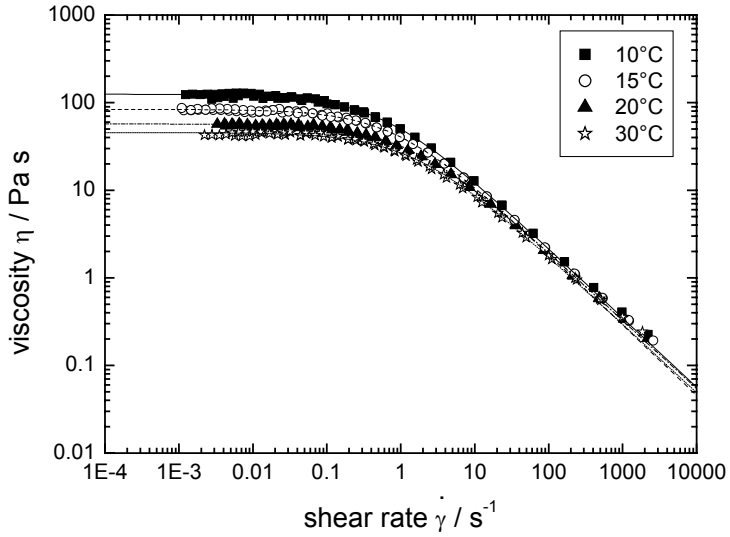

Figure 2. *Viscosity as a function of shear rate for different temperatures for the linear chain PNiPAM in D_2O at a concentration of 4.7 wt%. The lines represent fits according to the equation given by Cross[112].*

Figure 2 displays flow curves representative of concentrated solutions (4.7 wt%) of the linear PNiPAM polymer in D_2O. The flow curves are characterized by a clear zero shear plateau η_0 at low shear rates and strong shear thinning at higher shear rates. However, there is only a small influence of temperature on the viscosity. Changing the temperature from 10 °C to 30 °C gives rise to a decrease of η_0 by a factor of 2.7 from η_0 = 124 Pas to η_0 = 46 Pas. In the shear thinning regime no influence of the temperature on the viscosity can be detected. The high molar mass macromolecules form a highly entangled polymer solution at concentrations well above the overlap concentration. Such solutions are not very sensitive to changes in the size of the individual macromolecules, as long as the concentration stays well above the overlap concentration. The viscoelastic properties do not

reveal a pronounced temperature dependence either. The steady state viscosity η and the dynamic complex viscosity η^* as a function of shear rate $\dot{\gamma}$ and angular frequency ω, respectively, coincide on a single curve for all temperatures revealing that the Cox-Merz-rule[111] applies. These results indicate that the rheological behavior is determined by the mechanical interactions of the entangled network. Apparently, the influence of specific physical or chemical interactions is negliable.

The experimental flow curves were fitted using an expression given by Cross[112]

$$\frac{\eta}{\eta_0} = \frac{1}{1 + (\tau \dot{\gamma})^n} \qquad (1)$$

which is known to provide a good description of the viscosity of concentrated polymer solutions. Zero shear viscosity η_0, relaxation time τ and power law exponent *n* were obtained for various concentrations and temperatures. For the 4.7 wt% microgel suspension shown in figure 2 a power law exponent *n* = 0.78 was obtained for all temperatures. The concentration and temperature dependence of η_0 is given in figure 3. The course of the viscosity as a function of concentration is similar for all temperatures. At low concentrations the viscosity increases slightly with increasing concentration. At concentrations above the overlap concentration *c** a strong dependence of η_0 on *c* is observed.

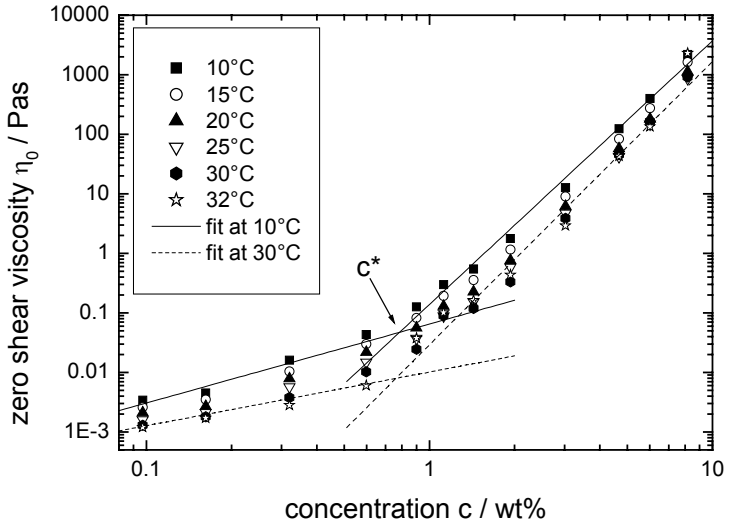

Figure 3. *Zero shear viscosity as a function of concentration for different temperatures for the linear chain PNiPAM in D_2O. The lines represent power law fits to the 10 °C and 30 °C data at low (0.1 - 0.6 wt%) and at high concentrations (0.9 - 8.2 wt%), respectively.*

At concentrations well above *c**, a power law behavior of $\eta_0 \propto c^q$ is observed. That corresponds to a scaling behavior of the specific viscosity $\eta_{spec.} \propto (c\,[\eta])^q$ for large values of

$c\,[\eta]$ with the intrinsic viscosity $[\eta] \approx 1/c^*$. Since $[\eta]$ is related to the molecular weight by the Mark-Houwink-Sakurada equation $[\eta] = K_v M^{\alpha}$, a power law behavior of $\eta_{spec.} \propto c^q M^{q\alpha}$ is obtained. For high molecular weight polymer melts an exponent of $q\,\alpha = 3.4$ is expected. For undisturbed polymer coils in polymer melts, $\alpha = 0.5$ is found. Therefore, $\eta_{spec.}$ of concentrated polymer θ-solutions at high $c\,[\eta]$ values reveal a $c^{6.8}$ dependence. Non-draining polymer coils in a good solvent with $\alpha = 0.764$ exhibit an increase to $\eta_{spec.} \propto c^{4.45}$. These scaling concepts should hold for all polymers regardless of their chemical composition.[113] For the temperature sensitive linear chain PNiPAM we observed an increase of q with increasing temperature. At low temperatures (10 °C) a value of $q = 4.5$ indicates good solvent conditions that become worse at elevated temperatures. At 20 °C the exponent $q = 4.7$ and at 30 °C $q = 5.3$ was obtained. At higher temperatures (32 °C) the exponent $q = 5.6$ is still below $q = 6.8$ for θ–polymer solutions, since the temperature is still below the θ–temperature. The temperature dependence of the power law exponents of concentrated polymer solutions agrees well with the decrease of the second virial coefficient A_2 with heating we observed in dilute solution by SLS.

A power law behavior of the relaxation times τ obtained from the Cross-fits with concentration is observed for all temperatures ($\tau \propto c^n$). At high concentrations τ is nearly temperature independent since the relaxation process of the polymer chain is determined by the relaxation of the entangled network. In contrast, τ is temperature dependent at lower concentrations, and a decrease of τ is observed with increasing temperature. The temperature dependent size of the polymer coil influences the relaxation behavior more strongly when the network is not highly entangled. The power law exponents n increase with rising temperature indicating a slight decrease in entanglements. At low temperatures (10 °C) we observed a slope of $n = 3.1$, at 20 °C $n = 3.3$ and at 32 °C $n = 3.9$ was obtained.

6.3.3 Rheology of the PNiPAM microgel

Flow curves representative of concentrated PNIPAM microgel suspensions (5.1 wt%) are displayed in figure 4. Shear thinning is observed and the microgel sample reveals a strong influence of temperature on the flow behavior. The viscosity decreases by 2-3 orders of magnitude when the temperature is raised from 10 °C to 30 °C. This behavior is caused by the strong dependence of the size of the microgel particles on temperature. It has been shown before that the effective volume fraction of the microgel particles decreases with temperature, and a master curve of the zero shear viscosity is obtained when the effective volume fraction is used as concentration parameter.[20] For the microgel investigated in this study a sufficient number of zero shear viscosities required to obtain a master curve could

not be experimentally observed since the radius of the microgel employed in these studies is large. One can define the dimensionless Peclet number

$$P_e \equiv \dot{\gamma} t_D = \dot{\gamma} \frac{6\pi \eta_s a^3}{k_B T} \qquad (2)$$

to relate the shear rate $\dot{\gamma}$ with the time t_D for a particle to diffuse a distance equal to its radius *a* in a solvent of viscosity η_s . A plateau in η_0 can only be observed when the applied shear rate does not disturb the equilibrium distribution of interparticle spacings. For the large particles the low shear rate limit of P_e<1 was out of the experimentally accessible range.

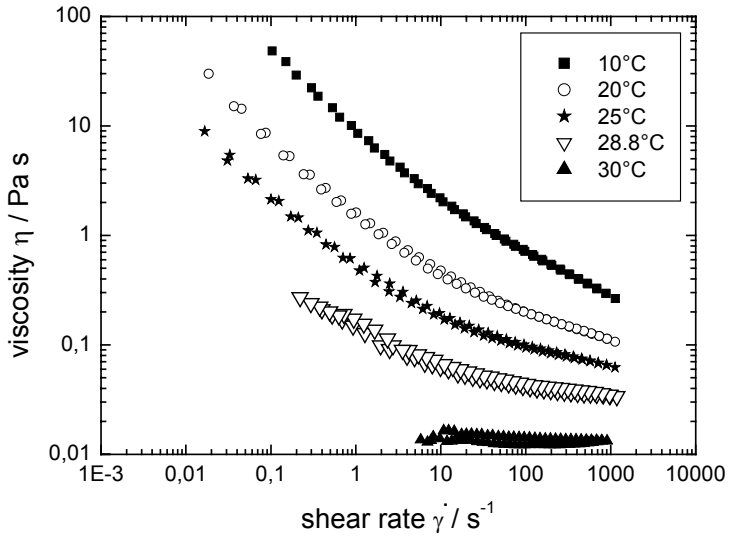

Figure 4. *Viscosity as a function of shear rate for different temperatures for the PNiPAM microgel in D_2O at a concentration of 5.1 wt%. The microgel particles reveal a pronounced temperature dependence of viscosity.*

The different temperature sensitivity of concentrated microgel suspensions as compared to linear polymer solutions is due to the different microstructure. An entangled network is present in the former whereas a close packed structure of spheres is formed in the later. This gives rise to a strong temperature sensitivity of the flow and the viscoelastic behavior of the microgel suspensions whereas solutions of the linear chain PNiPAM exhibit no significant temperature dependence of the rheological behavior.

6.3.4 Shear induced demixing

A convenient technique to study phase separation of polymer solutions is to measure the optical transmission. Usually the solution is sheared at a constant shear rate and the transmitted light intensity is determined as the temperature is increased. In our experiments a heating rate of 0.1 K/min was used. The turbidity obtained from two microgel suspensions at concentrations of 8.0 and 10.0 wt% at varied shear rates is shown in figure 5.

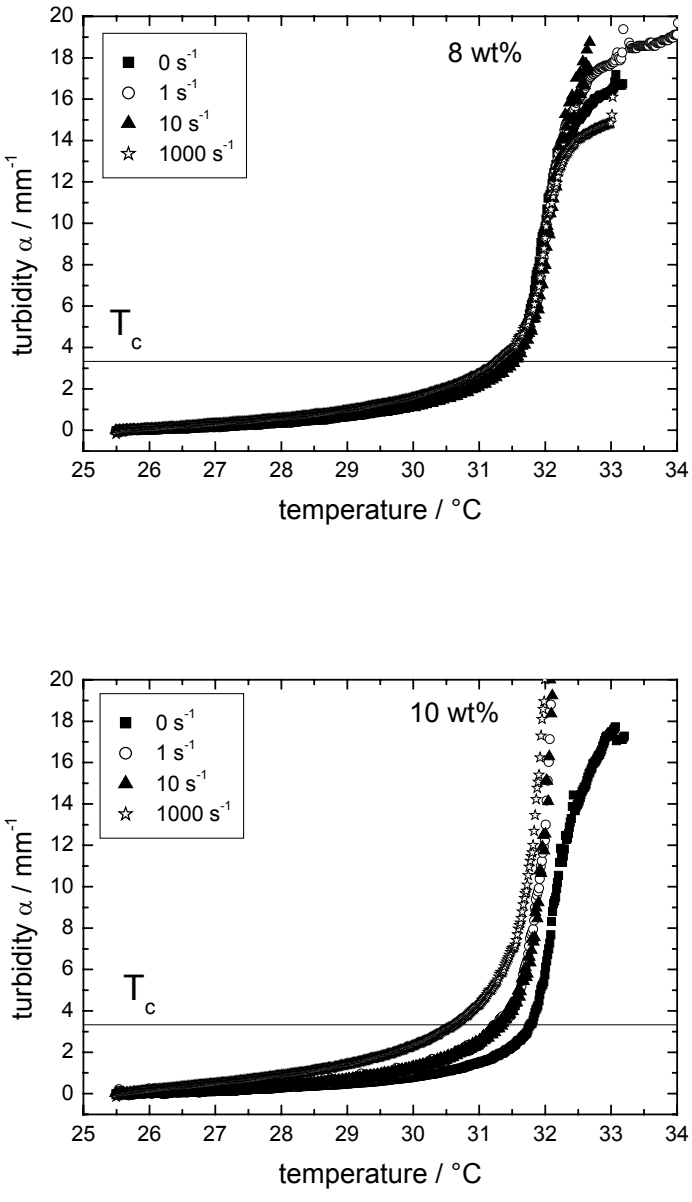

Figure 5. *Turbidity as a function of temperature for a 8.0 wt% (top) and a 10.0 wt% (bottom) PNiPAM microgel suspension. An influence of shear flow on T_c is only observed for the 10.0 wt% microgel.*

Both samples became turbid with increasing temperature, however, a shear-induced shift of the curve was only observed in the concentrated sample. The shift of the turbidity curve to lower temperatures at a higher shear rate demonstrates that shear flow caused phase separation at lower temperature relative to the quiescent state. The turbidity curves can be characterized by the cloud point temperature T_c. In this study we defined T_c as the temperature corresponding to a developing turbidity of α = 3.33 mm^{-1}, or a transmission of I_t/I_0 = 1/e = 0.368, as indicated in the figures.

The behavior of a solution of the linear PNiPAM at a concentration of 4.0 wt% is shown in figure 6. Again shear induced phase separation is observed. The shear-induced shift of the turbidity curve is more pronounced than in the microgel samples.

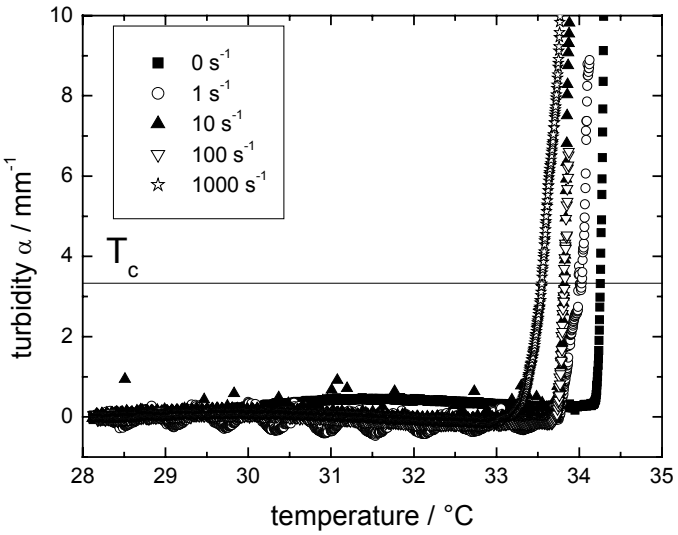

Figure 6. *Turbidity as a function of temperature for a linear chain PNiPAM solution at 4.0 wt%*

In addition isothermal rheo-optical experiments were performed with the linear chain polymer (4.7 wt%) at temperatures approximately 1 K below T_C in the quiescent state (32.7 °C). The sample was presheared at $\dot{\gamma}$ = 5 s^{-1} for 10 minutes. Then a shear rate of $\dot{\gamma}$ = 1000 s^{-1} was applied for 2 minutes. A strong turbidity developed immediately after the high shear rate was applied, indicating shear induced demixing. After reduction of the shear rate to $\dot{\gamma}$ = 5 s^{-1} the sample became transparent immediately, indicating that the shear induced phase transition is reversible. Isothermal experiments were performed with the microgel (10.0 wt%) as well and similar results were obtained. These experiments revealed

again that the shear flow induces a phase separation for the temperature sensitive polymers regardless of their macromolecular architecture.

SANS is a further useful technique to study the temperature induced volume-transition in thermosensitive colloidal microgels.[63,66,68,69,70,71,72] Crowther et al.[63] describe the temperature induced deswelling of PNiPAM microgel particles in the *q* range of 0.01 - 0.1 $Å^{-1}$. In the swollen state at temperatures below the LCST their data shows contributions from polymer chains in a solution-like environment (Ornstein-Zernike scattering). At temperatures above the LCST the scattering profiles exhibit a Porod form ($I \propto q^{-4}$) of scattering relative to the size of the colloidal particles indicating scattering from a dilute dispersion of non-interacting hard spheres. Dingenouts and coworkers[68,69,70] report on a continuous volume-transition in core-shell particles consisting of a poly(styrene) core and a PNIPAM shell. They demonstrate that the shell has a well defined compact structure above the LCST. The swelling of the shell is described in terms of an affine expansion of the network, followed by a slight decrease of the volume fraction with increasing distance to the surface of the core. To our knowledge not much is known about the shear induced phase separation of thermoresponsive microgels. To gain a more detailed understanding of the shear induced structures rheo-SANS experiments were carried out.

First results of the rheo-SANS experiments in the low q-regime of a 10.0 wt% PNiPAM microgel at rest and under sheared condition are presented in figure 7. All scattering patterns remained isotropic even at shear rates of $\dot{\gamma}$ = 500 s^{-1} and elevated temperatures. Hence, no deformation of the microgel particles was observed under shear flow. At temperatures well below the LCST (29.2 °C) no significant change in the intensity distribution *I(q)* is observed when a shear flow is applied. In the quiescent state and under shear the scattered intensity exhibits pronounced form factor minima at the same *q*-values. At temperatures above the LCST (34.4 °C) the PNiPAM microgel suspension demixes. Porod scattering ($I \propto q^{-4}$) is observed in the high *q*-regime as a result of scattering from a sharp interface of the collapsed particle. The scattering profile remains unchanged after shear flow was applied. At temperatures near the LCST (31.5 °C), a strong increase of the scattered intensity is observed when the suspension is sheared. The minima of the form factor obtained at rest vanish under shear flow indicating the shear induced particle collapse. The rheo-SANS studies provided information about the structure of a single particle although the suspensions were highly concentrated (10.0 wt%). For the large particles investigated in this study the main contribution of the scattering in the high q-regime arises from the form factor describing the temperature or shear induced collapse of a single particle. In contrast, the rheo-turbidity measurements revealed the shear induced macroscopic phase separation of the concentrated PNiPAM suspensions. Additional rheo-SANS experiments were performed

employing PNiPAM microgels with different cross-linking densities and particle sizes and a detailed fitting model for *I(q)* was developed in collaboration with Jan Skov Pedersen, University of Aarhus, Denmark. These studies will be presented in a following article.[89]

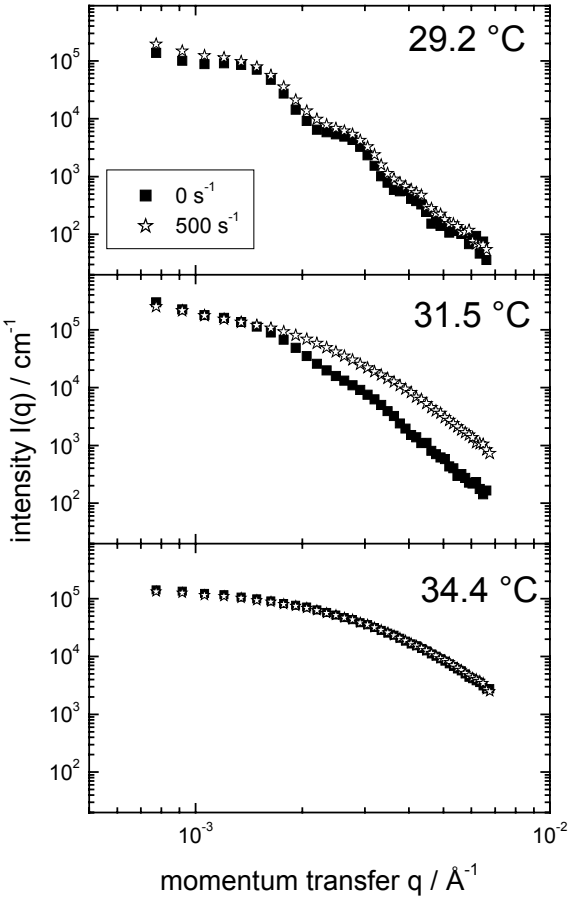

Figure 7. *SANS scattering intensity distribution I(q) versus momentum transfer q of the PNiPAM microgel at 10.0 wt% for different temperatures at rest and under shear flow. The shear flow strongly influences the form factor at 31.5 °C.*

Figure 8 displays the cloud curves for both molecular architectures at rest and under sheared conditions. The cloud point temperatures T_C of the microgel are apparently lower than the T_C of the linear PNiPAM. At a concentration of 1.0 wt% the T_C of the microgel (T_C = 32.2 °C) is 1.8 K lower than the T_C of the linear PNiPAM (T_C = 34.0 °C). The cloud point temperatures determined by the onset of a developing turbidity in the rheo-optical experiment are slightly lower than the phase-transitions-temperatures obtained from DSC measurements. Temperatures of 33.6 °C for the microgel and 34.8 °C for the linear polymer were found by DSC in D_2O. Otake and coworkers[114] report, that the transition temperature of macroscopic PNiPAM gels is always slightly higher (1-2 K) than that of linear PNiPAM

solutions. They attribute this effect to the different mobility of the polymer chains in different molecular architectures and to surface effects of the polymer globule in the solution.

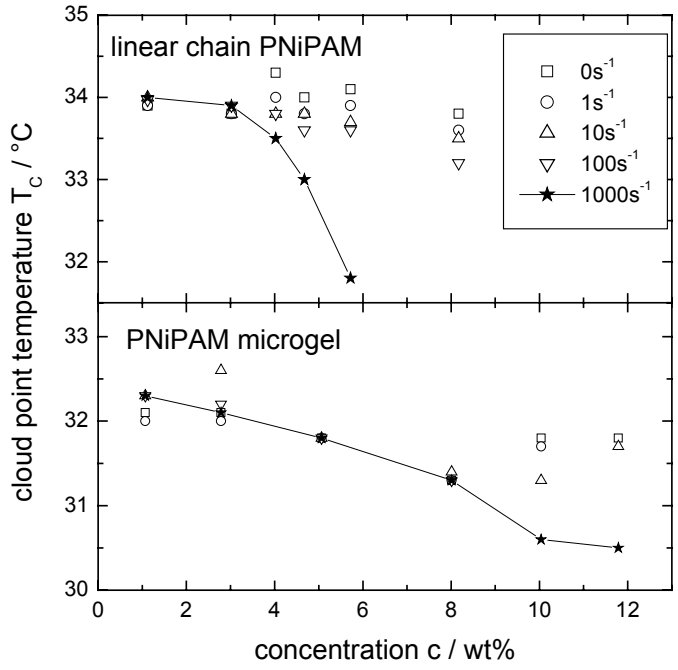

Figure 8. *Cloud curves of the linear chain PNiPAM (top) and the PNiPAM microgel (bottom) in D_2O at rest and at various shear rates. Shear induced demixing was observed for both polymer architectures at high concentrations. The lines are guides to the eye.*

A significant shear induced shift of T_C is observed only when the polymer concentration was sufficiently high. A shift of 1.0 K was noted for the linear PNiPAM at $\dot{\gamma}$ = 1000 s^{-1} for a concentration of 4.7 wt%. At higher concentrations the effect becomes even more pronounced. For the crosslinked microgel at $\dot{\gamma}$ = 1000 s^{-1} a concentration of 10.0 wt% or higher was required to observe a shift of T_c by 1.2 K. Hence, an influence of shear flow on the miscibility gap was observed only when high Weissenberg numbers ($W_i \equiv \dot{\gamma}\,\tau$) were applied. A 4.0 wt% solution of the linear PNiPAM at 32 °C exhibits τ = 0.09 s and a shift of T_C by 0.8 K was observed when W_i = 90 was reached.

Shear induced demixing can occur in the PNiPAM/water system independent of the macromolecular architecture. The behavior of the linear PNiPAM in semi-dilute solution is similar to that of PS in DOP. Shear flow leads to a strong enhancement of concentration fluctuations and the turbidity rise is observed at lower shear rates when the temperature is closer to the miscibility gap.

Concentrated colloidal suspensions of rigid particles display rich structural changes when strong shear forces are applied. A prominent and technologically important feature is the observation of shear thinning and shear thickening with increasing shear rate, which are related to shear induced structures including string and bundle like ordering.[26] Verduin et al.[35] investigated the influence of shear flow on the structure of a gel-forming suspension. Stearyl coated silica particles which behave as sticky hard spheres were suspended in benzene. The phase diagram reveals typical bimodal and spinodal lines but at high volume fraction the gel line occurs first when the temperature is decreased and the interaction potential becomes more attractive. In rheo-optical experiments an increase of turbidity was observed at very low shear rates indicating the formation of larger structures (mainly along the flow direction). Thus shear flow destabilized the solution. Higher shear rates, however, shifted the cloud point in the other direction.

The PNiPAM-microgel particles investigated in this study have different properties as compared to attractive hard sphere colloids. With increasing temperature the solvent becomes worse and eventually the interaction potential becomes attractive. Since the microgel particles are swollen by the solvent, the temperature increase also causes the particles to collapse, which does not occur in colloidal suspensions of rigid particles. Therefore, altering the temperature of the thermoresponsive PNiPAM particles leads to changes in the volume fraction as well as interaction potential. Hence the macroscopic behavior is very different since the liquid to solid transition is shifted to higher concentrations with increasing temperature.

A common feature of the PNiPAM microgel and linear PNiPAM samples is the strong influence of concentration on phase separation under shear. Shear induced demixing was found at 10.0 wt% but not at 8.0 wt% for the microgel and at 4.0 wt% but not at 3.0 wt% for the linear PNiPAM.

Figure 9 displays results obtained from low amplitude oscillatory shear experiments for the 8.0 and 10.0 wt% microgel samples. At 30.2 °C both concentrations behave as a viscoelastic solid and the storage modulus is larger than the loss modulus. Near the equilibrium cloud temperature the two samples reveal a characteristic difference in the viscoelastic properties. At 32.0 °C the lower concentrated sample behaves as a viscoelastic liquid and the loss modulus exceeds the storage modulus. The 10.0 wt% sample, however, revealed a dominant elastic behavior. This indicates that the presence of an elastic material with a close packing of particles is necessary in order to influence the phase separation process by shear flow.

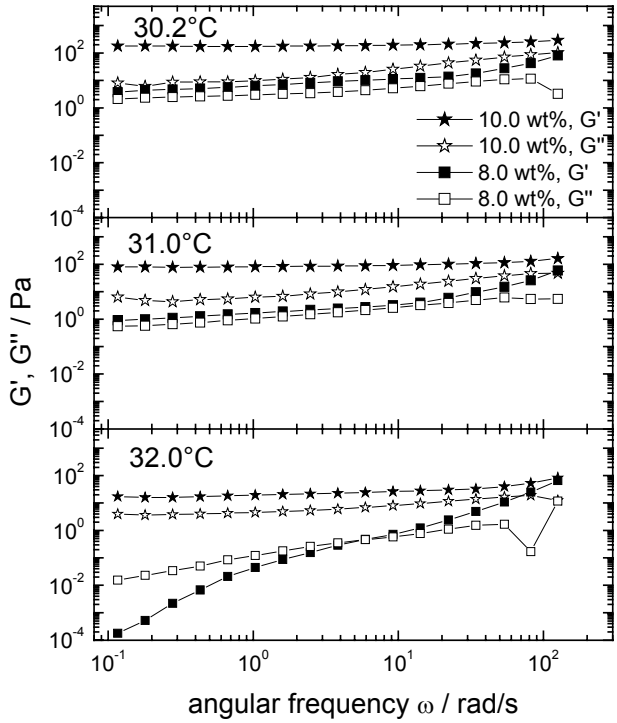

Figure 9. *Storage modulus G´(filled symbols) and loss modulus G´´ (open symbols) as a function of angular frequency ω for the PNiPAM microgel at a concentration of 8.0 wt% and 10.0 wt% at different temperatures. At 32.0 °C the 8.0 wt% sample is liquid whereas the 10.0 wt% microgel is solid.*

The temperature dependent solid-liquid transition can also be detected by dynamic light scattering (DLS). The transition from a non-ergodic to an ergodic system is revealed in the decay of the time correlation function (TCF) and the speckle pattern. At 32.3 °C the 8.0 wt% sample displays a mono-exponential decay of the TCF which is no longer observed with the 10.0 wt% sample. Hence, the 8.0 wt% suspension is liquid and the 10.0 wt% sample solid at 32.3 °C. The DLS experiments are in good agreement with the rheological experiments.

The observation that the cloud curve is only affected by shear flow when the sample has dominant elastic properties indicates that the shear induced phase separation process is not only related to the attractive interaction potential of the microgel particles. Even at a concentration of 8 wt% the shear flow reached the limit of high Peclet numbers and should be sufficient to induce particle collisions and aggregation. Instead, it appears that a solvent squeezing mechanism is responsible for the shear induced demixing at high concentration. The coupling between concentration fluctuations and shear stress in entangled polymer solution can lead to stress relaxation via solvent squeezing[115]. A similar mechanism can be suggested for microgel particles if the particles are densely packed such that relaxation via

particle diffusion is hindered. The long time self diffusion of the particles is strongly suppressed above the liquid-solid transition. However, in contrast to rigid particles, the microgel particles can be compressed. Thus a coupling between the shear stress and fluctuation in the local packing density can result in squeezing of solvent giving rise to an enhancement of concentration fluctuations and turbidity.

It should be noted, that shear induced demixing was not only observed for the microgel presented here but also for a PNiPAM microgel with the same cross-linking density (1.5 mol%) but smaller particle size. In contrast, for a PNiPAM microgel with a higher degree of cross-linking density (5.5 mol%) shear induced demixing was not observed. The solvent inside the particle seems to be immobilized because of the high cross-linking density. The particles can not be compressed as much as the particles with a lower degree of cross-linking. Thus, the stress relaxation through solvent squeezing might be hindered. The increase of turbidity with increasing temperature is contributed to an aggregation of the particles.

6.4 Conclusions

Rheological properties of aqueous solutions of linear PNiPAM and of PNiPAM microgel particles were studied. The flow behavior and the viscoelastic properties of the linear polymer solutions revealed no pronounced temperature dependence. As along as the concentration stays well above the overlap concentration the rheological properties are not very sensitive to temperature induced changes in the size of an individual macromolecule. In contrast, a pronounced influence of temperature on those rheological properties was found for the microgel, since the effective volume fraction which determines the flow and viscoelastic behavior, strongly depends on temperature. A scaling behavior of the characteristic relaxation time of the linear PNiPAM with concentration is described.

Shear induced phase separation was observed for aqueous solutions of linear PNiPAM and of PNiPAM microgel particles. The cloud curve was shifted to lower temperatures with increasing shear rate. With the microgel system with a cross-linking density of 1.5 mol%, an influence of shear flow on the turbidity was only observed when the particle density was sufficiently high to be above the liquid-solid transition. This indicates that a coupling of shear stress with the concentration fluctuations leading to solvent squeezing is only possible when the particles are densely packed. For a PNiPAM microgel with a higher degree of cross-linking (5.5 mol%) shear induced demixing was not observed. The stress relaxation through solvent squeezing might be hindered since the particles can not be compressed as much as the ones with a lower degree of cross-linking.

ACKNOWLEDGMENT. Financial support by the Deutsche Forschungsgemeinschaft and the Fonds der Chemischen Industrie is gratefully acknowledged. We thank Jaro Ricka and Rene Nyffenegger, University of Berne, Switzerland, for the possibility to synthesize the linear PNiPAM in their lab. We thank Peter Lindner, Institute Laue-Langevin, Grenoble, France, for his support with the SANS experiments at the D11 beamline.

7 SANS Study of Shear Induced Structures in Solutions of linear PNiPAM

ABSTRACT: The influence of shear flow on the structure of concentrated aqueous PNiPAM solutions near the lower critical solution temperature is investigated by means of small angle neutron scattering. Two samples, both in the semi-dilute regime above the overlap concentration are studied. The scattering curve of the less concentrated sample is not influenced by shear flow, although high shear rates are reached. The more concentrated sample, however, displays shear induced demixing under strong shear flow conditions. Experiments at different shear rates indicate the existence of a threshold shear stress and the phase separation process becomes faster with increasing stress. The two dimensional scattering patterns remain isotropic even during the phase separation process and the correlation length as obtained from Ornstein-Zernike plot increases. The influence of shear flow on the phase separation process is thus similar to a temperature increase. The results are in excellent agreement with data from recent rheo-optical experiments where shear induced phase separation was also observed for the concentrated solution at high shear rates. Apparently strong shear flow has an analogous effect as a temperature increase.

7.1 Introduction

It is well known that shear flow can influence the phase separation of polymer solutions.[39] Several techniques have been employed to study the influence of shear on demixing of solutions of linear chain poly(styrene) (PS) in dioctylphthalate (DOP) including turbidity, dichroism, small angle light scattering (SALS) and small angle neutron scattering (SANS).[40,41,42] With PS in DOP a so-called butterfly pattern in SALS and SANS which indicates shear-induced concentration fluctuations is often observed in semi-dilute solutions above the overlap concentration c^*. Butterfly scattering patterns have also been observed with polymer networks and some colloidal systems.[43,44,45,46,47] In these complex fluids the viscoelastic properties, especially the first normal stress difference, play an important role for the coupling between density fluctuations and shear stress.[48] In further experiments with dilute PS/DOP solutions, shear-induced aggregation was observed below c^* indicating entanglements may not be necessary for fluctuation enhancements.[49]

Much less is known about aqueous polymer solutions where phase separation occurs upon heating. The temperature at which phase separation is first observed is known as the lower critical solution temperature (LCST). The most widely studied system displaying LCST behavior in aqueous solution is poly(*N*-isopropylacrylamide) (PNiPAM).[4] Temperature-

sensitive PNiPAM polymers have been studied extensively, primarily, due to their potential technological applications, including drug delivery systems and biotechnology.[2,9] PNiPAM undergoes a temperature-induced phase transition at the LCST of 31-34 °C. The phase transition has varied effects depending on the architecture of the polymer system, whether linear chain PNiPAM, chemically cross-linked microgels or macroscopic gels are discussed. For dilute solutions of linear PNiPAM, the contraction of the polymer chain is observed with increasing temperature and the transition from an expanded coil to a compact globule occurs. Cross-linked microgels and macrogels exhibit a temperature-induced volume phase transition from a highly swollen to a collapsed state.

Badiger et al.[52] observed shear-induced demixing in aqueous solutions of linear PNiPAM which was attributed to the destruction of intersegmental clusters formed in the stagnant state. Wolf et al. suggested a general thermodynamic approach in which the total energy of a polymer solution consists of the usual Flory-Huggins-Gibbs energy with an added term to describe the stored elastic energy.[53] Other approaches describe the dynamic coupling between concentration fluctuations and shear stress.[54,55,56] In this approach a stress applied causes squeezing of the solvent out of the more entangled regions which consequently enhances the concentration fluctuations. In addition, aggregation, flocculation and for example the formation of large scale bundle ordering have been observed in colloidal systems under shear.[36]

Differences in the microstructures of colloidal and polymer solutions give rise to very different properties near the miscibility gap. Recently, we reported on the shear-induced phase separation for aqueous solutions of linear chain PNiPAM and for suspensions of PNiPAM microgels.[73] A shear induced shift of the cloud curve to lower temperatures was observed in rheo-optical experiments.

Whereas optical techniques as e.g. turbidity, probe concentration fluctuations on a rather large length scale, small-angle neutron scattering (SANS) is an important technique to investigate spatial heterogeneities on a length scale of few nanometers. The phase separation of concentrated PNiPAM solutions and gels in the quiescent state has been investigated by means of SANS by Shibayama et al.[116] The scattering curves were fitted with an Ornstein-Zernike model and they observed that the correlation length diverged at the spinodal temperature.

In this contribution we investigate the influence of shear flow on the phase separation of concentrated aqueous solution of linear chain PNiPAM by means of small-angle neutron scattering. Analogue experiments with PNiPAM microgel solutions will be reported elsewhere.[117]

7.2 Experimental Part

Synthesis and characterization of the linear chain polymer are described elsewhere.[73] The weight-average molar mass M_w and the radius of gyration R_g of the linear chain PNiPAM were determined from static light scattering experiments (SLS) in dilute solution and $M_w = 3.9 \times 10^6$ g/mol and R_g(25.8°C) = 114 nm was obtained.

Small-angle neutron scattering experiments under shear (rheo-SANS) were performed at the instrument D11 of the Institute Laue-Langevin (ILL) in Grenoble, France. The neutron wavelength was λ = 6 Å with a spread of $\Delta\lambda / \lambda$ = 9 %. The data were collected on a two-dimensional multidetector (64 x 64 elements of 1 x 1 cm^2), and corrected for background and empty cell scattering. Sample-detector distances of 36.0 and 10.5 m were employed. The incoherent scattering of H_2O was used for absolute calibration according to standard procedures and software available at the ILL ($GRAS_{ans}P$ V. 3.25). A Bohlin CVO-120-HR rheometer was adjusted to the D11 beamline. Measurements were performed using a Searle shear cell of quartz cylinders with a gap of 1 mm. The scattering experiments were performed in the radial position yielding information in the plane formed by the flow and vorticity directions. Further processing of the isotropic two-dimensional SANS pattern was done by radially averaging to obtain a one-dimensional data set. All experiments were carried out at full contrast using D_2O as the solvent.

7.3 Results and Discussion

Macromolecules form a transient network of entangled chains in semi-dilute polymer solution, where the polymer concentration *c* is above the overlap concentration *c**. The average distance between entanglement points is described by the so-called mesh size or correlation length ξ which is large compared to the size of a monomer unit. For distances small compared to ξ, the polymer chain will exhibit single coil behavior and possess a random or self-avoiding walk conformation. At larger distances, the semi-dilute solution emulates a polymer melt, since the sample space is densely packed with polymer segments of the blob size ξ. Consequently, for good solvent conditions *I(q)* should show a different behavior than dilute solutions on length scales for $\xi > 1/q$. Here $q = \left(4\pi/\lambda\right)\sin\left(\theta/2\right)$ denotes the magnitude of the scattering (with the scattering angle θ). The scattering intensity *I(q)* in the semi-dilute regime for $\xi < 1/q$ is well described by the so-called Ornstein-Zernike equation, which is a Lorentzian function, and is given by

$$I(q) = \frac{I(0)}{1 + \xi^2 q^2} \qquad (1)$$

where *I(0)* denotes the scattering intensity at $q = 0$. Figure 1 shows the scattering intensity distribution normalized by concentration, *I(q)/c*, of PNiPAM solutions at different concentrations at 25°C. The curves nicely overlap at high q and a slope of $q^{-1.65}$ is observed in the double logarithmic plot. Thus, the asymptotic scaling behavior in the high q-regime is in good agreement with the predictions of the asymptotic q-dependence for a polymer in good solvent conditions according to a self avoiding walk model $I(q) \propto q^{-1.66}$. A strong increase of the scattering intensity in the low q-regime is observed for the samples at a concentration of 0.50 wt% and 4.60 wt%. At concentrations above the overlap concentration c^* additional long range inhomogeneties are often observed giving rise to an increase of the forward scattering intensity $I(q \rightarrow 0)$. Correlations length ξ of 2 and 1nm were obtained from Ornstein-Zernike plots for the 0.5 and 4.6 wt% samples, respectively, which agrees nicely with the data reported by Shibayama et al.[116]

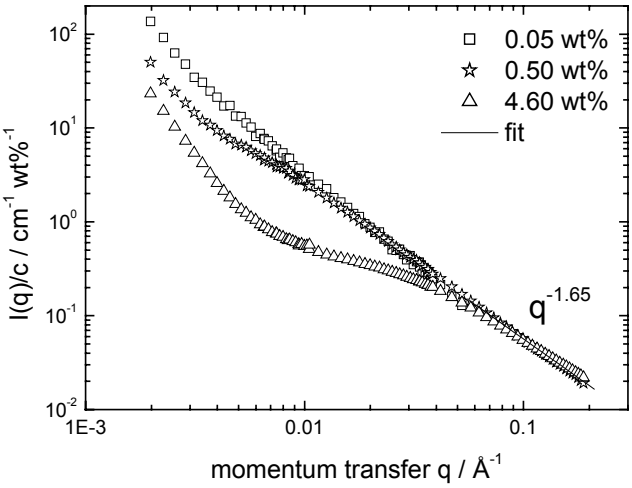

Figure 1. *SANS curves normalized by concentration, I(q)/c, of PNiPAM solutions at 25°C and different concentrations.*

Figure 2 displays results from a 1.1 wt% solution at a constant temperature of 32.3°C which is approximately 1K below the LCST in the quiescent state. The top left part illustrates the shear protocol: the sample was sheared at different applied shear stresses and the evolution of the shear rate was recorded. At the lowest shear stress, the sample did not reach stationary shear flow, but at higher stresses the steady state was reached quickly. Shear thinning was found which is typical of concentrated polymer solution and indicates that the shear rates were already above the characteristic relaxation time of the sample.

The other two plots in figure 2 display SANS data: first the angular dependent scattering intensity *I(q)/c* shown in a double logarithmic plot vs. q (top right). The bottom part shows an Ornstein-Zernike plot of the same data. The scattering intensity *I(q)/c* is well described by the

Ornstein-Zernike equation (1) and it is apparent that shear flow has no influence on the scattering intensity at this temperature. An average correlation length of ξ=10.4 nm was obtained. At this concentration the previously discussed rheo-turbidity measurements revealed no influence of shear flow on the phase separation as well.

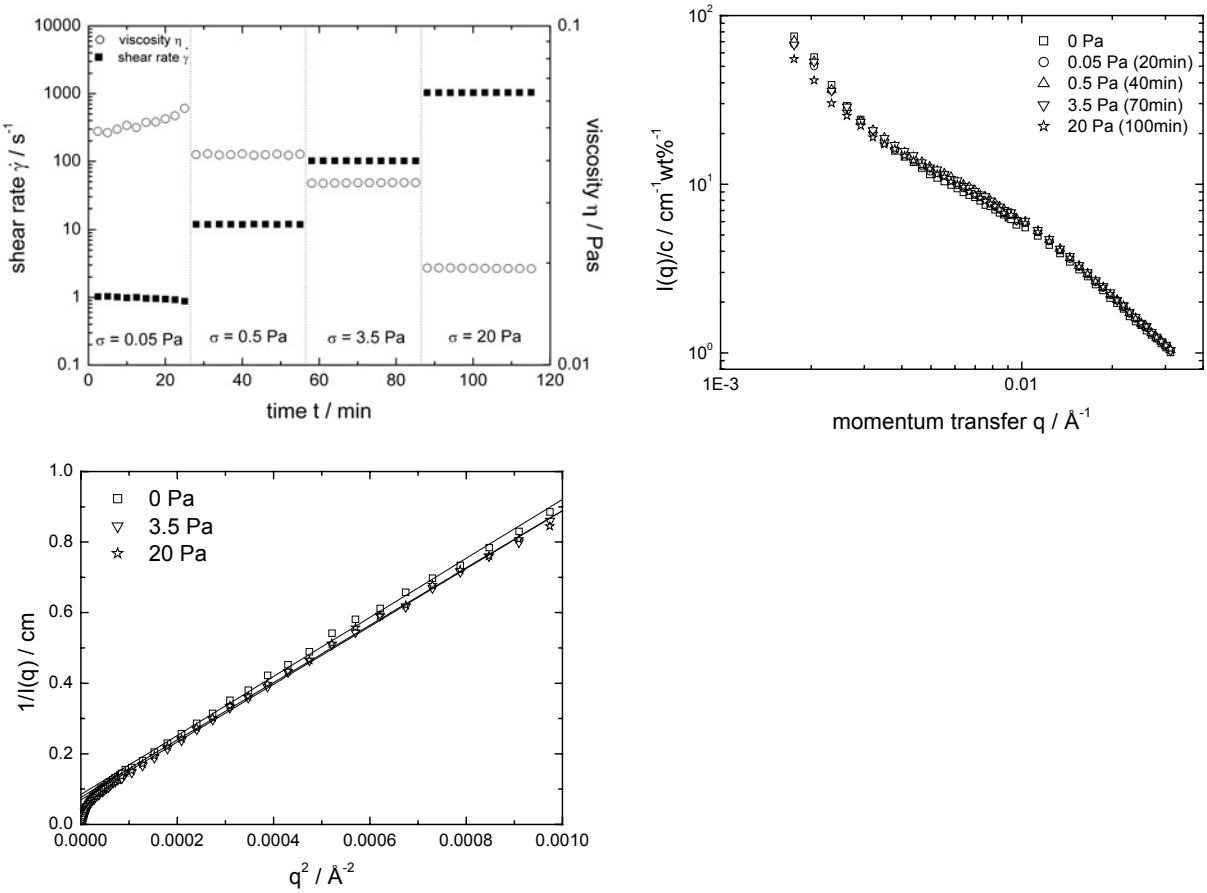

Figure 2. *Rheological and rheo-SANS data from a PNiPAM solution at 1.1wt% and 32.3°C. The experiment was performed under controlled stress conditions. Top left: viscosity and shear rate; top right: SANS data; bottom: Ornstein-Zernike plot of SANS data.*

However, the scattering intensity was dramatically influenced by shear flow for the 4.0 wt% solution, see figure 3. The SANS intensity *I(q)/c* was strongly enhanced when a shear stress of 180 Pa was applied to the sample. The 2D scattering patterns remained isotropic at all shear stresses. Again the scattering intensity could be fitted with the Ornstein-Zernike model and the results are summarized in table 1. Both, correlation length ξ and the scattering intensity $I(q \rightarrow 0)$ strongly increased at high stress. Apparently, phase separation was induced by shear flow. These results agree nicely with rheo-optical data where shear induced demixing was observed when the sample was subjected to strong shear flow. The scattering patterns we observed at high shear stress resemble those obtained by Shibayama et al. when the phase separation was induced by rising temperature.

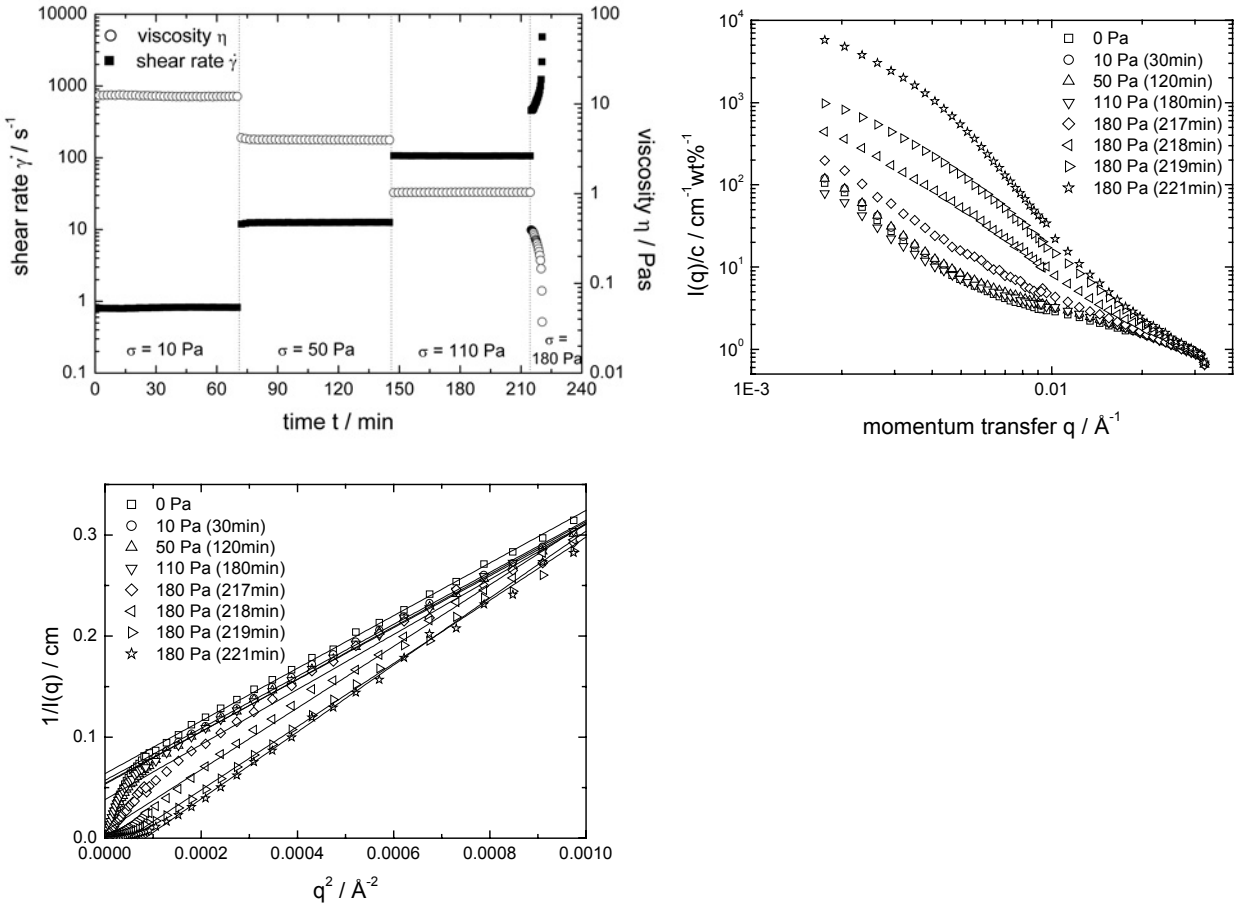

Figure 3. *Rheological and rheo-SANS data from a PNiPAM solution at 4.0wt% and 32.3°C. The experiment was performed under controlled stress conditions. Top left: viscosity and shear rate; top right: SANS data; bottom: Ornstein-Zernike plot of SANS data.*

time* / min** ***(according to shear protocol)	***application time of shear stress***	***I(q→0)* / cm^{-1}**	***ξ* / nm**
0 min	0 Pa	15.66	6.4
30 min	10 Pa for 70min	17.5	6.7
120 min	50Pa for 75 min	18.4	6.9
180 min	110 Pa for 70 min	18.7	7.0
217 min	180 Pa for 2 min	26.2	8.4
218 min	180 Pa for 3 min	145.8	21.1

Table 1. *Ornstein-Zernike fitting results from a PNiPAM solution at 4.0wt% and 32.3°C under various sheared conditions.*

As already mentioned above, the two-dimensional scattering patterns remained isotropic even at the highest applied stress. This indicates that the shear induced demixing process is isotropic on a short, local length scale. Similar behavior was observed with concentrated suspensions of PNiPAM microgels. Shear induced demixing was also found and the scattering intensity at high *q* where the particle form factor is probed remained isotropic as well.[117]

Results from a step-up / step-down experiment are shown in figure 4. The sample was presheared at 80 Pa where phase separation is not yet induced. Then the shear stress was increased to 165 Pa and the evolution of viscosity and SANS intensity was recorded. Finally, the shear stress was reduced back to 80 Pa. Obviously a shear stress of 165 Pa is also sufficient in order to induced phase separation. The phase separation process itself is fully reversible, when the stress is reduced to 80 Pa, the scattering curve relaxed back to its initial intensity.

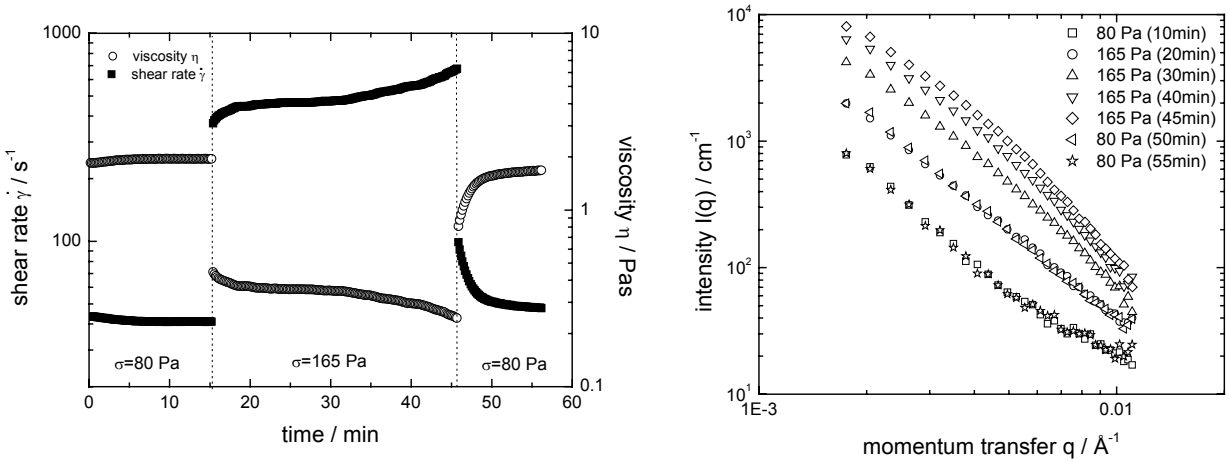

Figure 4. *Rheological and rheo-SANS data from a PNiPAM solution at 4.0wt% and 32.3°C. The experiment was performed under controlled stress conditions. Left: viscosity and shear rate; Right: SANS data. Similar to figure 3, but different shear stresses were applied.*

However, the shear-induced demixing process is slower at a shear stress of 165 Pa as compared to the experiment at 180 Pa. The kinetics of the demixing process for both shear stresses are compared in figure 5. At a shear stress of 165 Pa, the relative scattering intensities *I(t)/I(t=0)* obtained at $q = 0.0021\ Å^{-1}$ increased by a factor of ca. 10 in ca. 30 min. In contrast, application of a shear stress of 180 Pa for only 5 min gave rise to an increase of the low *q*-intensity by a factor of approximately 80. These experiments at different shear rates indicate the existence of a threshold shear stress and the phase separation process becomes faster with increasing stress.

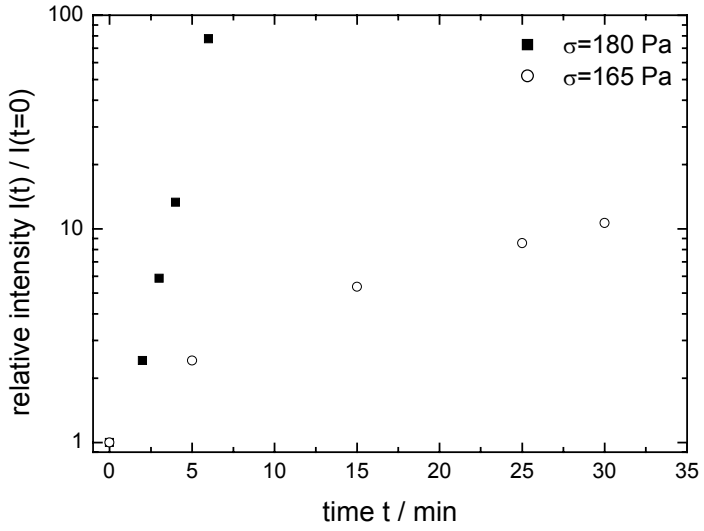

Figure 5. *Time resolved relative SANS intensity I(t)/I(t=0) determined at q = 0.0021 Å^{-1} from a PNiPAM solution at 4.0wt% at T = 32.3°C (see figure 3 and 4). The application of the shear stresses (165 Pa and 180 Pa) started at t = 0 min.*

Phase separation in aqueous PNiPAM solutions is considered to be caused by hydrophobic interaction and the breaking of H-bonds and spectroscopic data showed a change of the polymer backbone conformation. Recently, Badiger and Wolf investigated a 2 wt% solution of PNiPAM in H_2O and observed shear induced demixing in rheo-turbidity experiments.[52] They interpreted the shear-induced phase separation in terms of a destruction of favorable clusters. There are, however, some differences in the two studies; in our case we did not observe a significant viscosity increase during phase separation. One could speculate that the strong shear flow induces a change of the polymer backbone conformation which enhances phase separation. A stretching of the macromolecules should lead to an anisotropic structure which however, was not found in the SANS experiments.

7.4 Conclusions

The influence of shear flow on the structure of concentrated aqueous PNiPAM solutions is investigated by means of small angle neutron scattering. The high *q*-region of the scattering patterns at rest can be described by an Ornstein-Zernike approach and the correlation length decreases with concentration and increases with temperature in agreement with results by Shibayama et al.

The influence of shear flow on the solution structure close to the LCST is investigated for two samples, both at concentrations above the overlap concentration. The scattering curve of

the less concentrated sample (1 wt%) is not influenced by shear flow, although high shear rates are reached. The more concentrated 4 wt% sample, however, displays shear induced demixing under strong shear flow conditions. Experiments at different shear rates indicate the existence of a threshold shear stress and the phase separation process becomes faster with increasing stress.

The two dimensional scattering patterns remain isotropic even during the phase separation process and the correlation length as obtained from Ornstein-Zernike plot increases. The influence of shear flow on the phase separation process is thus similar to a temperature increase. The results are in excellent agreement with data from rheo-optical experiments where shear induced phase separation was also observed for the concentrated solution at high shear rates. Apparently strong shear flow has an analogous effect as a temperature increase. Since the LCST of aqueous PNiPAM solutions is in an experimentally convenient temperature range, this system is ideal to investigate the kinetics of shear induced phase separation. Such experiments are in progress and will be reported later.

Acknowledgements: Financial support by the Deutsche Forschungsgemeinschaft is gratefully acknowledged.

8 Summary and Outlook

8.1 Summary

The influence of the polymer architecture on the structure formation of thermoresponsive polymers in the quiescent state and under shear flow was studied in the present work. In the first section of this work, the internal structure of a PNiPAM microgel particle was studied via small-angle neutron scattering (SANS) in dilute suspension. In addition, a modeling expression to describe the form of the particle was introduced. The second section sought to encompass both the structure of a single microgel particle, and the larger, many-particle microstructure that is present in concentrated suspensions. SANS investigations were again performed over a wide *q*-range, and the model was extended to include a static structure factor term. A study of the influence of shear on both the internal particle structure and the particle-particle correlations completed the characterization of the microgel suspensions under shear flow. In the final two chapters, the corresponding results for solutions of linear chain PNiPAM are presented. The polymer was first studied by rheology and rheo-turbidity, then in concentrated solution both at rest and under shear by SANS.

I) In order to gain a thorough understanding of the full range of PNiPAM microgel behaviors, we first undertake to characterize the structure of an individual particle in dilute solution. We employ SANS as our primary experimental technique along with a direct modeling expression for the scattering intensity distribution. The model was found to describe very well the experimental data at all temperatures over an extensive *q*-range. The overall particle form as well as the internal structure of the microgel network were included in the model expression. The inhomogeneous distribution of cross-linking density through a particle was accounted for with a radial density profile that decreased gradually at the sphere surface following an error function. The structural changes induced by temperature, cross-linking density and particle size were revealed by the density profiles. The polymer volume fraction inside the particle increased dramatically with increasing temperature accompanied by a decrease of the smearing of the particle surface. Above the LCST, the particle surface sharpened significantly and a radial profile with an almost box-shape was observed. The overall swelling behavior of the particle is dominated by the swelling of the outer, less cross-linked regions of the microgel at temperatures near the LCST. The overall particle size obtained by SANS was smaller than the hydrodynamic radius obtained by DLS. This is explained by a few dangling polymer chains attached to the particle surface contributing to the hydrodynamic radius. In the swollen state, an increase of the cross-linking density

resulted in an increase of the polymer volume fraction in the inner region of the particle and a reduction of the fuzziness of the particle surface. The influence of the cross-linking densities on the structure of the PNiPAM microgels was explained with the kinetics of the emulsion copolymerization used to prepare the microgel colloids. A reduction of the surfactant concentration employed in the emulsion copolymerization lead to larger particles. A significant decrease of the polymer volume fraction inside the colloid was observed with increasing particle size. Obviously, the structural inhomogeneities of microgels need to be considered when such systems are employed.

II) Once an expression had been derived to describe the structure of a single particle in dilute suspension, we are able to answer the question of whether concentrated thermoresponsive PNiPAM microgels can be used as model systems for concentrated colloidal suspensions. The model expression for the particle form factor was extended by a model hard sphere structure factor in order to describe experimental data at high concentration. The particle form factor accounted for the inhomogeneous distribution of the polymer segment density throughout an individual particle whereas the Percus-Yevick hard sphere structure factor described the correlations between different particles. Average radial density profiles were calculated from the amplitude of the form factor and the structure factor. By this procedure a direct real space description of the spatial ordering in the neighborhood of a single particle was obtained. The model expression described the experimental scattering intensity distributions very well over the entire q-regime for a broad range of concentrations at temperatures below as well as above the LCST. The main conclusions are:

a) The overall particle size and the correlation length of the concentration fluctuations of the internal polymer network decreased with concentration revealing the increasing compression of the spheres. In contrast to suspensions of rigid hard spheres, the concentration dependence of the particle form factor of the swollen PNiPAM microgels needed to be accounted for when structure factors of concentrated suspensions were discussed.

b) The particle-particle interaction potential did not change significantly between 25°C and 32°C. Even approximately 1K below the LCST the experimental scattering intensity distributions were described very well by the hard sphere structure factor by using an equivalent hard sphere particle size and volume fraction. The hard sphere parameters $R_{HS}(c)$ and $\eta_{HS}(c)$ differed from R_{SANS} and the effective volume fraction ϕ_{eff}. At 39°C, which was well above the LCST, the interaction potential became strongly attractive leading to macroscopic phase separation. The collapsed microgel spheres formed aggregates consisting of flocculated particles without significant long-range order. Instead only one well-defined layer of surrounding neighbour particles was observed. Hence, an attractive interaction potential in

concentrated suspensions of PNiPAM microgels led to distinctively different structures as compared to attractive hard sphere colloids.

c) As mentioned above, concentrated suspensions of PNiPAM microgel particles could be described within the frame work of a hard sphere structure factor when equivalent hard sphere parameters R_{HS} and η_{HS} were employed. Microgels with different degrees of cross-linking and particle size resembled true hard sphere behavior up to effective volume fractions of ϕ_{eff}<0.35. At higher effective volume fractions ϕ_{eff}>0.35 strong deviations from true hard spheres were observed. Interpenetration of the outer, less cross-linked regions of the soft spheres as well as particle compression occurred at higher concentrations. The equilibrium colloidal phase behavior also revealed a soft sphere behavior as indicated by the shift of the freezing transition ϕ_f towards higher effective volume fractions. The divergence of the relative zero shear viscosity $\eta_{0,rel}$ occurred at higher effective volume fractions ϕ_{eff} as well and the power law concentration dependence of the plateau modulus G_P revealed typical soft sphere behavior.

Thermoresponsive PNiPAM microgels can be considered a model system in colloidal science when the above mentioned properties are taken into account. The temperature sensitivity leads to several advantages over other systems: i) The preparation of concentrated samples at low temperatures is facilitated since the suspensions can be prepared at elevated temperatures with low viscosity and cooling will lead to homogeneous particle swelling. ii) The liquid-solid transition (crystallization and glass transition) can be investigated both as a function of concentration at constant temperature and as a function of temperature at a constant particle number density. iii) The aggregation behavior near the LCST can be used to study the onset of film formation.

III) From the study of the structures of concentrated suspensions in the quiescent state, we conclude that the interaction potential of thermoresponsive PNiPAM microgels can be varied from repulsive at temperatures below the LCST to attractive at temperatures above the LCST. In contrast to suspensions of rigid spheres, the effective volume fraction can be changed by temperature while the mass concentration and particle number density are kept constant. Above the LCST the microgel particles eventually collapse. In addition to the structural characterization of concentrated PNiPAM microgel suspensions at rest, the influence of shear flow on the structure formation was investigated.

Studying PNiPAM microgels with different particle sizes in the same q-regime provided complementary information about shear-induced changes of both the internal particle structure as well as the overall microstructural phenomena. The shear-induced particle arrangements strongly depend on the interaction potential. When the interaction potential was repulsive at temperatures below the LCST, individual swollen PNiPAM particles in

concentrated suspension were not deformed significantly even at high shear rates. Shear-induced ordering was observed at high shear rates resulting in the formation of two dimensional hexagonal close packed layers that aligned along the flow direction giving rise to shear thinning. The formation of sliding hexagonal close packed layers under shear flow is therefore proposed to be a general property of colloidal dispersion independent of the internal structure of the particle. At temperatures near the LCST, when the particle interaction potential was not yet strongly attractive, shear flow induced the collapse of an individual particle in concentrated suspension at high shear rates. A so-called butterfly scattering pattern indicated the shear-induced enhancement of concentration fluctuations along the flow direction and phase separation occurred finally.

IV) In the last sections of this work, we employ various characterization techniques to describe aqueous solutions of linear chain PNiPAM. Rheological properties of linear PNiPAM solutions and of PNiPAM microgel particles were compared. The flow behavior and the viscoelastic properties of the linear polymer solutions revealed no pronounced temperature dependence. As along as the concentration stayed well above the overlap concentration the rheological properties were not very sensitive to temperature induced changes in the size of an individual macromolecule. In contrast, a pronounced influence of temperature on those rheological properties was found for the microgel, since the effective volume fraction which determined the flow and viscoelastic behavior, strongly depended on temperature. A scaling behavior of the characteristic relaxation time of the linear PNiPAM with concentration was described.

Shear induced phase separation was observed for aqueous solutions of linear PNiPAM and of PNiPAM microgel particles. The cloud curve was shifted to lower temperatures with increasing shear rate. With the microgel system with a cross-linking density of 1.5 mol%, an influence of shear flow on the turbidity was only observed when the particle density was sufficiently high to be above the liquid-solid transition. This indicated that a coupling of shear stress with the concentration fluctuations leading to solvent squeezing was only possible when the particles were densely packed. For a PNiPAM microgel with a higher degree of cross-linking (5.5 mol%) shear induced demixing was not observed. The stress relaxation through solvent squeezing might be hindered since the particles could not be compressed as much as the ones with a lower degree of cross-linking.

V) The influence of shear flow on the structure of concentrated aqueous linear chain PNiPAM solutions was investigated by means of small angle neutron scattering. The high q-region of the scattering patterns at rest were described by an Ornstein-Zernike approach and the correlation length decreased with concentration and increased with temperature.

The influence of shear flow on the solution structure close to the LCST was studied for two samples, both at concentrations above the overlap concentration. The scattering curve of the less concentrated sample was not influenced by shear flow, although high shear rates were reached. The more concentrated sample, however, displayed shear induced demixing under strong shear flow conditions. Experiments at different shear rates indicated the existence of a threshold shear stress and the phase separation process became faster with increasing stress.

The two dimensional scattering patterns remained isotropic even during the phase separation process and the correlation length as obtained from Ornstein-Zernike plot increased. The influence of shear flow on the phase separation process is thus similar to a temperature increase. The results were in excellent agreement with data from rheo-optical experiments mentioned above where shear induced phase separation was also observed for the concentrated solution at high shear rates. Apparently strong shear flow has an analogous effect as a temperature increase. Since the LCST of aqueous PNiPAM solutions is in an experimentally convenient temperature range, this system is ideal to investigate the kinetics of shear induced phase separation.

8.2 Outlook

We have demonstrated that swollen thermoresponsive PNiPAM microgel particles reveal a very different internal structure than homogenous spheres. The inhomogeneity arises from an uneven incorporation of the cross-linker during synthesis. The resulting PNiPAM microgels appear to be similar to model colloidal systems, but with additional surface fuzziness. In order to optimize the potential biotechnological applications of the microgel particles, it would be desirable to have microgels with a homogenous internal particle structure. Since the cross-linker is consumed faster than the monomer during the emulsion copolymerization, a homogenous distribution of cross-linking density throughout the particle might be achieved by so-called starved-feed polymerization techniques. In this method, the cross-linker is added slowly to the reacting solution. The kinetics of the starved-feed copolymerization could be followed using online calorimetry. The structure of the PNiPAM particles obtained by this approach could be characterized employing various scattering methods in combination with the model for the intensity distribution that was newly established in this work. The polymer density profiles should reveal the changes in the particle structure.

In this work the equilibrium structures of concentrated PNiPAM suspensions were intensively studied in the liquid, crystalline and glassy states with small angle neutron scattering techniques. In each case the primary results were the static structure factor and the form factor of the particles. While the form and structure factors provide essential information on the static properties of single particles and larger structures, respectively, SANS does not provide data on the dynamic properties of microgel suspensions. We have observed that the microgel particles can be modeled as hard sphere colloids in terms of their structure factors and as modified fuzzy hard spheres in their form. It is possible, however, that the high degree of swelling and the deformability of the particles might lead to significant differences in terms of their dynamic behaviors. We therefore additionally recommend that the microgels be studied with dynamic light scattering techniques. Since concentrated PNiPAM suspensions are turbid, standard dynamic light scattering experiments cannot be performed and a cross-correlated dynamic light scattering setup which could separate singly scattered light, would be required.

In order to compete with traditional colloidal suspensions for additional applications in the food and personal care industries, it is essential that the interaction parameters of the microgels be as tunable as possible. Chemical modifications of the PNiPAM microgel particle surface may allow for a wider range of behaviors, including gel- and glass-formation at lower volume fractions, more sharply increasing viscosities, and multi-step temperature sensitivities. Polyelectrolytes adsorbed onto the particle surface could give rise to an additional pH sensitivity, comparable to that often found in electrostatically stabilized hard spheres. In addition, for specific pharmaceutical applications, the encapsulation and release of proteins in the microgel network could be studied by fluorescence labeling techniques.

We have shown that concentrated solutions of linear chain PNiPAM reveal a threshold shear stress at which shear induced phase separation occurred. The phase separation process became significantly faster with increasing shear stress. To our knowledge very little is known about the influence of shear flow on the kinetics of the concentration fluctuations near the miscibility gap. Shear flow should give rise to an elongation of the polymer coil along the flow direction eventually leading to birefringence. Thus, it would be challenging to study the demixing under shear with time-resolved methods like flow-birefringence and rheo-SALS. Those methods would allow for determination of the shear induced structures with a time resolution of approximately one second, much faster than the time resolution of rheo-SANS of ca. one minute.

Overall, we conclude that there is tremendous potential for applications of the PNiPAM microgels. With this study we have made great progress toward a thorough characterization of the structures present in microgel suspensions. However, the great advantage of colloidal systems at this time is their well-characterized, and therefore predictable behavior. The possibilities for tuning the microgel behaviors are certainly as varied as with hard sphere colloids, with an advantageous additional thermo-sensitivity. We therefore believe that microgels will continue to be the subject of much interest well into the future.

9 References

[1] Larson, R. G. *The Structure and Rheology of Complex Fluids*, Oxford University Press, **1999**.

[2] Pelton, R. *Adv. Colloid Interface Sci*. **2000**, *85*, 1.

[3] Antonietti, M. *Angew. Chem.* **1988**, *100*, 1813.

[4] Schild, H. G. *Prog. Polym. Sci.* **1992**, *17*, 163.

[5] Klug, E. D. J. *Polym. Sci. Part G* **1971**, *36*, 491.

[6] Eisele, M.; Burchard, W. *Makromol. Chem.* **1990**, *191*, 169.

[7] Pelton, R. *Adv. Colloid Interface Sci.* **2000**, *85*, 1.

[8] Dhara, D.; Chatterji; P.R. *Rev. Macromol. Chem. Phys.* **2000**, C*40*, 51.

[9] Saunders, B. R.; Vincent, B. *Adv. Coll. Inter. Sci.* **1999**, *80*, 1.

[10] Kawasaki, H.; Sasaki, S.; Maeda, H. *J. Phys. Chem. B* **1997**, *101*, 4184.

[11] Zhang, Y.Q.; Tanaka, T.; Shibayama, M. *Nature* **1992**, *360*, 142.

[12] Inomata, H.; Wada, N.; Yagia, Y.; Goto, S.; Saito, S. *Polymer* **1995**, *36*, 875.

[13] Shibayama, M.; Fujikawa, Y.; Nomura, S. *Macromolecules* **1996**, *29*, 6535.

[14] Foss, D. R.; Brady, J. F. *J. Rheol.* **2000**, *44*, 629.

[15] Meeker, S. P.; Poon, W. C. K.; Pusey, P. N. *Phys. Rev. E* **1997**, *55*, 5718.

[16] Pusey, P. N.; Segre, P. N.; Behrend, O. P.; Meeker, S. P.; Poon, W. C. K. *Physica A* **1997**, *235*, 1.

[17] Pusey, P. N.; van Megen, W. *Nature* **1986**, *320*, 340.

[18] Derber, S.; Palberg, T.; Schätzel, K.; Vogel, J. *Physica A* **1997**, *235*, 204.

[19] Bartsch, E.; Frenz, V.; Baschnagel, J.; Schärtl, W.; Sillescu, H. *J. Chem. Phys.* **1997**, *106*, 3743.

[20] Senff, H.; Richtering, W. *J. Chem. Phys.* **1999**, *111*, 1705.

[21] Hellweg, T.; Dewhurst, C. D.; Brückner, E.; Kratz, K.; Eimer, W. *Colloid Polym. Sci.* **2000**, *278*, 972.

[22] Debord, J. D. *J. Phys. Chem. B* **2000**, *104*, 6327.

[23] Debord, J. D.; Eustis, S.; Debord, S. B.; Lofye, M. T.; Lyon, L. A. *Adv. Mater.* **2002**, *14*, 658.

[24] Debord, S. B.; Lyon, L. A. *J. Phys. Chem. B* **2003**, *107*, 2927.

[25] Mellema, J. *Curr. Opin. Colloid Interface Sci.* **1997**, *2*, 411.

[26] Loose, W.; Hess, S.. *Rheol. Acta.* **1989**, *28*, 91.

[27] Bossis, G.; Brady, J. F. *J. Chem. Phys.* **1984**, *80*, 5141.

[28] Ackerson, B. J.; Hayter, J. B.; Clark, N. A.; Cotter, L. *J. Chem. Phys.* **1986**, *84*, 2344.

[29] Ackerson, B. J.; Pusey, P. N. *Phys. Rev. Lett.* **1988**, *61*, 1033.

[30] Chen, L. B.; Zukoski, C. F.; Ackerson, B. J.; Hanley, H. J. M.; Straty, G. C.; Barker, J.; Glinka, G. J. *Phys. Rev. Lett.* **1992**, *69*, 668.

[31] Laun, H. M.; Bung, R.; Hess, S.; Loose, W.; Hess, O.; Hahn, K.; Hädicke, E.; Hingmann, R.; Schmidt, F.; Lindner, P. *J. Rheol.* **1992**, *36*, 743.

[32] Dux, Ch.; Musa, S.; Reus, V.; Versmold, H.; Schwahn, D.; Lindner, P. *J. Chem Phys.* **1998**, *109*, 2556.

[33] Versmold, H.; Musa, S.; Bierbaum, A. *J. Chem Phys.* **2002**, *116*, 2658.

[34] Young, S. L.; Wagner, N. J. *Rheol. Acta.* **2003**, *42*, 199.

[35] Verduin, H.; de Gans, B. J.; Dhont, J. K. G. *Langmuir* **1996**, *12*, 2947.

[36] Vermant, J.; Raynaud, L.; Mewis, J.; Ernst, B.; Fuller, G. G. *J. Colloid Interface Sci.* **1999**, *211*, 221.

[37] Wang, H.; Lettinga, M. P.; Dhont, J. K. G. *J. Phys.: Condens. Matter* **2002**, *14*, 7599.

[38] Lenstra, T. A. J.; Dhont, J. K. G. *Phys. Rev. E* **2001**, *63*, 61401.

[39] Rangel-Nafaile, C.;Metzner, A.B.; Wissbrun, K.F. *Macromolecules* **1984**, *17*, 1187.

[40] Morfin, I.; Lindner, P.; Boué, F. *Macromolecules* **1999**, *32*, 7208.

[41] Saito, S.; Hashimoto, T.; Morfin, J.; Lindner, P.; Boué, F. *Macromolecules* **2002**, *35*, 445.

[42] Saito, S.; Hashimoto, T. *J. Chem.Phys.* **2001**, *114*, 10531.

[43] Bastide, J.; Leibler, L.; Prost, J. *Macromolecules* **1990***, 23*, 1821.

[44] Moses, E.; Kume, T.; Hashimoto, T. *Phys.Rev.Lett*. **1994**, *72*,2037.

[45] DeGroot, J. V.; Macosko, C. W.; Kume, T.; Hashimoto, T. *J. Colloid Interface Sci.* **1994**, *166*, 404.

[46] Belzung, B.; Lequeux, F.; Vermant, J.; Mewis, J. *J. Colloid Interface Sci.* **2000**, *224*, 179.

[47] Weigel, R.; Läuger, J.; Richtering, W.; Lindner, P. *J. Phys. II France* **1996**, *6*, 529.

[48] van Egmond, J.W. *Macromolecules* **1997**, *30*, 8045.

[49] Pönitsch, M.; Hollfelder, T.; Springer, J. *Polym. Bull.* **1998**, *40*, 345.

[50] Badiger, M. V.; Lutz, A.; Wolf, B. A. *Polymer* **2000**, *41*, 1377.

[51] Schmidt. J.; Burchard, W.; Richtering, W. *Biomacromolecules* **2003**, *4*, 453.

[52] Badiger, M.; Wolf, B.A. *Macromol. Chem. Phys.* **2003,** *204*, 600.

[53] Wolf, B.A. *Macromolecules* **1984**, *17*, 615.

[54] Helfand, E.; Fredrickson, G. H. *Phys .Rev. E* **1989**, *62*, 2468.

[55] Milner, S. T. *Phys. Rev. E* **1993**, *48*, 3674.

[56] Onuki, A. *J. Phys. Condens. Matter* **1997**, *9*, 6119.

[57] Wu, X.; Pelton, R. H.; Hamielec, A. E.; Woods, D. R.; McPhee, W. *Colloid Polym. Sci.* **1994**, *272*, 467.

[58] Guillermo, A.; Cohen Addad, J. P.; Bazile, J. P.; Duracher, D.; Elaissari, A.; Pichot, C. *J. Polym. Sci. Part B: Polym. Phys.* **2000**, *38*, 889.

[59] Shibayama, M.; Tanaka, T.; Han, C. C. *J. Chem. Phys.* **1992**, *97*, 6829.

[60] Shibayama, M.; Tanaka, T.; Han, C. C. *J. Chem. Phys.* **1992**, *97*, 6842.

[61] Shibayama, M. *Macromol. Chem. Phys.* **1998**, *199*, 1.

[62] Mears, S. J.; Deng, Y.; Cosgrove, T.; Pelton, R. *Langmuir* **1997**, *13*, 1904.

[63] Crowther, H. M.; Saunders, B. R.; Mears, S. J.; Cosgrove, T.; Vincent, B.; King, S. M.; Yu, G. E. *Coll. Surf. A* **1999**, *152*, 327.

[64] Saunders, B. R.; Crowther, H. W.; Morris, G. E.; Mears, S. J.; Cosgrove, T.; Vincent, B. *Coll. Surf. A* **1999**, *149*, 57.

[65] Kratz, K.; Hellweg, T.; Eimer, W. *Polymer* **2001**, *42*, 6631.

[66] Kratz, K.; Lapp, A.; Eimer, W.; Hellweg, T. *Coll. Surf. A* **2002**, *197*, 55.

[67] Fernandez-Barbero, A.; Fernandez-Nieves, A.; Grillo, I.; Lopez-Cabarcos, E. *Phys. Rev. E* **2002**, *66*, 51803.

[68] Dingenouts, N.; Norhausen, Ch.; Ballauff, M. *Ber. Bunsenges. Phys. Chem.* **1998**, *102*, 1594.

[69] Dingenouts, N.; Norhausen, Ch.; Ballauff, M. *Macromolecules* **1998**, *31*, 8912.

[70] Seelenmeyer, S.; Deike, I.; Dingenouts, N.; Rosenfeldt, S.; Norhausen, Ch.; Ballauff, M.; Narayanan, T. *J. Appl. Crystallogr.* **2000**, *33*, 574.

[71] Dingenouts, N.; Seelenmeyer, S.; Deike, I.; Rosenfeldt, S.; Ballauff, M.; Lindner, P.; Narayanan, T. *Phys. Chem. Chem. Phys.* **2001**, *3*, 1169.

[72] Seelenmeyer, S.; Deike, I.; Rosenfeldt, S.; Norhausen, Ch.; Dingenouts, N.; Ballauff, M.; Narayanan, T.; Lindner, P. *J. Chem. Phys.* **2001**, *114*, 10471.

[73] Stieger,M.; Richtering, W. *Macromolecules* **2003**, *36*, 8811.

[74] Fritz, G.; Scherf, G.; Glatter, O. *J. Phys. Chem. B* **2000**, *104*, 3463.

[75] Pedersen, J. S. *Adv. Coll. Inter. Sci.* **1997**, *70*, 171.

[76] Svaneborg, C.; Pedersen, J. S. *Phys. Rev. E.* **2001**, *64*, 10802.

[77] Pedersen, J. S.; Svaneborg, C. *Curr. Opinion Coll. Inter. Sci.* **2002**, *7*, 158.

[78] Kinning, D. J.; Thomas, E. L. *Macromolecules* **1984**, *17*, 1712.

[79] Pedersen, J. S.; Posselt, D.; Mortensen, K. *J. Appl. Crystallogr.* **1990**, *23*, 321.

[80] Freltoft, T.; Kjems, J. K.; Sinha, S. K. *Phys. Rev. B* **1986**, *33*, 269.

[81] Senff, H.; Richtering, W. *Coll. Polym. Sci.* **2000**, *278*, 830.

[82] McPhee, W.; Tam, K. C.; Pelton, R. *J. Coll. Inter. Sci.* **1993**, **156**, 24.

[83] Jansen, J. W.; de Kriuf, C. G.; Vrij, A. *J. Colloid Interface Sci.* **1986**, *114*, 471; **1986**, *114*, 481; **1986**, *114*, 492.

[84] Rouw, P. W.; Woutersen, A. T. J. M.; Ackerson, B. J.; de Kruif, C. G. *Physica A* **1989**, *156*, 876.

[85] Vrij, A.; Penders, M. H. G. M.; Rouw, P. W.; de Kruif, C. G.; Dhont, J. K. G.; Smits, C. S.; Lekkerkerker, H. N. W. *Farady Discuss. Chem. Soc.* **1990**, *90*, 31.

[86] de Hek, H.; Vrij, A. *J. Colloid Interface Sci.* **1981**, *84*, 409.

[87] Bartsch, E.; Kirsch, S.; Lindner, P.; Scherer, T.; Stölken, S. *Ber. Bunsenges. Phys. Chem.* **1998**, *11*, 1597.

[88] Eckert, T.; Bartsch, E. *Phys. Rev. Lett.* **2002**, *89*, 125701.

[89] Stieger, M.; Richtering, W.; Pedersen, J. S.; Lindner, P. *J. Chem. Phys.* **2004**, *in press*.

[90] Wu, J.; Huang, G.; Hu, Z. *Macromolecules* **2003**, *36*, 440.

[91] Batchelor, G. K. *J. Fluid Mech.* **1997**, *83*, 97.

[92] Pedersen, J. S.; Svaneborg, C.; Almdal, K.; Hamley, I. W.; Young, R. N. *Macromolecules* **2003**, *36*, 416.

[93] Pedersen, J. S.; Gerstenberg, M. C. *Colloids Surfaces A* **2003**, *213*, 175.

[94] Sommer, C.; Pedersen, J. S.; Garamus, V. *in preparation*.

[95] Agrawal, R.; Kofke, D. A. *Mol. Phys.* **1995**, *85*, 23.

[96] Krieger, I. M.; Dougherty, T. J. *Trans. Soc. Rheol.* **1959**, *3*, 137.

[97] Zwanzig, R.; Mountain, R. D. *J. Chem. Phys.* **1965**, *43*, 4464.

[98] Buscall, R.; Goodwin, J. W; Hawkins, M. W.; Ottewill, R. H. *J. Chem. Soc. Faraday Trans.1* **1982**, *78*, 2889.

[99] Wagner, N. J. *J. Colloid Interface Sci.* **1993**, *161*, 169.

[100] Loose, W.; Ackerson, B. J. *J. Chem Phys.* **1994**, *101*, 7211.

[101] Stieger, M.; Pedersen, J. S.; Lindner, P.; Richtering, W. *Langmuir* **2004**, *submitted*.

[102] Stieger, M.; Lindner, P.; Richtering, W. *e-Polymers* **2004**, *in preparation*.

[103] Meewes, M.; Ricka, J.; de Silva, M.; Nyffenegger, R.; Binkert, T. *Macromolecules* **1991**, *24*, 5811.

[104] Kulicke, W.; Klein, J. *Angew. Makromol. Chem.* **1987**, *69*, 169.

[105] Senff, H. *phD thesis*, University of Freiburg, Germany, **1999.**

[106] Zipfel, J.; Berghausen, J.; Schmidt, G.; Lindner, P.; Tsianou, M.; Alexandridis, P.; Richtering, W. *Phys. Chem. Chem. Phys* **1999**, *1*, 3905.

[107] Kubota, K.; Fujishige, S.; Ando, I. *Polym. J.* **1990**, *22*, 15.

[108] Wu, C. *Polymer* **1998**, *39*, 4609.

[109] Hansen, J.C.; Maier, D.; Honerkamp, J.; Richtering, W.; Horn, F.M.; Senff, H. *J. Colloid Interface Sci.* **1999**, *215*, 72.

[110] Shirota, H.; Endo, N.; Horie, K. *Chem. Phys.* **1998**, *238*, 487.

[111] Cox, W.P.; Merz, E.H. *J. Polym. Sci.* **1958**, *28*, 619.

[112] Cross, M. *J. Coll. Sci.* **1965**, *20*, 417.

[113] Elias, H.G. in *Makromoleküle Band 2*, 6th ed., Wiley-VCH Verlag, Weinheim (Germany), **2001**, p 395.

[114] Otake, K.; Inomata, H.; Konno, M.; Saito, S. *Macromolecules* **1990**, *23*, 283.

[115] Saito, S.; Koizumi, S.; Matsuzaka, K.; Suehiro, S.; Hashimoto, T. *Macromolecules* **2000**, *33*, 2153.

[116] Shibayama, M.; Tanaka, T.; Han, C. C. *J. Chem. Phys.* **1992**, *97*, 6829.

[117] Stieger, M.; Lindner, P. ; Richtering, W. *J. Phys.: Condens. Matter* **2004**, *submitted*.